Progress in Retinal and Eye Research xxx (xxxx) xxx

Contents lists available at ScienceDirect

Progress in Retinal and Eye Research

journal homepage: www.elsevier.com/locate/preteyeres

Myopia: Histology, clinical features, and potential implications for the etiology of axial elongation

Jost B. Jonas [a,b,*,1], Rahul A. Jonas [c,1], Mukharram M. Bikbov [d], Ya Xing Wang [e], Songhomitra Panda-Jonas [f]

[a] Department of Ophthalmology, Medical Faculty Mannheim of the Ruprecht-Karis-University, Mannheim, Germany
[b] Institute for Clinical and Scientific Ophthalmology and Acupuncture Jonas & Panda, Heidelberg, Germany
[c] Department of Ophthalmology, University of Cologne, Cologne, Germany
[d] Ufa Eye Research Institute, Ufa, Russia
[e] Beijing Institute of Ophthalmology, Beijing Tongren Hospital, Capital Medical University, Beijing Ophthalmology and Visual Sciences Key Laboratory, Beijing, China
[f] Privatpraxis Prof Jonas und Dr Panda-Jonas, Heidelberg, Germany

ARTICLE INFO

Keywords:
Myopia
Axial elongation
Myopic maculopathy
Bruch's membrane
Parapapillary gamma zone
Glaucoma

ABSTRACT

Myopic axial elongation is associated with various non-pathological changes. These include a decrease in photoreceptor cell and retinal pigment epithelium (RPE) cell density and retinal layer thickness, mainly in the retro-equatorial to equatorial regions; choroidal and scleral thinning pronounced at the posterior pole and least marked at the ora serrata; and a shift in Bruch's membrane opening (BMO) occurring in moderately myopic eyes and typically in the temporal/inferior direction. The BMO shift leads to an overhang of Bruch's membrane (BM) into the nasal intrapapillary compartment and BM absence in the temporal region (i.e., parapapillary gamma zone), optic disc ovalization due to shortening of the ophthalmoscopically visible horizontal disc diameter, fovea–optic disc distance elongation, reduction in angle kappa, and straightening/stretching of the papillomacular retinal blood vessels and retinal nerve fibers. Highly myopic eyes additionally show an enlargement of all layers of the optic nerve canal, elongation and thinning of the lamina cribrosa, peripapillary scleral flange (i.e., parapapillary delta zone) and peripapillary choroidal border tissue, and development of circular parapapillary beta, gamma, and delta zone. Pathological features of high myopia include development of macular linear RPE defects (lacquer cracks), which widen to round RPE defects (patchy atrophies) with central BM defects, macular neovascularization, myopic macular retinoschisis, and glaucomatous/glaucoma-like and non-glaucomatous optic neuropathy. BM thickness is unrelated to axial length. Including the change in eye shape from a sphere in emmetropia to a prolate (rotational) ellipsoid in myopia, the features may be explained by a primary BM enlargement in the retro-equatorial/equatorial region leading to axial elongation.

1. Introduction

Myopic axial elongation is associated with pronounced anatomical changes of the eye (Haarman et al., 2020; Morgan et al., 2012; Ohno-Matsui et al., 2021). Exploring and understanding the anatomical characteristics of myopic eyes may help us better describe the histological correlates of ophthalmoscopical features of the myopic eye, to compare structural findings obtained by optical coherence tomography (OCT) with light-microscopical histology, to predict visual effects of the ophthalmoscopical appearance of the myopic fundus, and to gain a more comprehensive understanding of the process of axial elongation in myopia. Therefore, we assessed the anatomical features of myopic eyes using light microscopy, OCT, and ophthalmoscopy and correlated them with each other. We discuss these morphological findings with the results of previous experimental and clinical studies on the potential mechanism of axial elongation as part of the process of emmetropization and myopization.

* Corresponding author. Universitäts-Augenklinik, Theodor-Kutzer-Ufer 1-3, 68167, Mannheim, Germany.
E-mail address: Jost.Jonas@medma.uni-heidelberg.de (J.B. Jonas).
[1] JBJ and RAJ contributed equally to the study and share first authorship.

https://doi.org/10.1016/j.preteyeres.2022.101156
Received 22 August 2022; Received in revised form 27 October 2022; Accepted 14 December 2022

2. Sclera

2.1. Scleral thickness

Numerous studies on human globes and experimental studies on animals have revealed that axial elongation is associated with a thinning of the sclera posterior to the equator; these studies also addressed the role that the sclera may play in the process of axial elongation, emmetropization, and myopization (Coudrillier et al., 2012; Harper and Summers, 2015; Heine, 1899; Jonas, J.B. et al., 2014a; Maruko et al., 2012; McBrien et al., 2000; 2001, 2003, 2009; Morgan et al., 2012; Norman et al., 2010; Olsen et al., 1998; Rada et al., 2006; Shen et al., 2015; Vurgese et al., 2012).

Histomorphometry studies showed that the scleral thickness, measured at and posterior to the equator in human eyes, was lower in myopic eyes with an axial length >26 mm than in eyes with an axial length ≤26 mm (Olsen et al., 1998; Shen et al., 2015; Vurgese et al., 2012). In eyes with an axial length ≤26 mm and >26.0 mm, the scleral thickness decreased in an inter-regional comparison from the limbus (0.50 ± 0.11 mm and 0.46 ± 0.06 mm, respectively) to the ora serrata (0.43 ± 0.14 mm and 0.40 ± 0.13, respectively) and to the equator (0.42 ± 0.15 mm and 0.35 ± 0.14, respectively), from where it increased towards the midpoint posterior pole/equator (0.65 ± 0.15 mm and 0.47 ± 0.19 mm, respectively) to the peri-optic nerve head region (0.86 ± 0.21 mm and 0.63 ± 0.28 mm, respectively), and finally to the posterior pole (0.94 ± 0.18 mm and 0.67 ± 0.33 mm, respectively) (Vurgese et al., 2012). The differences in scleral thickness between the eyes with an axial length ≤26 mm vs. >26 mm were significant for all eye regions at and posterior to the equator, while the scleral thickness at the ora serrata ($p = 0.32$) and at the limbus ($p = 0.17$) did not differ significantly. In a high-field micro–magnetic resonance imaging (MRI) of 11 enucleated human globes, Norman and colleagues measured a maximal scleral thickness at the posterior pole of 1.0 ± 0.18 mm (Norman et al., 2010). This value was similar to the posterior scleral thickness measured histomorphometrically in eyes with an axial length ≤26 mm (0.94 ± 0.18 mm).

The peripapillary scleral flange consists of the inner layer of the posterior sclera, which continues into the lamina cribrosa and which is partially separated from the lamina cribrosa by the peripapillary border tissue of the scleral flange (Fig. 1). It forms the anterior end of the orbital cerebrospinal fluid space and is the biomechanical anchor of the lamina cribrosa (Ren et al., 2009). The outer layer of the posterior sclera merges into the optic nerve dura mater. The peripapillary scleral flange has a mean thickness of 0.39 ± 0.09 mm (axial length ≤26 mm) and 0.33 ± 0.12 mm (axial length >26 mm) in eyes with an axial length ≤26 mm and >26.0 mm, respectively. The peripapillary scleral flange is thinner than the sclera at any location of the globe (Fig. 1).

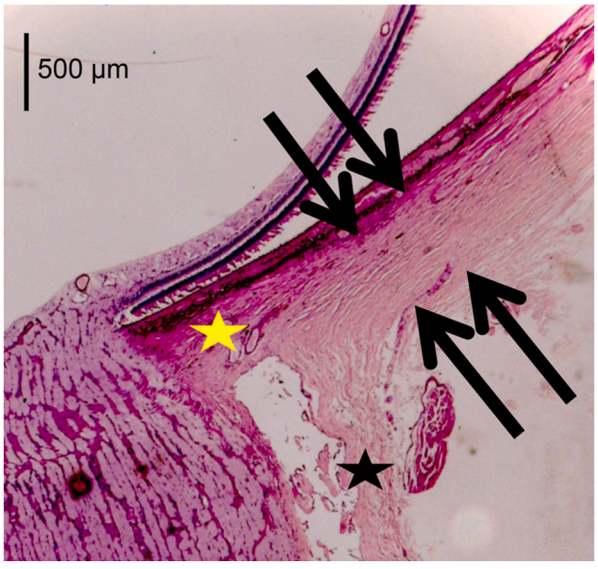

Fig. 1. Histo-photograph showing the posterior sclera (black arrows) splitting off into the peripapillary scleral flange (yellow asterisk) and into the optic nerve dura mater (black asterisk).

The finding that the peripapillary scleral flange is the thinnest part of the whole ocular coat suggests that it a "locus minoris resistenciae" (region of least resistance). It explains the occurrence of a traumatic avulsion of the optic nerve at the level of the peripapillary scleral flange (Omari et al., 2022). In that condition, the peripapillary scleral flange and the retinal nerve fibers rupture, leading to a retraction of the optic nervewhile the optic nerve meninges form a hollow tube. In highly myopic eyes, the peripapillary scleral flange can reach a thinness of 50 µm. Considering that the peripapillary scleral flange is the biomechanical anchor of the lamina cribrosa, the myopic thinning of the flange may potentially explain an increased vulnerability of the optic nerve head and optic nerve in highly myopic eyes (Jonas, JB et al., 2017a; Ren et al., 2009; Xu, L et al., 2017).

A study by Avetisov and colleagues examined scleral thickness changes occurring from birth to adulthood in emmetropic and in myopic human eyes (Avetisov et al., 1983). Avetisov and coworkers found that ontogenetic eye formation was accompanied by a thickening of all scleral regions, most markedly in the posterior section. They observed an accumulation of collagen and elastin in the posterior pole in association with a reduced share of soluble collagen fractions, a lower content of glycosaminoglycans in the equatorial region, and an increase of tensile strength and elasticity modulus. The authors discussed that a higher risk of myopia could be associated with a reduced content of collagen in the posterior scleral region, a delayed decrease of the soluble collagen fractions in the posterior and equatorial regions, and a diminished tensile strength.

Other experimental investigations suggest that the myopia-related increase in eye size results from an active scleral remodeling. This process included the production of a weakened scleral matrix, as summarized in Rada et al. (2006). Another study reported that scleral elasticity increased within the first 24 h of the development of myopia in tree shrews (McBrien et al., 2000, 2001, 2009). The scleral creep rate (defined as tissue extension vs. time) was elevated in the sclera of tree shrew eyes developing myopia and reduced in eyes recovering from myopia. These myopic changes were thought to be due to changes in matrix constituents, caused by scleral myofibroblasts. The latter are regulated by tissue stress and growth factors such as transforming growth factor-β (TGF-β). Changes in these regulatory factors have been observed during myopia development, implicating cellular factors in the subsequently weakened sclera. Liu and colleagues found a reduced expression of tissue inhibitor of metalloproteinase-2 (TIMP-2) in the sclera of tree shrew eyes undergoing myopization (Liu, HH et al., 2017). If TIMP-2 was exogenously added, myopia development and axial elongation were significantly decreased, and posterior scleral collagen degradation was inhibited. Liu et al. concluded that the reduction in TIMP-2 contributes to an increased degradative activity in the sclera and discussed that replenishment of TIMP-2 may significantly reduce the rate of both scleral collagen degradation and myopia development (Liu, HH et al., 2017; McBrien, 2013).

Interpretations of these findings must remain mindful that data are based on changes occurring within the first 24 h of myopia development in tree shrews; however, myopia develops over decades in humans. In addition, humans do not recover from myopia to any significant extent relative to tree shews (Zhu et al., 2013). Although tree shrews have often been deemed a better model than birds or primates (including humans), they reach maturity within 4 months, as compared with more than one or two decades in humans. Further, tree shrews do not have a fovea in their cone-dominant (~95% cones) retina.

2.2. Scleral thickness associations

Scleral thickness measurements obtained histomorphometrically in the anterior ocular segment are correlated with each other, but they are not markedly related to scleral thickness measurements made in the posterior segment. Similarly, posterior scleral thickness measurements are related to each other, but they are not profoundly correlated with anterior scleral thickness measurements (Vurgese et al., 2012). The scleral thickness values recorded posterior to the equator are inversely correlated with longer axial length (Vurgese et al., 2012). The regression lines are steeper and the correlation coefficients are higher, the closer the measurements are taken to the posterior region. In non–axially elongated eyes, the association between scleral thickness and axial length is not statistically significant, except for a relatively weak association between axial length and the scleral thickness at the posterior pole. Subsequently, the sclera is significantly thinner at and posterior to the equator in eyes with an axial length >26 mm vs ≤ 26 mm, while the scleral thickness at the ora serrata and at the limbus does not differ significantly between both groups. In clinical studies, the anterior scleral thickness was slightly inversely correlated with longer axial length (Dhakal et al., 2020; Sung et al., 2021). One study found that scleral thickness in the inferior anterior segment decreased in thickness in myopia, whereas the scleral thickness in the nasal and temporal meridians in the anterior segment were not correlated with myopic refractive error (Dhakal et al., 2020).

The thickness of the peripapillary scleral flange is positively correlated with central lamina cribrosa thickness and inversely correlated with longer axial length. None of the scleral measurements taken at the various locations of the globe are associated with central or peripheral corneal thickness, independently of axial length. This finding is in line with other studies (Oliveira et al., 2006), including the population-based Central India Eye and Medical Study, in which central corneal thickness was not found to be correlated with axial length (Nangia et al., 2010). The observation that the scleral thickness in the anterior segment does not correlate with the scleral thickness in the posterior segment suggests that myopic axial elongation, including moderate myopia, takes place predominantly in the posterior segment.

2.3. Scleral cross section area and volume

The scleral cross-section area, measured at or behind the equator, decreases with longer axial length (Jonas, JB et al., 2014a). The scleral volume is not related to axial length in individuals older than 3 years (Jonas, JB et al., 2014a; Shen et al., 2016a), which suggests that axial elongation is associated more with a re-modelling of the available scleral tissue than with an active growth of new scleral tissue (Bryant and McDonnell, 1998; McBrien et al., 2000; Rada et al., 2006). McBrien and colleagues observed significant scleral thinning and scleral tissue loss, especially at the posterior pole, in young tree shrews with induced myopia (McBrien et al., 2001). After a period of 12 days of myopia induction, the collagen fibril diameter distribution was not significantly altered; however, after a period of 3–20 months of myopia induction, significant reductions in the collagen fibril diameter were found, particularly at the posterior pole. McBrien and colleagues concluded that a loss of scleral tissue and subsequent scleral thinning occurred rapidly during development of axial myopia, while an increased number of small-diameter collagen fibrils in the sclera of highly myopic eyes of tree shrews was observed only in the longer term. As discussed above, it remains unclear to what degree these findings obtained in tree shrews are applicable in humans.

2.4. Posterior staphyloma

A feature of highly myopic eyes, but occurring also in some non–highly myopic eyes, are posterior staphylomas, which are outpouchings of a circumscribed region of the posterior sclera (Curtin, 1977; Hayashi, M et al., 2013; Lee, S et al., 2015; Liu et al., 2021; Maruko et al., 2011; Mehta et al., 2006; Moriyama et al., 2011; Nakao et al., 2022; Ohno-Matsui, 2014; Ohno-Matsui and Jonas, JB, 2019; Park, JH et al., 2016; Park, UC et al., 2021; Saito et al., 2021; Scott et al., 2005; Shinohara et al., 2016, 2017, 2018; Spaide, 2013; Tanaka et al., 2019; Wang, NK et al., 2016). Upon OCT-based histology, a posterior staphyloma is characterized by a relatively abrupt scleral thinning starting at the staphyloma edge, a pronounced de-arrangement of scleral collagen fibrils, and a marked choroidal thinning. The latter adds to an axial elongation–associated choroidal thinning and is most pronounced at the staphyloma border. Although occurring predominantly in highly myopic eyes, posterior staphylomas can also be detected in some non–highly myopic eyes, such as in eyes with retinitis pigmentosa or localized Bruch's membrane (BM) defects. Localized BM defects in eyes with congenital colobomas and in eyes with macular toxoplasmotic scars are usually accompanied by localized scleral staphylomas (Jonas, JB and Panda-Jonas, 2016; Xu, X et al., 2019a) (Fig. 2).

According to a recent histological study, a staphylomatous region—as compared to a corresponding region without sclera staphyloma—is characterized by marked scleral thinning and spatially correlated BM defects, while the thickness and density of the choriocapillaris and RPE cell layer and BM thickness did not differ significantly between the staphylomatous vs. non-staphylomatous regions (Jonas, JB et al., 2020a). While the pathogenesis of posterior staphylomas has so far remained elusive, the clinical and histological findings may suggest that local factors in BM and the choroid and/or a locally decreased biomechanical resistance of the sclera against a posteriorly expanding BM may play a role. The markedly thinned sclera in the staphylomatous region in spatial association with localized BM defects may suggest that a locally reduced resistance of the sclera against a backward-pushing BM may lead to a local outpouching of the sclera. BM may then, following the increased scleral circumference, become overextended, and localized BM ruptures may develop. This notion supports an active role for BM in axial elongation in myopic eyes. Alternatively, BM defects may develop initially, perhaps due to differences between the meridians in BM growth in the fundus midperiphery (see below). The localized BM defects may lead to a local outpouching of the sclera, similar to the occurrence of scleral staphylomas in spatial association with congenital BM defects, as in the case of colobomas, or in association with acquired BM defects in non–highly myopic eyes, such as in the case of toxoplasmotic scarring (Jonas, JB and Panda-Jonas, 2016).

3. Choroid

The choriocapillaris is a dense, mono-layered capillary network, the basal membrane of which covers the posterior surface of BM (Jonas, JB et al., 2011; Lejoyeux et al., 2022; Schachat et al., 2017) (Fig. 3). The choriocapillaris is the inner layer of the choroid. As shown in numerous clinical studies, the thickness of the choroid decreases with longer axial length (Hoseini-Yazdi et al., 2019; Flores-Moreno et al., 2013; Fujiwara et al., 2009; Ikuno and Tano, 2009; Jonas et al., 2019; Margolis and Spaide, 2009; Moriyama et al., 2007; Spaide et al., 2008; Wei et al., 2013). The axial length–associated reduction in choroidal thickness is most marked in the subfoveal region and decreases towards the periphery. In a study of 27 healthy young adults, Hoseini-Yazdi and colleagues did not find significant differences in choroidal thickness at a distance of 14 mm from the fovea between emmetropic eyes and myopic eyes (Hoseini-Yazdi et al., 2019). The subfoveal choroidal thickness decreases by approximately 32 μm (95% confidence interval [CI]: 37.1–26.0) for each millimeter increase in axial length, and by 4.1 μm (95%CI: 4.6–3.7) for each year increase in age, after adjusting for additional parameters such as sex (Fujiwara et al., 2009; Spaide et al., 2008; Wei et al., 2013).

The choroidal thickness reduction affects most prominently the layer of the medium- and large-sized choroidal vessels (Xu et al., 2017). Correspondingly, the percentage of the large choroidal vessel layer and

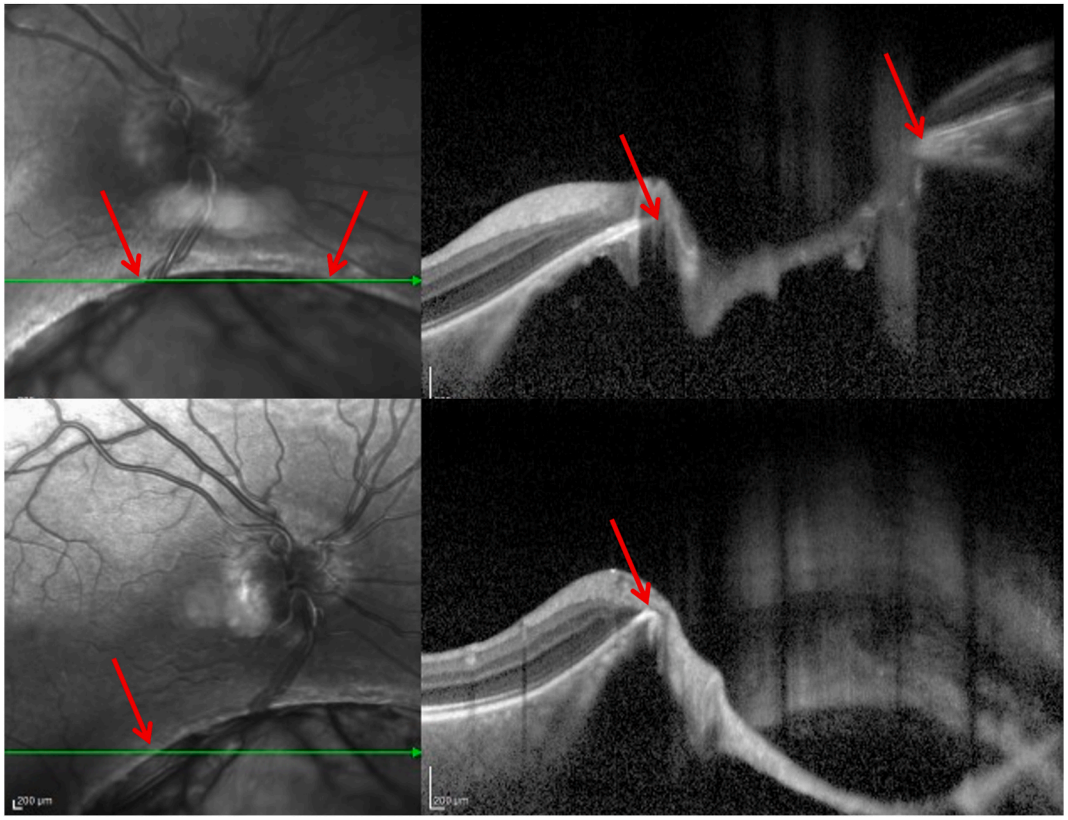

Fig. 2. Optical coherence tomographic (OCT) image of a coloboma, showing the defect in Bruch's membrane (red arrows).

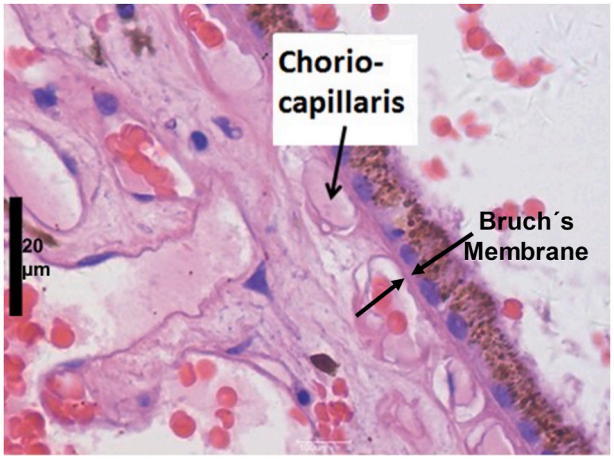

Fig. 3. Histo-photograph showing Bruch's membrane and the choriocapillaris.

of the medium-sized choroidal vessel layer on the total choroidal thickness decreases with longer axial length (Xu et al., 2017; Zhao et al., 2018). In contrast to the thickness of the medium- and large-sized choroidal vessels, the thickness of the choriocapillaris, measured histomorphometrically, may not be related to axial length (Panda-Jonas et al., 2021). Complementing the histomorphometric findings, OCT-angiographic studies reported that myopic eyes and non-myopic eyes did not differ significantly in the choriocapillaris perfusion area and that the choriocapillaris perfusion area in the foveal region was not associated with axial length (Al-Sheikh et al., 2017; Cheng, W et al., 2021, 2022). Mo and colleagues found that OCT-angiographic patterns of the choriocapillaris did not vary between emmetropic eyes and highly myopic eyes with or without pathological myopia (Mo et al., 2017). Scherm and colleagues reported that the subfoveal pattern of the choriocapillaris was not associated with axial length or choroidal thickness (Scherm et al., 2019).

In another OCT-angiographic clinical study, Al-Sheikh and associates found a lower total number of signal voids in the choriocapillaris, whereas the total and average flow void area was significantly higher, in a myopic study group compared with in a non-myopic control group (Al-Sheikh et al., 2017). The myopia-associated decrease in total choroidal thickness was not significantly associated with quantitative parameters of the choriocapillaris (Al-Sheikh et al., 2017). Jiang and coworkers found no differences in the overall vascular density in the choriocapillaris, as measured by OCT-angiography, between highly and non–highly myopic persons (Jiang et al., 2021). Applying swept-source optical coherence tomography angiography, Cheng and colleagues reported that longer axial length was associated with a higher choriocapillaris flow deficit in the perifoveal region, but not in the parafoveal region or in the fovea (Cheng, W et al., 2022).

In contrast to the histomorphometric study and the clinical studies mentioned above, a study using OCT-angiography reported that the choroidal vascularity and choriocapillaris blood perfusion decreased with longer axial length and choroidal thinning, and that both parameters were lower in the more myopic eyes of anisomyopic adults (Wu et al., 2021). In a community-based cohort of young adults, choroidal thickness showed changes during early adulthood. Choroidal thickening was less marked in eyes that were longer at baseline, and the choroid thinned in eyes that showed myopia progression (Lee, SS et al., 2022a). In eyes with myopic maculopathy, regions of patchy atrophy (categories 3 and 4 of myopic maculopathy) showed a complete loss of the choriocapillaris and of the large choroidal vessels (Sayanagi et al., 2017). Eyes with category 2 of myopic maculopathy ("diffuse choroidal atrophy") revealed a low-density pattern of the choriocapillaris. In another clinical investigation, a lower choriocapillaris flow was detected in myopic eyes with diffuse chorioretinal atrophy (stage 2 of myopic

maculopathy), in eyes with patchy atrophies (categories 2 and 3 of myopic maculopathy), and in some eyes with tessellated fundus (Wong, CW et al., 2019). One of the reasons for the differences between the studies may be the inclusion of eyes with pathological myopia in some clinical study populations. Macular BM defects in eyes with category 3+ of myopic maculopathy do not have a choriocapillaris in the region of the patchy atrophy. If areas with BM defects were included into the measurements, the mean thickness and density of the choriocapillaris as averaged across the total examination area would be lower, as if the patchy atrophy regions were excluded.

4. Bruch's membrane

Bruch's membrane (BM) consists of a collagenous layer, an elastic layer, and a collagenous layer, and it is covered on both sides by basal membranes; on its inner side by the basal membrane of the RPE, and on its outer side by the basal membrane of the choriocapillaris (Curcio and Johnson, 2012; Guymer and Bird, 2006) (Fig. 3).

According to histomorphometric studies on enucleated Caucasian human eyes, BM is thickest in the region of the pars plana, while its thickness does not differ markedly between other locations at or behind the equator of the eye (Jonas, JB et al., 2014b). BM thickness is not significantly associated with axial length (Jonas, JB et al., 2014b). Consequently, the ratio of scleral thickness to BM thickness and the ratio of choroidal thickness to BM thickness significantly decreases with longer axial length for measurements taken posterior to the equator, since retinal and choroidal thickness, measured at or posterior to the equator, decrease with longer axial length. In a parallel manner, a study on enucleated Chinese eyes revealed that in eyes without congenital glaucoma, BM was the thickest at the ora serrata, followed by the posterior pole, the posterior pole/equator midpoint, and, finally, the equator (Bai et al., 2017). Also in the Chinese eyes, BM thickness was not significantly correlated with axial length at any location. Similar findings were obtained in a histomorphometric study on guinea pigs (Deng et al., 2019). Since the distance between the ora serrata and the posterior pole elongates with longer axial length, implying an enlargement of the surface area of BM, the finding that BM thickness is independent of axial length indicates an increase in BM volume along with axial elongation. It supports the notion that the process of axial elongation may be associated with a growth of BM. In contrast, the thickness of the choroid and sclera decrease with longer axial length, and choroidal and scleral volume are independent of axial length. These findings imply that the axial elongation–related thinning of the sclera and choroid is a re-arrangement of the available scleral and choroidal tissue, rather than active formation of new tissue (Jonas, JB et al., 2017b).

If BM actively enlarges during axial elongation, the question arises whether BM enlargement occurs in a diffuse manner or predominantly in special locations of the eye. Assuming that the numbers of RPE cells and photoreceptor cells are postnatally stable, and taking into account that BM underlies both cell layers, one may consider regional differences in associations between the RPE cell density or the photoreceptor density with axial length as surrogate for a localized enlargement of BM. Studies conducted separately on eyes of Caucasians and Chinese revealed that the densities of the photoreceptors and RPE cells in the region of the posterior pole/equator midpoint, at the equator and close to the ora serrata decreased with longer axial length (or alternatively with longer retinal length) (Bai et al., 2017; Jonas, JB et al., 2017c;.own unpublished data). The decrease was most marked at the posterior pole/equator midpoint, followed by the equator, and it was less marked close to the ora serrata. The RPE cell density at the posterior pole was not related to axial length. The densities of both cell types were positively correlated with each other, and the axial length–related decrease in cell density did not differ significantly between the RPE and photoreceptor cells at the equator and at the posterior pole/equator midpoint. Correspondingly, the ratio of photoreceptor density to RPE cell density was independent of axial length at those locations. These findings suggest that the axial elongation–associated enlargement of BM takes place predominantly in the retro-equatorial region, followed by the equatorial region.

Fitting with this notion, a study of RPE progenitor cells showed that in domestic pigs that underwent either experimental RPE debridement, subretinal amniotic membrane transplantation, or both, the *in vivo* incorporation of 5-bromo-2'-deoxyuridine (BrdU) in RPE cells was detectable in the peripheral fundus region, but not in the central region (Kiilgaard et al., 2007). As a corollary, after 1 and 4 days of cell culturing, pre-equatorial RPE cells incorporated significantly more [^{3}H] thymidine than had more centrally located RPE cells. The results suggest a higher proliferative capacity in peripheral vs. central RPE cells. As a corollary, the expression of genes related to extracellular matrix production or turnover differed between the periphery and the center of the fundus. A microarray analysis by Van Soest et al. (2007) found that the macular and peripheral RPE differed in the expression of 438 genes, 33 of which were related to the extracellular matrix and some of which encoded proteins known to be present in BM.

Studies on human eyes reported that BM thickness increased with older age (Pauleikhoff et al., 1990; Ramrattan et al., 1994). An age-related increase in BM thickness may be attributed to a lifelong production and deposition of basal membrane material, with BM being covered by two basal laminae (Curcio and Johnson, 2012; Guymer and Bird, 2006; Guymer et al., 1999; Pauleikhoff et al., 1990; Ramrattan et al., 1994).

4.1. Biomechanical properties of Bruch's membrane

The biomechanics of BM has been explored experimentally (Friberg and Lace, 1988; Ugarte et al., 2006; M. Wang et al., 2018) (Fig. 4). The elastic modulus of BM (with the choroid attached) was examined by Ugarte and colleagues, who investigated the pressure–deformation relationship and defined the elastic modulus of BM as a strain-to-stress ratio with units in mm/Pa (Ugarte et al., 2006). Applying various hydrostatic pressures (stress) to the surface of BM samples obtained from the mid-peripheral fundus region, Ugarte and colleagues found that the elasticity of BM (with the choroid attached) in human eyes decreased linearly with older age after the age of 21 years, with an approximate reduction of 1% per year of age, without a detected influence of the presence of age-related macular degeneration. The recoil capacity of BM was not affected by ageing. Using a linear elastic material model, Friberg and associates examined the elastic modulus of BM and found that the modulus of elasticity of BM (with the choroid attached) was significantly greater in posteriorly vs. anteriorly located samples (7.5 ± 7.0 vs. $2.2 \pm 1.5 \times 10^5$ N m^{-2}), with a mean elasticity modulus for all locations of $6.0 \pm 2.8 \times 10^5$ N m^{-2} and a mean stress at failure of $3.3 \pm 1.3 \times 10^5$ N m^{-2} (Friberg and Lace, 1988). The mean elasticity modulus of scleral strips

Fig. 4. Pig eye with the sclera peeled off showing the underlying dark uvea; the exposed uvea with Bruch's membrane and retina is withstanding an intraocular pressure caused by the squeezing fingers.

was $2.9 \pm 1.4 \times 10^6$ N m^{-2} for the anterior sclera and $1.8 \pm 1.1 \times 10^6$ N m^{-2} for the posterior sclera at stress levels ranging from 20 to 260×10^4 N m^{-2} (Friberg and Lace, 1988).

Applying uniaxial tensile tests and performing burst tests, Girard and colleagues determined the biomechanical properties and the rupture pressure of BM (with the choroid attached) in pig eyes (X. Wang et al., 2018). The uniaxial tensile tests revealed an average elastic (tangent) modulus of BM at 0% and 5% strain of 1.60 ± 0.81 MPa and 2.44 ± 1.02 MPa, respectively. The burst examinations demonstrated that BM could withstand an average intraocular pressure of 82 mm Hg before rupture. These findings indicated that BM is a nonlinear soft tissue (stiffer with stretch), similar to other collagenous tissues such as the dura or peripapillary sclera (Girard et al., 2009; Wang et al., 2016). The elastic modulus of BM is comparable or higher than that of the sclera (0.2–0.5 MPa for an intraocular pressure of approximately 15 mm Hg; 7.96 ± 1.00 MPa at 8% strain), of the cornea (0.1–0.5 MPa), of the retina (0.011 MPa), and of the iris (0.004 MPa) (Elsheikh et al., 2008; Ko et al., 2013; Leung et al., 2014; Liu, J and He, 2009; Liu, TX and Wang, 2013; Pierscionek et al., 2007; Whitcomb et al., 2009; Worthington et al., 2014).

The relatively high rupture pressure of BM, which is capable of maintaining the intraocular pressure up to a level of about 80 mm Hg, suggests that BM may be the second-strongest tissue in the eye, second only to the corneoscleral shell. It points at the biomechanical importance of BM for the structural stiffness and stability of the eye. Studies exploring the biomechanical properties of BM in axially elongated eyes are both lacking and warranted.

4.2. *Bruch's membrane defects*

In axially elongated eyes—especially in those with an axial length exceeding 26.5 mm—BM can develop secondary defects in the macular region (Du et al., 2020; Jonas et al., 2013a; Meng et al., 2022a; Ohno-Matsui et al., 2016a; You et al., 2016) (Figs. 5–9). They can be differentiated from the primary BM defect, which is the BM opening (BMO) of the optic nerve head. The secondary BM defects in the macular region are surrounded by larger defects in the RPE layer. In a recent histomorphometric study, the mean width of macular BM defects was 1.93 ± 1.62 mm (range: 0.22–6.24 mm) (own unpublished data). A higher prevalence and larger size of macular BM defects is associated with longer axial length and a higher prevalence of posterior staphylomas. The BM defects are smaller than the defects in the overlying RPE (1.9 ± 1.6 mm vs. 2.6 mm ± 1.7 mm), are larger than defects in the overlying retinal inner nuclear layer (0.4 ± 0.8 mm), and are larger than so-called inner limiting membrane (ILM) bridges (0.1 ± 0.3 mm) (own unpublished data). The choriocapillaris, BM and the RPE cell layer do not differ significantly in thickness between the border of the BM defect and neighboring regions. In the area of the macular BM defects, the RPE and the choriocapillaris are completely absent, and the layers of mid- and large-sized choroidal vessel are mostly missing. Correspondingly, the inner retinal layers have direct contact with the inner surface of the sclera in the region of the BM defect. Within the BM defects, the sclera is thinner (0.28 ± 0.19 mm vs. 0.36 ± 0.13 mm) relative to neighboring regions. It has remained unclear why these secondary macular BM defects show no leaking of fluid from the choroidal space into the retinal space.

The macular BM defects, as detected by light microscopy, correspond

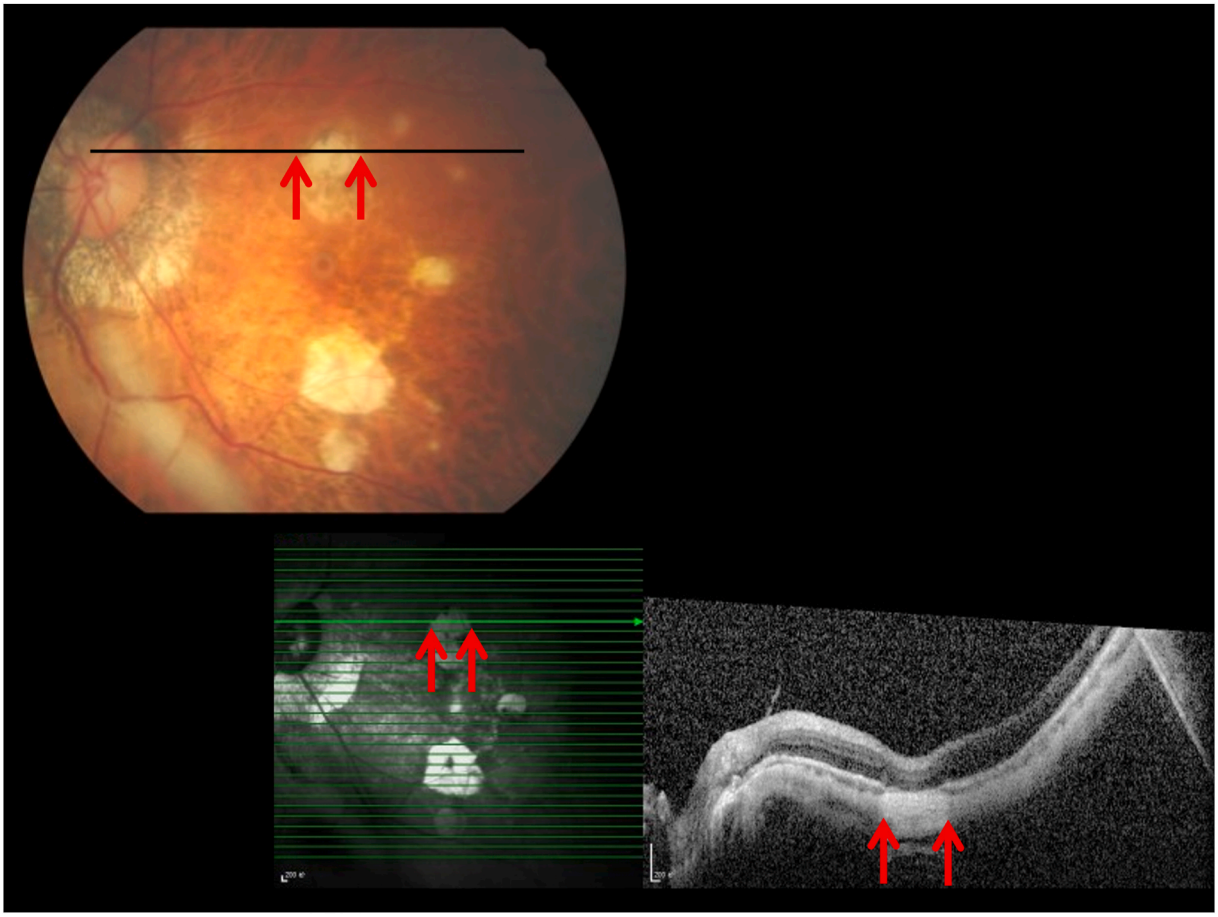

Fig. 5. Fundus photograph and optical coherence tomographic (OCT) image of the fundus of a highly myopic eye with a "patchy atrophy" (category 3 of myopic maculopathy); red arrows: end of retinal pigment epithelium layer and Bruch's membrane, indicating a defect in both layers.

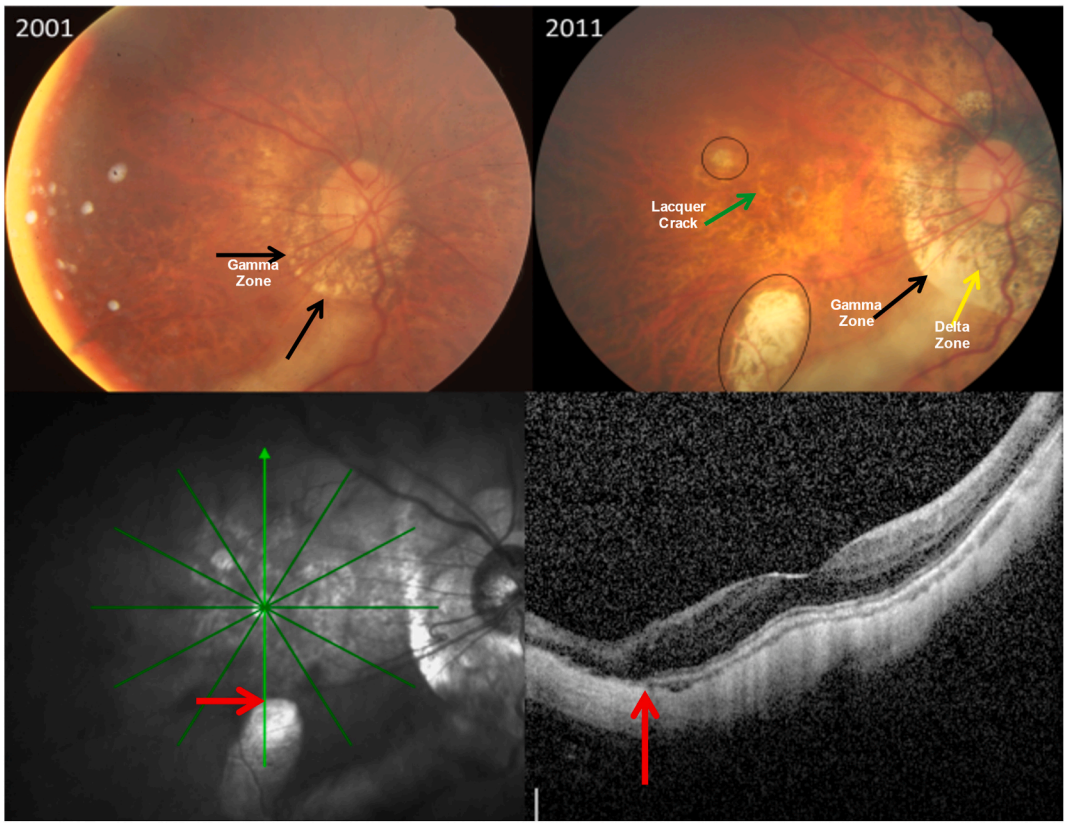

Fig. 6. Fundus photograph and optical coherence tomographic (OCT) image of the fundus of a highly myopic eye in 2001 (upper left image) and in 2011 (upper right eye), after having developed lacquer cracks (green arrow) and extrafoveal patchy atrophies (black ovals), in association with an enlarging parapapillary gamma zone and developing delta zone; the OCT images, taken in 2011, show a Bruch's membrane defect corresponding to the patchy atrophy.

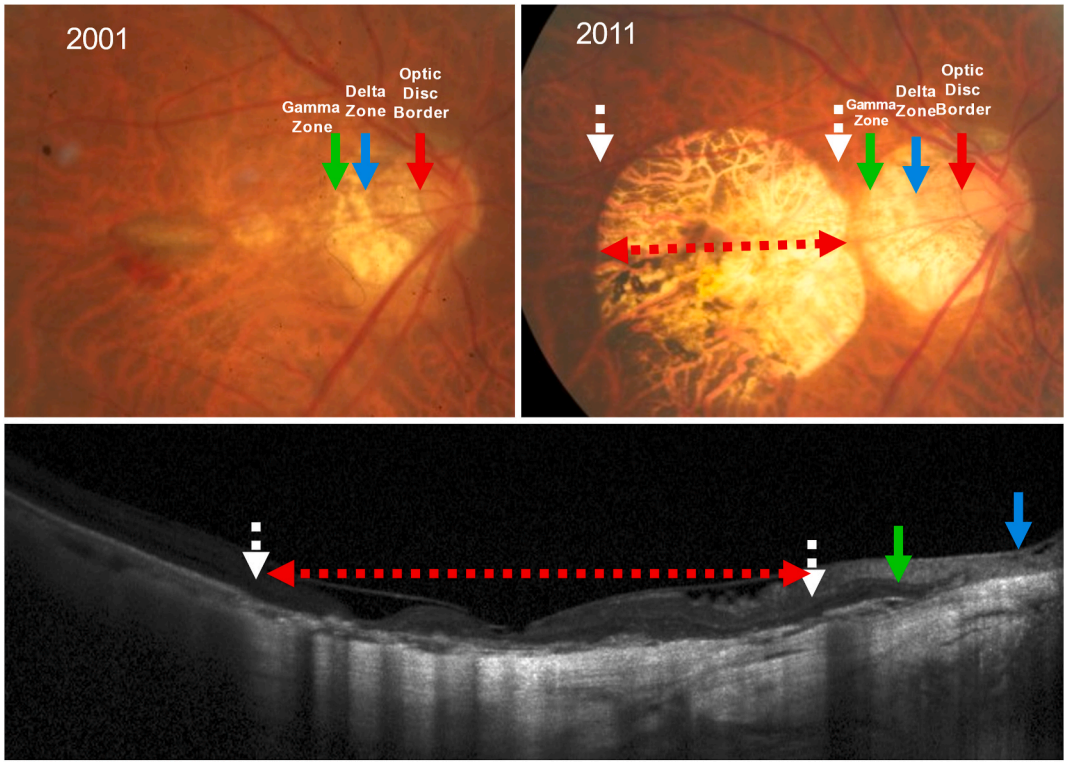

Fig. 7. Fundus photograph and optical coherence tomographic (OCT) image of the fundus of a highly myopic eye, having developed a fovea "patchy atrophy" (category 4 of myopic maculopathy) in 2011 (right upper image) out myopic macular of a macular neovascularization in 2001 (left upper image); Note: enlarging parapapillary gamma zone and delta zone.

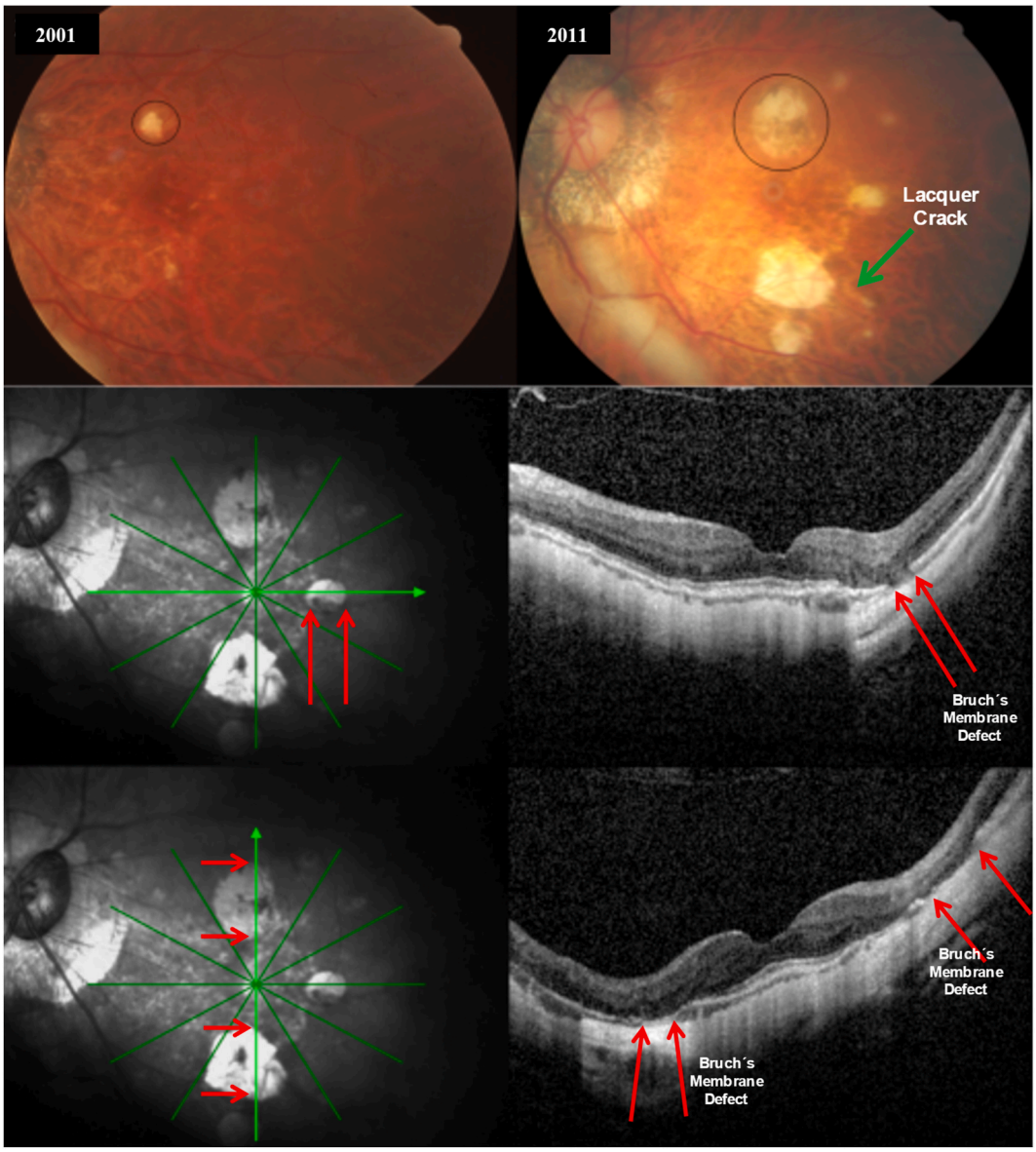

Fig. 8. Fundus photograph and optical coherence tomographic (OCT) image of the fundus of a highly myopic eye in 2001 (upper left image) and in 2011 (upper right eye), after having developed extrafoveal patchy atrophies; the OCT images, taken in 2011, show Bruch's membrane defects corresponding to the patchy atrophies; green arrow: lacquer crack.

to the macular patchy atrophies as the main element of the definition of stage (category) 3 of myopic maculopathy (Ohno-Matsui et al., 2015). The histology of the macular BM defects with the lack of RPE cells and photoreceptors implies that they correspond to an absolute scotoma in the visual field. Future studies are encouraged to explore whether BM defects without myopic macular neovascularization differ from those with myopic macular neovascularization (Xie et al., 2021).

It may be considered that, as described by Spaide and others, macular BM defects can occur also in non–highly myopic eyes, such as in patients with Stargardt's disease or in eyes with pseudoxanthoma elasticum and peripapillary atrophy (Park et al., 2012; Spaide and Jonas, 2015).

5. Retinal pigment epithelium (RPE)

The RPE forms a monolayer of hexagonally arranged cells, which are most dense in the foveal region. In a morphometric study on enucleated normal human donor eyes, the total number of RPE cells was 3,556,000 ± 491,000 (range: 2,130,500–4,653,200 (Panda-Jonas et al., 1996). The total RPE cell count increased along with a higher number of rods and cones, a larger total retinal surface area, and a larger optic disc area. The RPE cell density decreased from the fovea (4200 ± 730 cells/mm^2) to the mid-periphery (3000 ± 460 cells/mm^2) and to the outer peripheral fundus regions (1600 ± 411 cells/mm^2). In the retinal periphery, the RPE cell density was highest in the nasal fundus region compared with any other fundus quadrant. The RPE cell density decreased by about 0.3% per year with increasing age.

In recent histomorphometric studies of human eyes, the RPE cell density in the equatorial region and at the posterior pole/equator midpoint decreased with longer axial length, while it was less significantly or not at all associated with axial length at the ora serrata and at the posterior pole (Bai et al., 2017; Jonas, JB et al., 2017c, 2020b). In a similar manner, the RPE cell density in eyes of guinea pigs with lens-induced axial elongation decreased with longer axial length at the posterior pole/equator midpoint (and at the posterior pole) (Deng et al., 2019). In human eyes, the RPE cell density correlated with the density of the photoreceptors. Both parameters, measured in the retro-equatorial region (posterior pole/equator midpoint) and equatorial region,

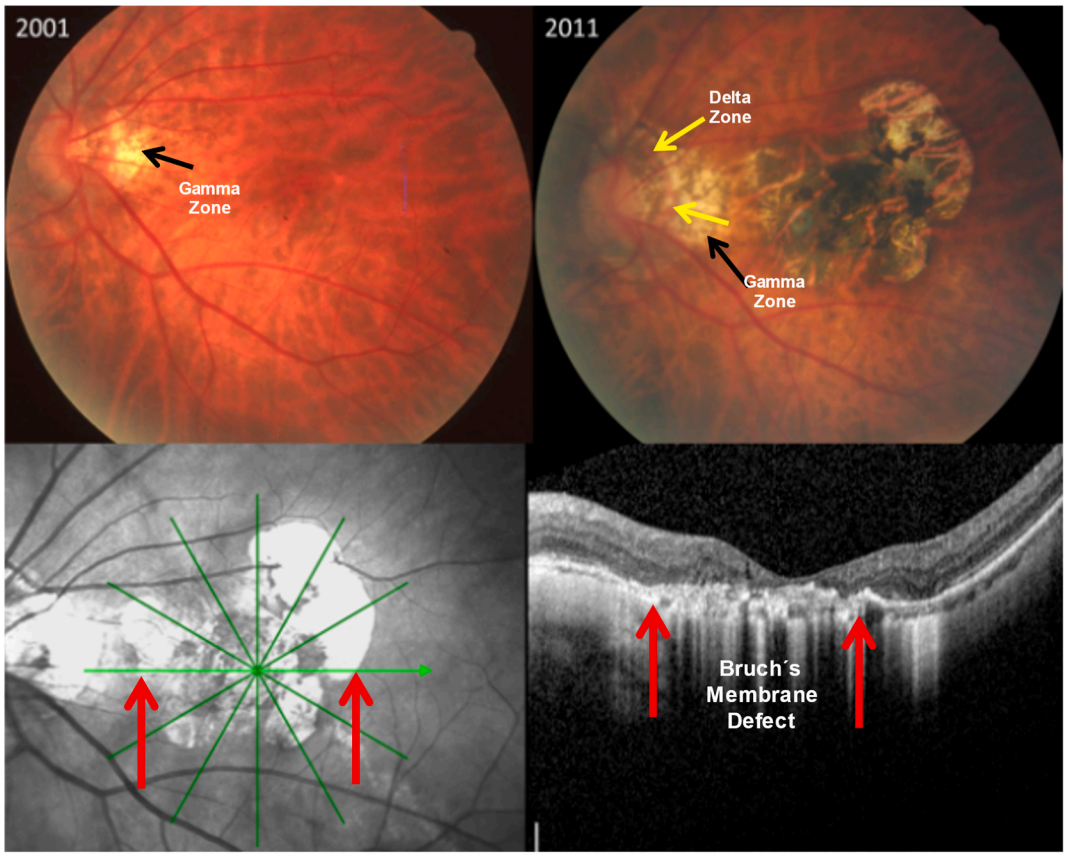

Fig. 9. Fundus photograph and optical coherence tomographic (OCT) image of the fundus of a highly myopic eye in 2001 (upper left image) and in 2011 (upper right eye), after having developed a foveal patchy atrophy; the OCT images, taken in 2011, show Bruch's membrane defects and central retinal pigment epithelium proliferations in the foveal region.

decreased with longer axial length and longer retinal length (Bai et al., 2017; Jonas, JB et al., 2017c; own unpublished data). Assuming a postnatal constancy in the number of RPE cells, the decrease in the RPE cell density found predominantly in the retro-equatorial region (posterior pole/equator midpoint) and equatorial region fits with the notion of an axial elongation-related regional enlargement of BM in the retro-equatorial and equatorial region (Jonas, JB et al., 2017b).

5.1. Secondary RPE defects

Highly myopic eyes with stage (category) 3 or 4 of myopic maculopathy show so-called patchy atrophies in their macular region. Upon OCT-based histology and as examined histologically by light microscopy, these patchy atrophies correspond to round RPE defects, a substantial proportion of which additionally show a BM defect in their centers (Jonas, JB et al., 2013a; Ohno-Matsui et al., 2016b; own unpublished data). The RPE defects with central BM defects are larger than the RPE defects without additional central BM defects. All macular BM defects have a defect in the overlying RPE layer. In the follow-up, RPE defects without central BM defect can enlarge and develop a central BM defect (Ohno-Matsui et al., 2016b).

These observations suggest that both forms—RPE defects without or with central BM defects—belong to the same entity and that the larger RPE defects with central BM defects represent a more advanced stage (own unpublished data). It may imply that an RPE defect is initially developed in patchy atrophies, followed by a central BM defect, while the RPE defect enlarges concurrently. One may suggest that an axial elongation-associated stretching effect is the etiological basis for both phenomena. Considering that the RPE basal membrane is much thinner than the BM, the RPE basal membrane (and the RPE cell layer), relative to the BM, may be biomechanically weaker and rupture first.

The first stage of an RPE rupture may be a lacquer crack, which OCT-based histology reveals is characterized by an increased transmission of light into the choroidal and scleral space in association with an RPE lesion. Corresponding linear BM defects are not typically detected in these regions (Xu et al., 2019b). If an axial elongation–induced rupture of the RPE occurs, first in the shape of a lacquer crack and later widening into a round defect (i.e., a patchy atrophy), one may wonder whether the RPE cells in the RPE defect region became lost or whether the RPE sheet developed a small opening and slipped away during the enlargement of the opening. The notion of a slippage of the RPE is supported by observations obtained in eyes with age-related macular degeneration in which prominent detachments of the RPE can be found. These RPE detachments may be detachments of the RPE basal membrane from the underlying BM (consisting of a collagenous, elastic, and collagenous layer). A detachment of the RPE cells from their basal membrane, with the latter then still resting on BM, may be unlikely, since the RPE cells, like other cells of ectodermal origin, are firmly attached to their basal membranes. In addition, a sheet of RPE cells without their connecting basal membrane may get dissolved and transform into a cell suspension.

Another example of a temporary RPE detachment is the development of RPE rolls at the margin of the BM opening at the optic nerve head. These parapapillary RPE rolls occur in association with a marked rise in intraocular pressure (IOP) and decrease in height when the IOP normalizes again (Wang, YX et al., 2015a). Another example is the decrease in the height of some RPE detachments in the macular region when the IOP increases (Wang, YX et al., 2015b). These examples may serve to support the notion that the RPE, with its basal membrane, is not firmly connected to the main layers of BM and may be able to slide. If the notion of a sliding RPE is valid, an axial elongation–related increased

strain within the RPE layer in the posterior ocular segment in highly myopic eyes may first lead to an enlargement of the physiologic opening of the RPE layer in the optic nerve head canal region; in other words, to the development and enlargement of a parapapillary (myopic) beta zone characterized by the presence of BM and the absence of RPE in the parapapillary region. Such a myopic beta zone is typically found in myopic eyes and arises from an enlargement of the RPE opening of the optic nerve head canal. The development of such a myopic beta zone may occur parallel to, but independent of, the development of a parapapillary gamma zone.

While the etiology of a myopic beta zone may be due to the axial elongation–associated enlargement of the inner surface of the eye, the development of a gamma zone in moderately myopic eyes may be caused by a temporal shift of the BMO in relationship to the lamina cribrosa. Such a temporal BMO shift may be caused by an enlargement of BM in the mid-periphery of the fundus (see below for further details). If the axial elongation–related enlargement of the RPE opening of the optic nerve head canal (i.e., myopic beta zone) does not lead to a sufficient relaxation within the RPE cell layer (and its basal membrane), secondary defects in the macular RPE layer may develop, first in the form of linear defects (lacquer cracks). Therefore, the RPE defects in the macular region may not be due to a loss of RPE cells but, rather, due to the development of an initially small (linear) RPE defect (lacquer crack), which eventually widens to a patchy atrophy. Typically, the lacquer cracks are orientated in a perpendicular angle to the shortest optic disc diameter and to the maximal with of parapapillary gamma zone (Jonas JB et al., 2022a; Jonas RA et al., 2021a). The enlargement of lacquer cracks to patchy atrophies has been observed clinically (Xu, X et al., 2019b). Fitting with the notion of a sliding RPE is the observation that the defect in the overlying photoreceptor layer (outer nuclear layer) in the region of the BM defects is smaller than the RPE defect (own unpublished data). This finding corroborates the idea that the RPE layer can slip away beneath the photoreceptors, while the less mobile photoreceptors remain firmly connected to the inner retinal structures.

6. Retinal photoreceptor layer

Assuming a postnatal constancy in the photoreceptor count, regional differences in associations between the photoreceptor density and axial length can be used as surrogate for regional differences in the enlargement of the underlying tissue; namely, BM and the sclera. Assessing the photoreceptor density in anterior–posterior histological sections of enucleated human eyes revealed a decreased density along with longer axial and retinal length (measured from the ora serrata to the posterior pole). The axial length–related decrease in the photoreceptor density was most marked at the posterior pole/equator midpoint, followed by the equatorial region, and, finally, the region near the ora serrata (own unpublished data). In that study, the photoreceptor density at the posterior pole was not measured. The regional photoreceptor density was correlated with the regional RPE cell density. In a similar study, the thickness of the retina (measured as thickness of the inner and outer nuclear layers combined) at the equator and at the posterior pole/equator midpoint decreased with longer axial length (Jonas, JB et al., 2016a). These observations support the hypothesis of a regional enlargement of the underlying tissue—BM and the sclera—in the fundus mid-periphery during the process of axial elongation.

The retinal thickness (as measured by OCT) in the foveal center and in the parafoveal regions is not significantly associated with axial length or even slightly increases with longer axial length (Deng et al., 2019; Jonas, JB et al., 2016a). Correspondingly, the thickness of the photoreceptor layer in the fovea region is not related, or not markedly related, to axial length (Kim, TY et al., 2020). In the study population of the UK biobank, the combined thickness of the layers from the inner nuclear layer to the RPE increased with more hyperopic refractive error, after adjusting for younger age, male sex, non-Black ethnicity, no smoking, lower systolic blood pressure, higher intraocular pressure, and higher corneal hysteresis (Chua et al., 2019). The topic has been addressed in other studies (Dabir et al., 2015; Eckmann-Hansen et al., 2021; Mirhajianmoghadam et al., 2020; Trinh et al., 2022; Wang, Y et al., 2019; Woog and Legras, 2019). Applying adaptive optics scanning laser ophthalmoscopy, Wang and colleagues found that the foveal cone mosaic was expanded in eyes with longer eyes, but not in proportion to eye length (Wang, Y et al., 2019). Considering the optics of a myopic eye, eyes with longer axial length, compared with eyes with normal axial length, had a higher cone angular sampling density (measured in cones/deg^2) in and around the fovea, despite the decrease in the cone density (measured as cones/mm^2). Eckmann-Hansen et al. (2021), also applying adaptive optics scanning laser ophthalmoscopy, found a 9.7% decrease in absolute cone density for each mm increase in axial length, while the angular cone density showed a 0.84% decrease for each mm increase in axial length. These results could explain why best corrected visual acuity was independent of axial length (Shao et al., 2014).

If the macular BM does not enlarge in axial elongation (Jonas, JB et al., 2015), the question arises as to why the thickness of the outer nuclear layer (slightly) decreases in longer eyes. A possible explanation may be that the retina, fixed to the ora serrata, increases in surface area during axial elongation. This would impart strain on the retina, leading to a retinal thinning predominantly in the mid-periphery of the fundus—and presumably leading to a decrease in photoreceptor density in that region—while the effect of the retinal stretching in the macular region may be the smallest relative to other fundus regions. However, it would nonetheless lead to a slight but statistically significant decrease in ONL thickness in the macular region.

7. Retina

7.1. Retinal length

Axial myopia is characterized by an elongation of the sagittal diameter of the eye and, to a minor degree, by an enlargement of the ocular coronal diameters (Atchison et al., 2004; Cheng, HM et al., 1992; Guo, Y et al., 2017; Heine, 1899; Jonas, JB et al., 2017d; Logan et al., 2004; Matsumura et al., 2019; Meyer-Schwickerath et al., 1984). Longer axial length is associated with a longer retina as measured from the ora serrata to the posterior pole and, to a minor degree, it is related to a longer ciliary body. For each millimeter increase in sagittal globe diameter, the retinal length increases linearly by 0.73 mm (95%CI: 0.65–0.81), and the ciliary body length increases by 0.16 mm (95%CI: 0.12–0.20) (Panda-Jonas et al., 2022). Ciliary body length is nearly constant beyond an axial length of 30 mm. Correspondingly, axial elongation is mainly associated with an increase in the length of the vitreous body compartment.

The elongation of the retina in myopic eyes has clinical importance. The retina elongates by 4.3 mm, if the axial length increases from 24 mm in a roughly emmetropic eye to 30 mm in a highly myopic eye. This retinal lengthening primarily affects the retinal structures connecting the deeper retinal layers with the optic disc; these structures are the ILM and the retinal nerve fibers. Assuming that the axons of the retinal ganglion cells are not elastic, any lengthening of the retinal nerve fibers will lead to a mechanical strain, which could result in their damage and loss, and it would result in a non-glaucomatous optic neuropathy. This assumption agrees with clinical findings that high axial myopia can be associated with a non-glaucomatous optic nerve damage (Bikbov et al., 2020). If one assumed that myopic enlargement did not differ between the equatorial region, the mid-peripheral region, and the central region at the posterior pole, the lengthening of the retinal nerve fibers would increase with the distance to the optic disc. In that case, retinal nerve fibers originating in the retinal periphery would be lengthened most. As discussed above, however, axial elongation is associated predominantly with an enlargement of the eye wall in the retro-equatorial and equatorial regions. In that case, all axons of the retinal ganglion cells located within or anteriorly to that region will be lengthened and stretched,

while the axons of the retinal ganglion cells located centrally to that location will be less affected. These assumptions fit with the clinical observation of a concentric constriction of the visual field in highly myopic eyes (Fledelius et al., 2019).

Other than the retinal nerve fibers, the ILM is the other structure directly extending from the retina to the optic disc. Any elongation of the retina will lead to an elongation of the ILM. Since the ILM, as a basal membrane (similar to the lens capsule or BM), is not elastic but stiff, an elongation of the ILM will increase its strain (Wang, X et al., 2018). Particularly in eyes with a posterior staphyloma in which the distance to the optic disc has locally further enlarged, the ILM stretch may lead to an intraretinal detachment of the ILM, similar to a washing-line phenomenon. Such a washing-line phenomenon could cause a secondary splitting of the retina, into an inner part clinging to the ILM, and an outer part with the retinal photoreceptors firmly connected to the RPE and BM. It could explain the development of a myopic macular retinoschisis.

Other than affecting the ILM and retinal nerve fiber layer, the increase in the distance to the optic disc also affects all other retinal layers, since the local enlargement of their underground (i.e., BM) leads to a decrease in their density (Fig. 10). This notion is based on the assumption that the retinal cells do not undergo mitosis in adolescence or later, and that axial elongation leads to an enlargement of the inner surface of BM in that region. A decreased photoreceptor cell density may directly cause a reduction in spatial resolution and, in association with a decreased density of the cells of the inner nuclear layer and retinal ganglion cell layer, an enlargement of receptive fields. Correspondingly, clinical studies have revealed that at peripheral retinal loci, resolution acuity declined linearly with the magnitude of myopic refractive error (Chui et al., 2005). Relative to emmetropic eyes, eyes with a myopic refractive error of −15 diopters had twice as much spacing between retinal receptive units and, thus, 50% of the peripheral resolution acuity (Chui et al., 2005).

7.2. Fovea–optic disc distance

The fovea–optic disc distance increases with longer axial length due to the development and enlargement of a temporal gamma zone (Jonas RA et al., 2015a) (Fig. 10). Since the distance between the superior and inferior temporal vascular arcade is independent of axial length, the angle between the temporal vascular arcade decreases with longer axial length (Jonas RA et al., 2015b, 2018a). What results is a crowding of the retinal nerve fiber layer in the temporal region of the optic nerve head and, correspondingly, to a relative thinning of the retinal nerve fiber layer in the other regions (Jonas, JB et al., 2022b; Jonas RA et al., 2015b; Zhang, Q et al., 2021). In particular, the locations of the peaks of the retinal nerve fiber layer thickness profiles move in the direction of the temporal position (Zhang, Q et al., 2021). These changes in the retinal nerve fiber layer thickness profile, occurring in association with the axial elongation–associated decrease in angle kappa, must be taken into account when diagnosing an optic nerve damage, based on the peripapillary retinal nerve fiber layer thickness profile.

The increase in the fovea–optic disc distance leads to an elongation, and potentially stretching, of the retinal nerve fibers running in the papillo-macular bundle (Jonas, RA et al., 2021b), which could lead to non-glaucomatous optic nerve damage. This might explain the occurrence of paracentral scotomas in highly myopic eyes in which the macular morphology cannot explain the etiology of paracentral scotomas (Bikbov et al., 2020). Retinal nerve fibers, which run primarily in an arcuate manner from their retinal ganglion cells to the optic disc, may compensate for the increased distance to the optic disc by taking a straighter course. Correspondingly, retinal vessels take a straighter course towards the optic disc in highly myopic eyes with progressive myopization (Jonas, RA et al., 2021b).

7.3. Cobblestones

So-called “cobblestones”, or retinal cobble stone degeneration, develop in the equatorial and pre-equatorial region of axially elongated eyes (Grossniklaus and Green, 1992). In a recent histomorphometric study on human enucleated globes, BM thickness and thickness and density of the choriocapillaris were significantly lower in the cobblestone region than in the area just beyond the cobblestone region, or in corresponding regions of eyes without cobblestones (Jonas, SB et al., 2022). The cobblestone regions were characterized by an apparently firm adhesion between a disorganized retina and a thinned and intact BM, an abrupt termination of the normally-appearing RPE layer at the cobblestone border, some islands of RPE cells within the cobblestone region and, except for the RPE islands, an absence of intraretinal or subretinal RPE proliferations and absence of regional scleral thinning. Interestingly, BM within the cobblestone regions, except for the areas of the RPE islands, appeared mostly to be monolayered, in contrast to its double-layered appearance beyond the cobblestone region. The inner layer of BM terminated in the border region of the cobblestone region, and it was absent within the cobblestone regions, except for the areas with RPE islands (Jonas, SB et al., 2022).

The etiology of cobblestones in myopic eyes has remained elusive to date. Grossniklaus discussed a relationship between mechanical stretching and a vascular compromise of the pathologically myopic eye and the development of choroidal ischemic atrophy of the RPE and overlying retina (Grossniklaus and Green, 1992). In a study applying

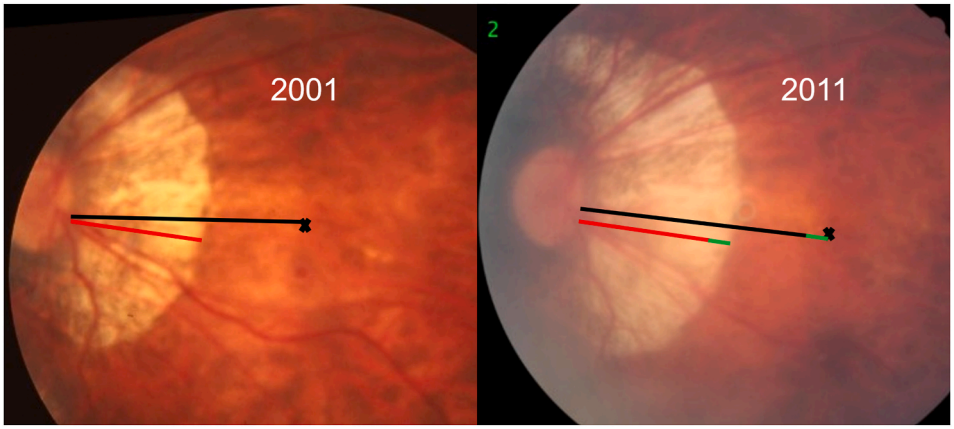

Fig. 10. Fundus photograph of the fundus of a highly myopic eye in 2001 (upper left image) and in 2011 (upper right eye, showing the elongation of the optic disc–fovea distance (2011: black bar; 2011: black bar + green bar [elongation from 2001 to 2011]), and the widening of the parapapillary gamma zone by the same amount (2001: red bar; 2011: red bar + green bar [elongation]).

OCT imaging of peripheral retinal lesions, Ghazi and colleagues described an enucleated and formalin-fixed eye with a cobblestone (paving stone) degeneration, which upon OCT examination showed an abnormally high reflectivity at the level of the BM line, while the equivalent histological image demonstrated, as in the histomorphometric study cited above, an absence of RPE, an outer retinal layer, and choriocapillaris (Ghazi et al., 2006). In the cobblestone region, the OCT did not show cystoid spaces, which are otherwise typical for a peripheral retinal cystoid degeneration with Blessig–Iwanoff cystoid spaces. Ghazi and colleagues considered that the hyperreflectivity seen on the OCT image may have resulted from increased signal transmission caused by the RPE cell loss, with backscattering from the residual choroid and inner sclera.

Based on the histological and clinical observations concerning the morphology of cobblestones, it is possible that the axial elongation–associated enlargement of the inner ocular surface leads to a stretching and increased strain within the RPE layer at the posterior pole and in the periphery of the fundus, where the main enlargement of the ocular coats (e.g., BM) may occur. Such a strain within the RPE layer may lead to focal defects in the RPE layer in the form of cobblestones, explaining the absence of RPE and the inner BM layer in the cobblestone region with a secondary destruction of the photoreceptor cell layer and thinning of the choriocapillaris, while the middle and inner retinal layers, the layer of medium- and large-sized choroidal vessels, and the sclera were stretched, but not directly affected.

7.4. Tissue shift in association with axial elongation

In the population-based longitudinal Beijing Eye Study 2001/2011 with a follow-up of 10 years, a shift of large choroidal vessels in relationship to retinal vessels was observed in 47 (55%) out of 85 highly myopic eyes (Jonas, JB et al., 2021a). The shift occurred most often in the disc–fovea line and corresponded to the gamma zone enlargement in eyes with a parapapillary gamma zone without choroidal vessels. In eyes in which a gamma zone showed some large choroidal vessels, the choroidal shift was smaller than the enlargement of the gamma zone. In the region of a developing or enlarging diffuse chorio-retinal atrophy (stage [category] 2 of myopic maculopathy) or a macular patchy atrophy (stage [category] 3 or 4 of myopic maculopathy), the choroidal inter-vessel distance increased, suggesting a choroidal vessel shift or spreading in a direction perpendicular to the longest diameter of the lesion. In eyes with a macular BM defect with choroidal vessels, the inter-vessel distance in the choroidal large vessel layer did not change notably (Jonas, JB et al., 2021a). The finding of a decrease in the large choroidal vessel density (i.e., an increase in the choroidal inter-vessel distance) confirms a previous report by Moryama and colleagues, who also observed a decrease in the number of large vessels in the choroid (Moriyama et al., 2007).

The changes in the position of the large choroidal vessels occurring in association with an enlargement of a parapapillary gamma zone may be explained by a shift of BMO into the temporal direction in axially elongating eyes (Figs. 10–12). The BMO shift leads to an overhanging of BM into the intrapapillary compartment at the nasal disc border, and to a compensatory lack of BM (i.e., gamma zone) in the temporal parapapillary region (Jonas, JB et al., 2017b; Reis et al., 2012; Zhang, Q et al., 2019). Since the large choroidal vessels are not connected to the underlying sclera—except for the few vortex veins in the equatorial region and for the short ciliary arteries in the peripapillary region—one may infer that the large choroidal vessels can shift on the sclera in a relatively unrestricted manner. The large and medium-sized choroidal vessels are connected with the choriocapillaris, which is firmly attached to BM through its basal membrane. It is possible that any shift in BM will lead to a similar shift of the choriocapillaris, and more or less to a similar shift of the large choroidal vessels. Since the retinal vessels are connected to the optic nerve head and become even slightly stretched by the gamma zone–associated elongation of the disc–fovea distance, their gamma zone enlargement–associated shift is limited (Jonas RA et al., 2021b; Kim, TW et al., 2012). Such a discrepancy in retinal vessel shift and choroidal vessel shift can lead to a change in the relative position of the retinal vessel-based landmarks compared with the position of large

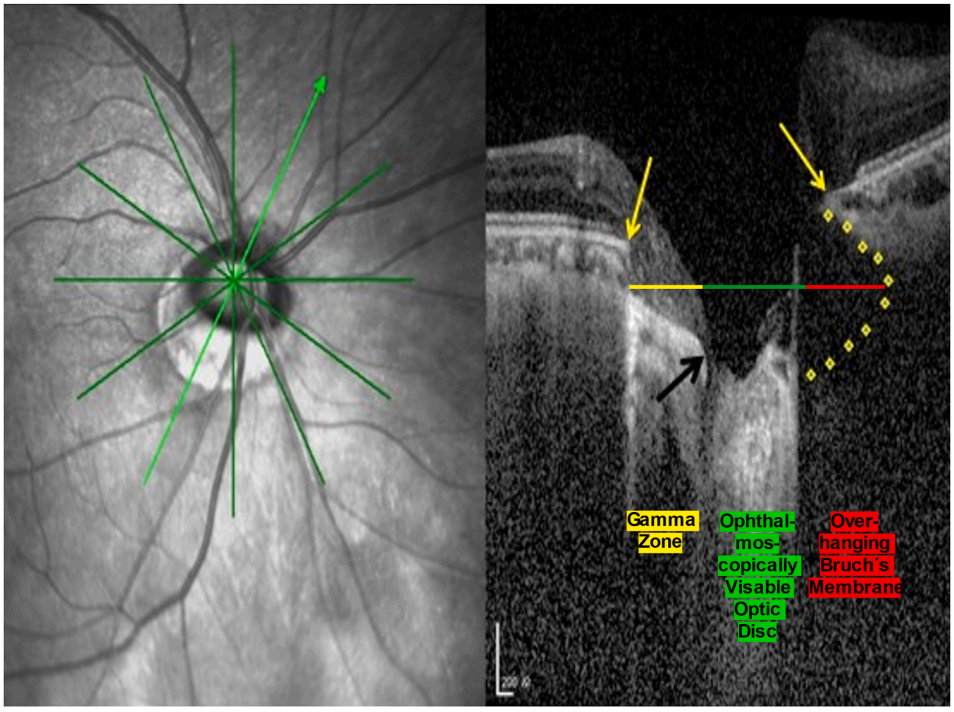

Fig. 11. Optical coherent tomographic image of the optic nerve head of a moderately myopic eye, showing the overhanging of Bruch's membrane into the intrapapillary compartment on one side of the optic disc and the corresponding absence of Bruch's membrane at the opposite side of the optic disc (gamma zone), leading to a reduction in the ophthalmoscopically visible optic disc.

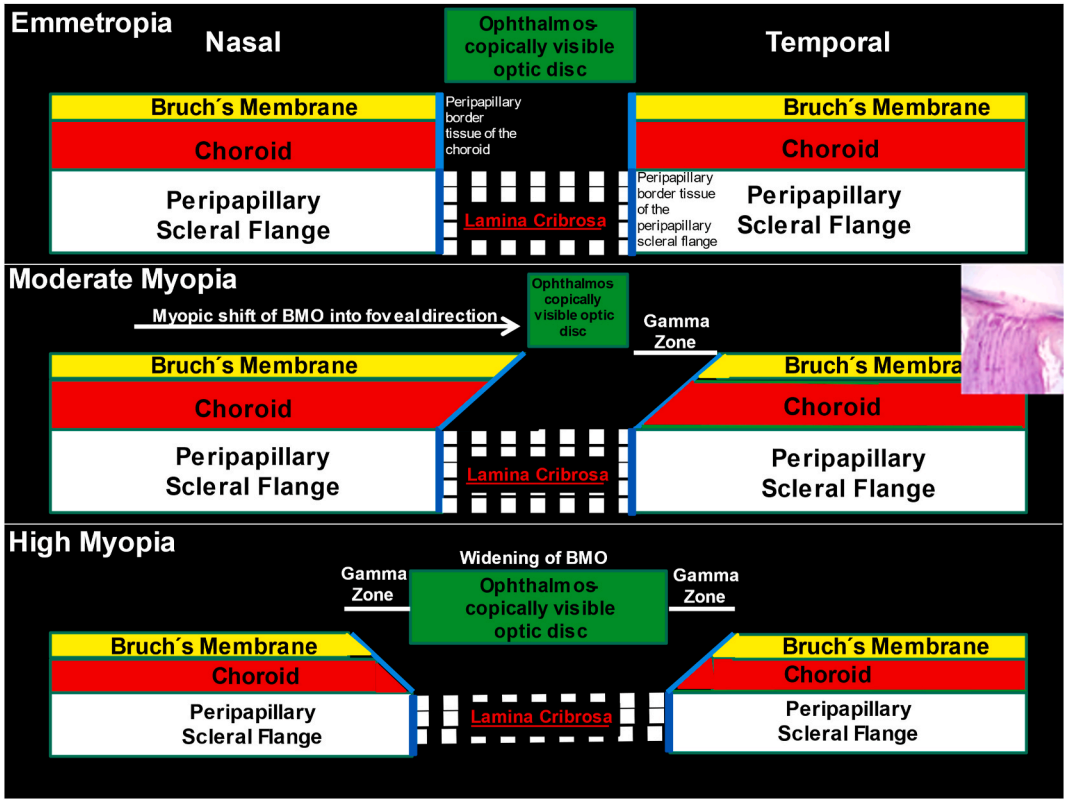

Fig. 12. Schematic of the spatial relationships between the Bruch's membrane opening, the choroidal opening, and the peripapillary scleral flange opening (lamina cribrosa) in moderate myopia and high myopia.

choroidal vessel–associated landmarks.

An additional factor influencing the axial elongation-related choroidal shift may be that the large choroidal vessels are fed by, and are connected with, the short posterior ciliary arteries which penetrate the sclera in the peripapillary region. The finding that the choroidal vessel shift was less pronounced in eyes showing large choroidal vessels in their gamma zone may suggest that in these eyes, the peripapillary ciliary artery system prevented a full shift of the large choroidal vessel layer. A partial immobility of the peripapillary choroidal vessels suggests that in some highly myopic eyes with an enlarging gamma zone, a strain within the large choroidal vessel layer may develop due to a BM-associated shifting of the choriocapillaris, while the peripapillary ciliary arteries prevent a full shift of the large choroidal vessels. It may also suggest that within the retinal layers, a strain develops between the inner retinal layers with the retinal vessels and the retinal nerve fibers both connected with the optic disc, and the deep retinal layers with the retinal photoreceptors firmly connected to the RPE and indirectly to the shifting BM.

Independently of the gamma zone enlargement, a shifting of the large choroidal vessels was also observed in regions with a developing or enlarging diffuse choroidal atrophy and in macular BM defects. If macular BM defects develop and enlarge, the choriocapillaris firmly connected with the shifting BM moves, together with BM, while the large choroidal vessels only loosely connected with the choriocapillaris may partially remain in the center of the BM defect. Since the inner retinal layer covering a BM defect may also partially shift, the spatial relationship between retinal vessel landmarks and choroidal vessel landmarks may change.

8. Optic nerve head

The optic nerve head consists of the optic nerve head canal (intrapapillary region) with the lamina cribrosa as its basis, and the parapapillary region. The latter includes alpha zone (irregular pigmentation due to RPE irregularities and peripheral location), beta zone (complete RPE loss with BM being present), gamma zone (absence of BM [and thus absence of RPE]), and delta zone (elongated and thinned peripapillary scleral flange) within the gamma zone and located at the optic disc border) (Burgoyne et al., 2005; Jonas, JB et al., 1999, 2017e,f; Wang, YX et al. 2020; 2021). The optic nerve head canal consists of the (1) opening in the retina (retinal ganglion cell layer opening, inner plexiform layer opening, inner nuclear layer opening, outer plexiform layer opening, and outer nuclear layer opening, with each of these layers closed against the intrapapillary compartment by the intrapapillary retinal ganglion cell axons [or retinal nerve fibers]); (2) RPE layer opening; (3) BMO; (4) opening in the choroid, sealed against the intrapapillary compartment by the peripapillary border tissue of the choroid; and (5) opening in the peripapillary scleral flange, covered by the lamina cribrosa (Zhang, Q et al., 2019; Wang YX et al., 2021).

8.1. Optic disc size

The optic disc may be defined as the ophthalmoscopically visible region having the lamina cribrosa as its bottom (uncovered or covered by neuroretinal rim) (Jonas, JB et al., 2017f; Wang, YX et al., 2021). If the BMO is fully aligned to the lamina cribrosa, the BMO size fits with the size of the lamina cribrosa and, thus, represents the optic disc size. In the case of a misalignment of the BMO in relationship to the lamina cribrosa (e.g., in the case of an overhanging of BM into the intrapapillary compartment), the optic disc size is smaller than the BMO size, since the optic disc is the equivalent of the area common to both the BMO and the lamina cribrosa (Araie et al., 2017; Reis et al., 2012; Strouthidis et al., 2009, 2010; Wang, YX et al., 2021; Zhang, Q et al., 2019). Besides a pronounced inter-individual variability of about 1:7 in non-highly myopic eyes of Caucasians (Jonas et al., 1988a; Papastathopoulos et al., 1995; Ramrattan et al., 1999; Sanfilippo et al., 2009; Varma et al.,

1994), the size of the optic disc depends on ethnic background (Wang, YX et al., 2021). The optic disc is largest in populations from Sub-Saharan Africa, followed by South Asians, Chinese and, eventually, European-descended individuals (Chi et al., 1989; Tsai et al., 1995; Varma et al., 1994; Wang, YX et al., 2021). Among individuals of European descent, disc size is not associated with iris color (Budde et al., 1998).

Disc size depends on the refractive error, showing a curvilinear relationship (Jonas, JB et al., 1999; Jonas, JB and Budde, 2000). The optic disc size is small in marked hyperopia and increases towards emmetropia. From emmetropia towards moderate myopia, the disc size tends to decrease, mainly from increasing misalignment between the BMO and the lamina cribrosa, such that the optic disc area in common between the BMO area and lamina cribrosa area decreases (Reis et al., 2012; Zhang, Q et al., 2019). In high myopia, further axial elongation leads to an enlargement of the BMO, and any part of BM previously overhanging into the intrapapillary compartment in moderate myopia is withdrawn to the parapapillary region (Jonas, JB et al., 2003, 2004; Lee, S et al., 2014; Sung et al., 2019; Zhang, Q et al., 2019). The withdrawal of the intrapapillary overhanging part of BM leads to an uncovering of the region having the lamina cribrosa (with or without neuroretinal rim) as its bottom; consequently, that region becomes fully assessable upon ophthalmoscopy. In addition, the lamina cribrosa area enlarges with longer axial length in highly myopic eyes. Therefore, optic disc enlargement in highly myopic eyes is due to two mechanisms: the axial elongation–associated enlargement of the BMO, uncovering the lamina cribrosa region, and an enlargement of the lamina cribrosa itself. The enlargement of the BMO and lamina cribrosa starts mainly at a cut-off value of approximately −8 diopters or an axial length of about 26.5 mm (Xu, L et al., 2007a, 2010; Zhang, Q et al., 2019).

The optic disc enlargement in high myopia leads to secondary (or acquired) macrodiscs, which can be differentiated from primary macrodiscs. While the size of primary macrodiscs is independent of age, refractive error, and axial length from early adulthood onwards, the size of secondary macrodiscs enlarges with further axial elongation (Jonas, JB et al., 1988a,b; Liu, HH et al., 2010a; Xu, L et al., 2007b, 2010). Since the latter depends on age, the size of secondary macrodiscs is indirectly associated with older age. While primary macrodiscs are associated with larger and flatter corneas and a higher prevalence of cilioretinal arteries, congenital optic nerve head pits and "Morning glory syndrome", secondary macrodiscs in highly myopic eyes do not show such associations (Jonas, JB and Königsreuther, 1994; Jonas, JB and Naumann, 1987; Jonas, JB et al., 1989a). The secondary macrodiscs can be differentiated into secondary macrodiscs in eyes with primary high myopia, and into secondary macrodiscs in eyes with secondary high myopia due to congenital glaucoma. In both, a larger optic disc is correlated with longer axial length (Jonas, JB and Dichtl, 1997; Jonas, JB et al., 1988c).

The association of high myopia with secondary macrodiscs has clinical significance (Dichtl et al., 1998). A larger optic disc size is related to a lower prevalence of optic disc drusen and non-arteritic anterior ischemic optic neuropathy, both conditions leading to non-glaucomatous optic nerve damage. Correspondingly, high myopia is a protective factor against both conditions. In histomorphometric studies, a larger optic disc size in non–highly myopic eyes correlated with a larger retinal surface area and a higher count of photoreceptors, RPE cells, and optic nerve fibers (Panda-Jonas et al., 1994, 1996; Wang, YX et al., 2021). While in highly myopic eyes, the axial elongation–associated increase in the optic disc size may correlate with the axial elongation–related increase in the retinal surface area, the size of secondary macrodiscs in highly myopic eyes may not correlate with the count of photoreceptors, RPE cells, and optic nerve fibers, under the condition that the retinal cells have no postnatal mitotic activity.

8.2. Optic disc shape

Defining the optic disc as the ophthalmoscopically visible part of the lamina cribrosa (uncovered or covered by neuroretinal rim), the optic disc shape depends on the shape of the lamina cribrosa and on the spatial relationship between the lamina cribrosa and the BMO. In a postmortem study on 107 freshly enucleated, unfixed, human donor eyes, the mean ratio of the minimal to maximal lamina cribrosa diameter was 0.86 ± 0.11, indicating a slightly oval, nearly circular shape (Jonas, JB et al., 1988c). A similar result was obtained when the optic disc shape was measured upon ophthalmoscopy, i.e., on fundus photographs (Jonas, JB et al., 1988a).

In moderately myopic eyes, the optic disc shape is often configurated in a vertical oval and is more obliquely oriented; in other words, the maximal disc diameter, often forming a rectangular angle with the optic disc–fovea line, is slightly rotated along the z-axis towards the temporal side (i.e., the superior disc pole is rotated towards the fovea) (How et al., 2009; Jonas, JB et al., 1988c, 1999; Rezapour et al., 2022a; Tay et al., 2005; Wang, YX et al., 2021; Xu, L et al., 2007b; You et al., 2008). The vertical ovalization of the disc shape increases during myopization in adolescence, simultaneously showing a shortening of the horizontal disc diameter, while the vertical disc diameter remains mostly unchanged (Guo, Y et al., 2015, 2018a; Hwang et al., 2012; Jonas, JB et al., 2022c; Nakazawa et al., 2008; Kim, TW et al., 2012; Samarawickrama et al., 2011; Yoon et al., 2019). Upon OCT-based histology, eyes with a vertical oval disc show an overhanging of BM into the intrapapillary compartment in the nasal superior region and, correspondingly, a parapapillary gamma zone in the temporal inferior region (Jonas, JB et al., 2017b; Reis et al., 2012; Zhang, Q et al., 2019).

In highly myopic eyes, the optic disc shape varies markedly between individuals, and can assume a markedly oval shape, with an oblique orientation of the maximal disc diameter. Since these eyes show a circular parapapillary gamma zone, indicating the absence of BM around the optic disc, an overhanging of BM into the intrapapillary compartment can no longer explain the vertical disc shape. Potentially, additional forces may influence the disc shape in highly myopic eyes. According to studies performed by Demer, Girard, and others, the optic nerve may become too short in markedly elongated eyes to allow a full adduction of these eyes (Chang et al., 2017; Demer, 2016; Wang et al., 2016a, b, 2017, 2018, 2021). If the optic nerve becomes too short, it leads to a backward pull—likely through the optic nerve dura mater—on the insertion of the optic nerve dura mater at the posterior sclera. That insertion line is the peripheral end of the peripapillary scleral flange, which, through the peripapillary border tissue of the peripapillary scleral flange, is connected with the lamina cribrosa.

Taking into account the orbital origin of the optic nerve in the nasal superior region of the orbit, one may infer that in adduction, the temporal and temporal inferior border of the optic nerve head (i.e., the end of the peripapillary scleral flange and, indirectly, the temporal border of the optic disc) is drawn backward. This could lead to a rotation of the optic disc around a line oriented perpendicularly to the direction of action of the optic nerve. With the optic nerve coming from the nasal superior region of the orbit, that line, with its 12 o'clock position, would be rotated towards the macula. Fitting with that notion, the maximal optic disc diameter in highly myopic eyes is often sagittally rotated with the superior disc pole towards the macula. Additionally, the potential backward pull of the optic nerve dura mater in highly myopic eyes may lead to the development of peripapillary suprachoroidal cavitations, as described below (Dai et al., 2015a; Jonas, JB et al., 2016a; Toranzo et al., 2005; You et al., 2013).

Aligning with the observations made about the relationship between length of the optic nerve and reduction of adduction of highly myopic eyes, Wang and colleagues reported that the optic nerve tortuosity in primary gaze, adduction, and in abduction was significantly lower in highly myopic eyes compared with non–highly myopic eyes (Wang, X et al., 2021). The authors suggested that eyes that would later become highly myopic were exposed to higher optic nerve traction forces during eye movements before the onset of myopia. In non–highly myopic eyes, the potential backward pull by the optic nerve dura mater may not play

a major role—at least, it may not lead to a change in the optic disc shape (Shang et al., 2019a).

Some moderately myopic eyes can have so-called "tilted discs", which are small optic discs, the maximal diameter of which is orientated horizontally, and which often show an inferior "crescent" or gamma zone (Cohen et al., 2022; How et al., 2009; Kim, MJ et al., 2014; Park, HY et al., 2015; Rebolleda et al., 2016; You et al., 2008). In contrast to its name as a tilted disc—and which may render this term a misnomer—these discs show a marked overhanging of BM into the intrapapillary compartment at the superior disc region and, correspondingly, an absence of BM (gamma zone) in the inferior parapapillary region. The BMO shift into inferior direction explains the horizontal shape of the optic disc as the ophthalmoscopically visible part of the optic nerve canal. "Tilted" discs may, therefore, not truly be tilted; rather, they may have a vertical misalignment of BMO in relationship to the lamina cribrosa. It remains to be discussed why in these eyes BM is overhanging at the superior region, in contrast to the nasal region as in eyes with a vertical oval disc shape.

Interestingly, eyes with "tilted discs" have a fovea that is located relatively inferiorly. This fact aligns with the hypothesis that, in these eyes, a movement of BM occurred in the inferior direction, leading to BM overhanging at the superior disc pole, to an inferior gamma zone, and to an inferior location of the fovea (Jonas, RA et al., 2021c). It should also be considered that the optic disc shape, as it appears upon ophthalmoscopy, can undergo a perspective distortion, due to the location of the optic disc nasally to the fovea (Dai et al., 2015b). The effect of a perspective distortion of the ophthalmoscopical optic disc image is, however, too small to sufficiently explain the vertical optic disc shape in myopic eyes.

8.3. Neuroretinal rim shape

Independent of axial length, the neuroretinal rim shape usually follows the inferior-superior-nasal-temporal (ISNT) rule (Jonas, JB et al., 1988a). This rule indicates that the neuroretinal rim is usually wider at the inferior disc pole, followed by the superior disc pole, the nasal disc region and, finally, the temporal disc area. As in non-myopic eyes, the rim can also be wider superiorly rather than inferiorly in many myopic eyes; whereas, in almost all eyes, the rim is most narrow in the temporal disc region. With neuroretinal rim shape and the ISNT rule being major parameters in the morphological diagnosis of glaucomatous optic nerve damage, it is clinically important that the rim shape in highly myopic eyes also usually follows the ISNT rule.

In highly myopic eyes, the enlargement and stretching of the lamina cribrosa (and optic disc) is associated with a flattening of the optic cup, as assessed upon ophthalmoscopy (Jonas, JB and Dichtl, 1997; Xu, L et al., 2007b). Such enlargement and stretching render the delineation of the optic cup from the neuroretinal rim more difficult, particularly in highly myopic eyes with glaucomatous optic nerve damage, since the depth of the glaucomatous optic cup is markedly flatter in highly myopic eyes than in non–highly myopic eyes with glaucoma (Chang and Singh, 2013; Jonas, JB and Dichtl, 1997; Tan et al., 2019; Xu, L et al., 2007b).

Highly myopic eyes can show, besides glaucomatous damage of the optic nerve, a non-glaucomatous optic neuropathy (Bikbov et al., 2020). Since non-glaucomatous optic nerve damage does not markedly change the shape and size of the neuroretinal rim, its detection in highly myopic eyes can be particularly difficult. Clues as to the presence and severity of a non-glaucomatous optic nerve damage in highly myopic eyes can be a marked pallor of the neuroretinal rim (with the rim shape fulfilling the ISNT rule), and thin retinal arterioles (as unspecific clue for any type of optic nerve damage). Besides morphological parameters, a general constriction of the outer isopters of the visual field and central perimetric defects, not explainable by myopic maculopathy, are additional clues for the presence of a non-glaucomatous optic neuropathy.

8.4. Lamina cribrosa

The lamina cribrosa covers the opening of the peripapillary scleral flange, simultaneously allows the exit of the retinal ganglion cell axons and central retinal vein and the entry of the central retinal artery, and, by tightening the intraocular compartment, it helps to preserve the intraocular pressure. In non–highly myopic eyes, the thickness and diameter of the lamina cribrosa is mostly independent of axial length. In highly myopic eyes, the lamina cribrosa markedly elongates and thins with longer axial length, while the lamina cribrosa volume remains constant and is independent of axial length (Jonas, JB et al., 1992a, 2003, 2004). The enlargement and thinning of the lamina cribrosa in highly myopic eyes, synonymous with the enlargement of the optic disc, is typical for high myopia, in contrast to moderate myopia. The lamina cribrosa thinning may be due to the axial elongation–associated increase in strain in the peripapillary sclera, leading to a posterior scleral thinning and enlargement of the peripapillary scleral opening (i.e., the lamina cribrosa).

In eyes with small-to-medium–sized optic discs and normal optic nerves, the complete posterior surface of the lamina cribrosa is covered and supported by the solid tissue of the optic nerve (Jonas, JB et al., 1992a, 2003). In highly myopic eyes with secondary macrodiscs, the lamina cribrosa is elongated and markedly thinned. Since the retrobulbar optic nerve does not expand in diameter with longer axial length, the periphery of the posterior surface of an enlarged lamina cribrosa in highly myopic eyes is not covered by the solid tissue of the optic nerve but has direct contact with the orbital cerebrospinal fluid space. The lack of a structural support for the peripheral posterior lamina cribrosa surface in highly myopic eyes may be one of the reasons for an increased prevalence of glaucomatous or glaucoma-like optic neuropathy in highly myopic eyes (Jonas, JB et al., 2017a, 2020c; Xu, L et al., 2007a). In addition, the peripheral outer lamina cribrosa surface region exposed to the cerebrospinal fluid space enlarges if the optic nerve gets thinner (e.g., in the case of glaucomatous or non-glaucomatous optic neuropathy in highly myopic eyes).

In non–highly myopic eyes, the thinning of the retrobulbar optic nerve in glaucomatous eyes is associated with the development of acquired optic disc pits, usually located sharply at the disc border in the superior or inferior disc region (Faridi et al., 2014; Javitt et al., 1990). These optic disc pits represent a local backward bulging of the lamina cribrosa into the cerebrospinal fluid space. It remains unclear whether such a herniation of the lamina cribrosa also occurs at the same frequency in secondary macrodiscs in highly myopic eyes, or whether the axial elongation–associated stretching tightens the lamina cribrosa and prevents its posterior bulge-like deformation (Kimura et al., 2014; Ohno-Matsui et al., 2012). Ohno-Matsui et al. detected pit-like clefts within the optic disc at the optic disc border at the superior or inferior disc pole, or within the parapapillary region in 32 (16.2%) of 198 highly myopic eyes, but in no emmetropic eyes (Ohno-Matsui et al., 2012). The prevalence of these pit-like abnormalities increased with longer axial length and larger optic disc size. Almost all eyes with pit-like clefts additionally showed a posterior staphyloma, and the pits were often associated with defects in the retinal nerve fiber layer, as observed in another study (Dai et al., 2013a; Ohno-Matsui et al., 2012).

8.5. Peripapillary border tissues

The two deepest layers (openings) in the optic nerve head canal (i.e., the peripapillary scleral flange opening and the choroidal opening) are separated from the intracanalicular compartment by a border tissue, which, histologically, is a continuation of the optic nerve pia mater and which ends at the end of the BM at the BMO (Figs. 13 and 14). This border tissue is differentiated into the peripapillary choroidal border tissue (Jacoby) and the peripapillary scleral flange border tissue (Elschnig) (Anderson, 1969, 1970; Bücklers, 1929; Elschnig, 1900, 1901; Hayreh, 1974; Hayreh and Vrabec, 1966; Hogan et al., 1971;

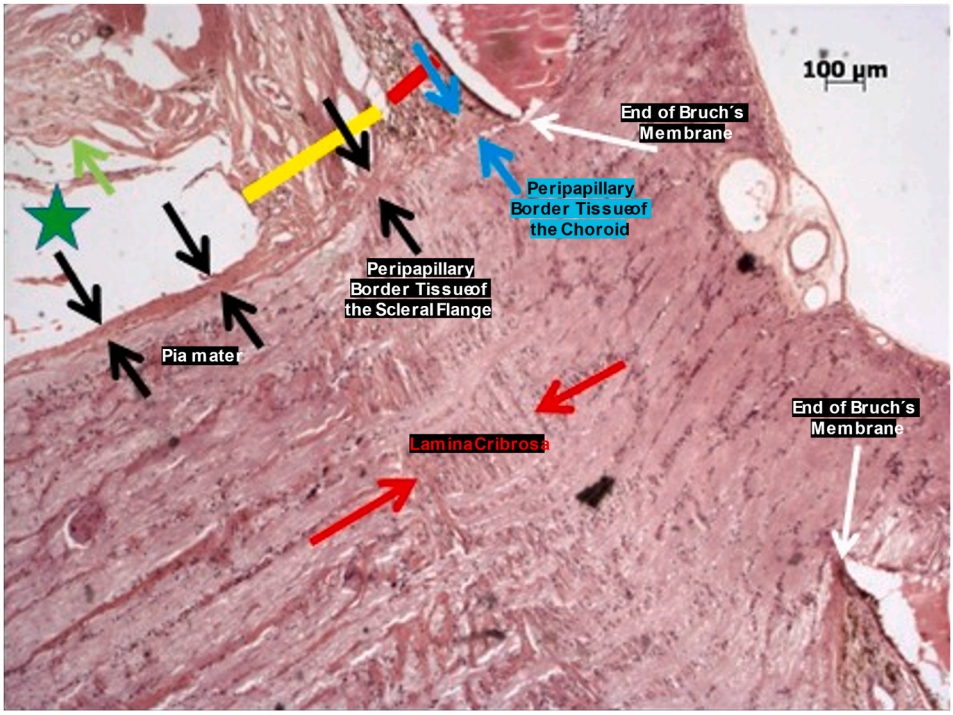

Fig. 13. Histo-photograph showing the peripapillary border tissues of the peripapillary scleral flange and of the choroid; yellow bar: peripapillary scleral flange; red bar: choroid.

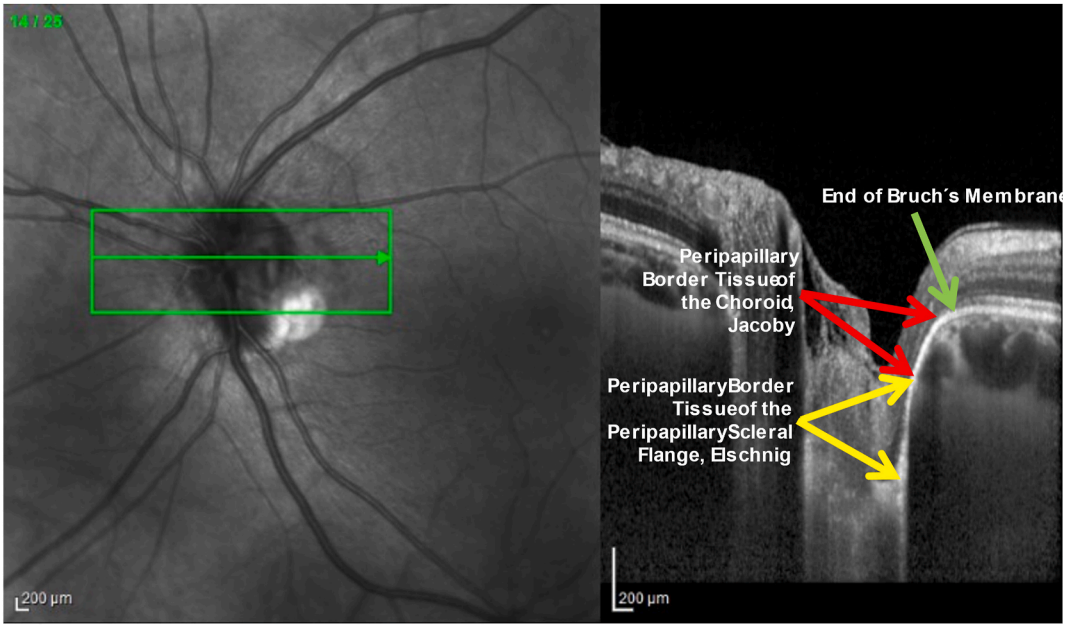

Fig. 14. Optical coherence tomographic image of the optic nerve head showing the peripapillary border tissues of the peripapillary scleral flange and of the choroid; yellow bar: peripapillary scleral flange; red bar: choroid.

Jacoby, 1905; Jonas, RA and Holbach, 2020; Kuhnt, 1879; Salzmann, 1912). The collagen fibers of the peripapillary scleral flange border tissue criss-cross with collagenous fibers coming from the peripapillary scleral flange and continue into the lamina cribrosa (Jonas, RA and Holbach, 2020). This criss-crossing of collagenous fibers may be important for the sagittal stabilization of the optic nerve head. Without such a stabilization in the anterior–posterior direction, the intraocular pressure being higher than the retro-laminar cerebrospinal fluid pressure could push or press backward the peripapillary retina, which is directly connected with the lamina cribrosa through the retinal ganglion cell axons and indirectly through the peripapillary choroidal border tissue.

The choroidal peripapillary border tissue connects the peripapillary scleral flange border tissue with the end of BM at the margin of the BMO. Besides the scleral spur in the anterior segment of the eye, the choroidal peripapillary border tissue is, thus, one of only two structures connecting the inner shell of the eye (consisting of the uvea, BM, RPE and retina, and lens) with the outer shell (i.e., the sclera). Both peripapillary border

tissues may, thus, have biomechanical importance. The merging line of the choroidal border tissue with the end of BM is the histological correlate of the peripapillary ring which surrounds the optic nerve upon ophthalmoscopy (Jonas, JB et al., 2014c). The choroidal peripapillary border tissue separating the choroidal space with the leaking choriocapillaris may be related to the choroid–optic nerve head blood barrier.

Axial elongation has an effect on both peripapillary border tissues. The choroidal border tissue elongates due to the development of parapapillary gamma zone (Jonas, RA and Holbach, 2020). The enlarging distance between the end of BM and the optic disc leads to a lengthening and thinning of the choroidal border tissue, which may even rupture in some highly myopic eyes; in such a case, BM may no longer be firmly and tautly connected to the optic disc. Such a rupture of the peripapillary choroidal border tissue with a disconnection of BM end from the optic disc may lead to and explain a corrugation of BM observed upon histology and on OCT images in some highly myopic eyes (Jonas, JB et al., 2018b) (Fig. 15). The volume of the choroidal border tissue is mostly independent of the axial elongation since the increase in its length is associated with a decrease in its thickness. The importance of the axial elongation–associated elongation and thinning of the choroidal border tissue and of a rupture and detachment of the peripapillary choroidal border tissue from the end of BM for the biomechanics of the lamina cribrosa has not yet been explored.

The peripapillary scleral flange border tissue can become shorter in eyes with axial elongation in association with the axial elongation–associated thinning of the lamina cribrosa. The same may hold true in eyes with glaucomatous optic neuropathy.

8.6. Parapapillary alpha, beta, gamma, and delta zones

In the parapapillary region, four zones can be differentiated: alpha, beta, gamma, and delta (Dai et al., 2013b; Fantes and Anderson, 1989; Jonas, JB et al., 1989b, 1992b, 2011, 2012, 2016b; Kubota et al., 1993; Sung et al., 2020) (Figs. 6, 7, 9, 10, 16 and 17).

8.6.1. Alpha zone

The alpha zone is present in almost all eyes and is located, as compared with all other parapapillary zones, most peripherally to the optic disc border, and it is characterized by an irregular hyperpigmentation and hypopigmentation due to irregularities in the parapapillary RPE (Fantes and Anderson, 1989; Jonas, JB et al., 1992b; Kubota et al., 1993). It is histologically defined by the presence of BM and an irregularly arranged RPE, which in some eyes appears to be rolled up at its end (Wang et al., 2015c). The alpha zone is largest and most frequently located in the temporal horizontal sector, followed by the inferior temporal sector and the superior temporal area, and it is smallest and most rarely found in the nasal parapapillary sector.

8.6.2. Beta zone

Upon light microscopy and OCT-based histology, the beta zone is characterized by the presence of BM and absence of RPE (Jonas, JB et al., 1989b, 1992b). In the part of the beta zone located closest to the optic disc border, the choriocapillaris is closed and retinal photoreceptors are missing (Fantes and Anderson, 1989; Jonas, JB et al., 1992b, 2011, 2012; Kubota et al., 1993; Zhang, Q et al., 2018). In an intermediate region of the beta zone, the choriocapillaris is open and photoreceptors are absent. In the peripheral part of the beta zone, the choriocapillaris is open and photoreceptors are present, but the RPE, by definition, is missing. If one extrapolates these longitudinal findings obtained in a cross-sectional study, they may suggest that during beta zone development, there is, first, a loss of RPE cells, followed by a loss of photoreceptors and, finally, a closure of the choriocapillaris. Corresponding to the histological anatomy, a beta zone represents an absolute scotoma in perimetry, and an alpha zone a relative scotoma (Akagi et al., 2013; Jonas, JB et al., 1991; Meyer et al., 1997; Rensch and Jonas, JB, 2008). Due to the mostly closed choriocapillaris, a beta zone appears as a

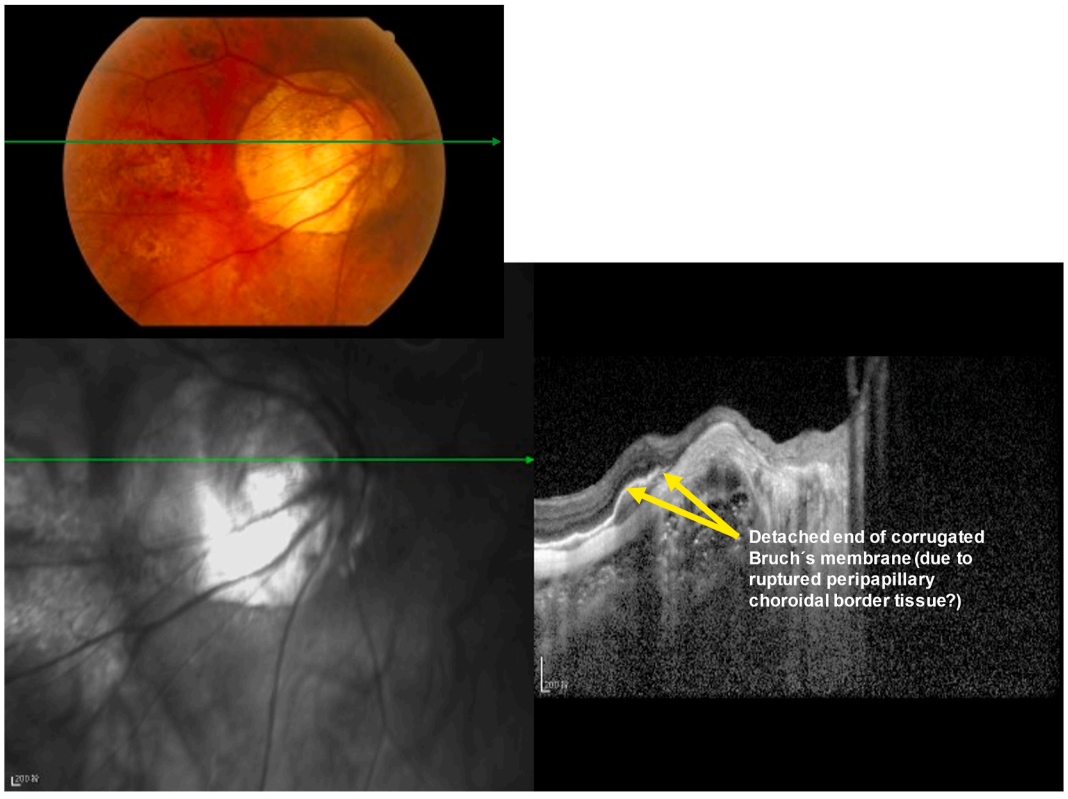

Fig. 15. Fundus photograph and optical coherence tomographic (OCT) image of the optic nerve head of a highly myopic eye, showing a corrugated Bruch's membrane, the end of which may be loosened from its anchoring in the optic nerve head, potentially due to a rupture of the peripapillary choroidal border tissue.

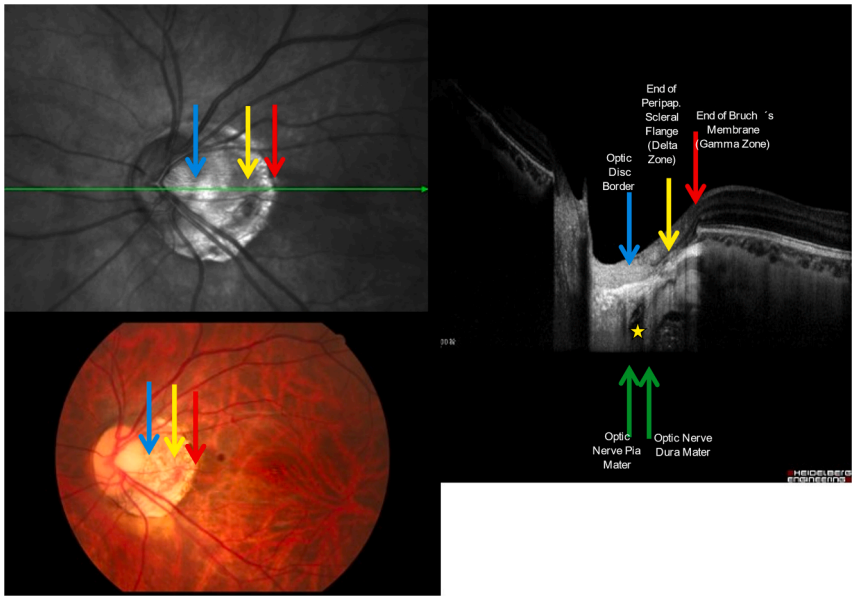

Fig. 16. Optical coherence tomographic (OCT) image and fundus photograph of the optic nerve head of a myopic eye, with parapapillary gamma zone and delta zone, and potentially the visualization of the orbital cerebrospinal fluid space (yellow asterisk) in the OCT image.

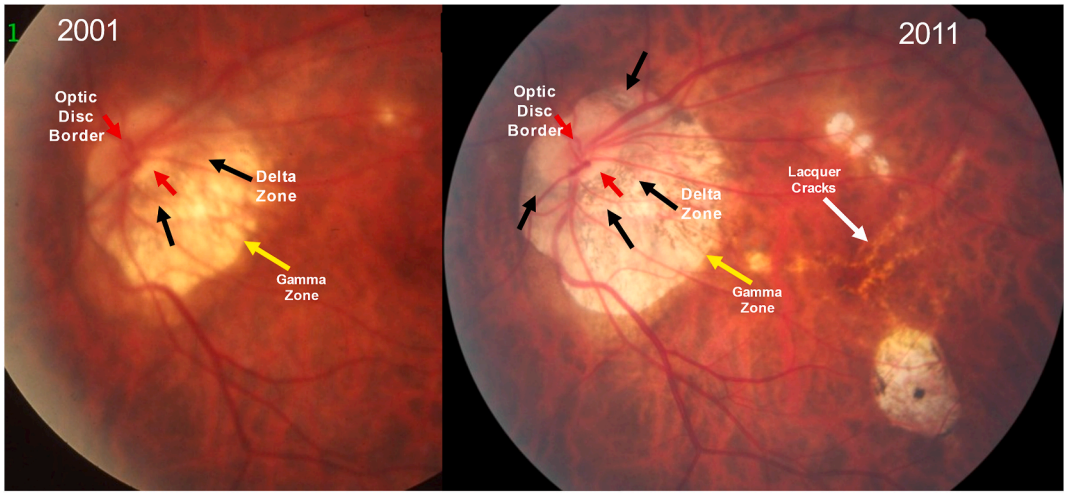

Fig. 17. Fundus photograph image of the fundus of a highly myopic eye, having developed extrafoveal "patchy atrophies" (category 3 of myopic maculopathy) in 2011 (right image; left image: same eye in 2001) and lacquer cracks (white arrow), in addition to an enlarging gamma zone and delta zone.

hypofluorescent area in angiography (O'Brart et al., 1997). The beta zone is the largest and is most frequently located in the temporal horizontal sector, followed by the inferior temporal area and the superior temporal region, while it is the smallest and is most rarely found in the nasal region (Jonas, JB et al., 1989b, 1992b).

The beta zone may be differentiated into a beta zone which developed in association with glaucomatous optic neuropathy ("glaucomatous beta zone"), and into a beta zone which developed in axially elongating eyes ("myopic beta zone"). In the case of non-myopic eyes, the occurrence and size of a beta zone is correlated with the glaucomatous loss of neuroretinal rim inside of the optic disc, glaucomatous visual field loss, decreasing diameter of the retinal arteries in eyes with glaucoma, and a decreasing diameter of the retrobulbar part of the optic nerve as measured sonographically (Anderson, 1983; Araie et al., 1994; Bak et al., 2020; De Moraes et al., 2017; Hayashi, K et al., 2012; Horn et al., 1997; Jonas, JB et al., 1992b, 2001; Manalastas et al., 2018; Miki et al., 2017; Park, KH et al., 1996; Skaat et al., 2016; Sugiyama et al., 1997; Tezel et al., 1997; Tuulonen et al., 1996; Uchida et al., 1998). The location of the glaucomatous beta zone is also spatially associated with the location of the most marked loss of neuroretinal rim inside of the optic disc and with the location of perimetric defects.

The glaucomatous beta zone may be due to an upfolding of the end of the parapapillary RPE in dependence of fluctuations of the intraocular pressure (Wang, YX et al., 2015c). The myopic beta zone may potentially develop in association with the axial elongation–associated enlargement of the RPE layer area. It may lead to an increased strain within the RPE layer and an increase in the size of the physiological opening of the RPE layer at the optic nerve head. As discussed above, the RPE layer and its basal membrane may not be firmly connected with the underlying BM and may be slip away from the optic disc. Independently of the etiology, a beta zone is associated, due to the absence of RPE cells, with an absolute scotoma (i.e., enlargement of the blind spot).

8.6.3. Gamma zone

The gamma zone is located between the beta zone (or alpha zone in the case of an absence of beta zone) on its peripheral side, and the

peripapillary ring on its central side (Asai et al., 2016; Banc and Bianchi Marzoli, 2022; Cheng, D et al., 2022; Dai et al., 2013b; Guo, Y et al., 2018a,b, 2021; Hu et al., 2016, 2021; Jonas, JB et al., 2011, 2012, 2016b, 2017a, 2018c, 2022d; Kim et al., 2020; Kim, M et al., 2018; Lee, EJ et al., 2017; Lee, KM et al., 2018a,b; Manjunath et al., 2011; Miki et al., 2017, 2019; Sakaguchi et al., 2017; Sawada et al., 2018; Shang et al., 2019b, 2022; Sung et al., 2018; Vianna et al., 2016; Yoo et al., 2016) (Figs. 6,7,9–11,16,17). In highly myopic eyes, the gamma zone can include a parapapillary delta zone in its central part (i.e., in the direction of the optic disc). The gamma zone is defined by the absence of both BM and RPE. Due to the absence of BM, the gamma zone does not contain choriocapillaris or deep retinal layers (Jonas, JB et al., 2012). It includes the inner limiting membrane on its inner surface, followed by retinal nerve fibers and the underlying sclera or peripapillary scleral flange. In some eyes it also includes few large choroidal vessels, and in some eyes the BM border can be located more peripherally than the border of the choroidal tissue, so that a small crescent of choroidal tissue (as discussed below) is located in the peripheral part of the gamma zone, uncovered by BM (Jonas, JB et al., 2012).

The development of a gamma zone may occur via two mechanisms (Jonas, JB et al., 2017b) (Fig. 12). As also suggested by the morphology of the optic nerve head in moderately myopic eyes, the BMO may shift in non–highly myopic eyes, usually in the direction of the macula. As also discussed above, this mechanism explains the overhanging of BM into the intrapapillary compartment at the nasal disc border, and, correspondingly, an absence of BM (i.e., gamma zone) in the temporal parapapillary region (Zhang, Q. et al., 2019). The shifting of the two layers of the optic nerve canal (BMO and choroidal opening) in relationship to the lamina cribrosa (as opening of the peripapillary scleral flange) leads to an oblique orientation of the ocular optic nerve head canal in dependence of the direction of the shift of the BMO (Girkin et al., 2017; Hong et al., 2019). The direction of the BM shift determines the location of the widest extension of the gamma zone in the non–highly myopic eyes.

Shifting of the BMO (and BM) as a mechanism responsible for the development of gamma zone in moderately myopic eyes also explains the occurrence of a so-called choroidal crescent in the peripheral region of the gamma zone in some eyes. Since BM primarily moves and drags the adjacent choriocapillaris and choroid, the latter may stay behind a bit, so that a small margin of choroid uncovered by BM in the peripheral region of the gamma zone may exist. The gamma zone is usually widest in the temporal inferior region, corresponding to the most common location of BM overhanging in the nasal superior disc quadrant. Exceptions are eyes with so-called “tilted optic discs”, in which an inferior gamma zone is associated with a BM overhanging in the superior disc region. In these eyes, the BM shift may have occurred from the superior to inferior direction. Correspondingly, the fovea in these eyes is located more inferiorly as compared to eyes with a temporal gamma zone (Jonas, RA et al., 2021c). In eyes with a so-called “inversio situs papillae”, BM overhanging is located in the temporal disc region, with a corresponding gamma zone in the nasal parapapillary region. The eyes with inversio situs papillae also have a large angle kappa (i.e., the angle between the temporal superior retinal arterial arcade and the temporal inferior arterial arcade), since the retinal vessels first leave the optic disc in a nasal superior and inferior direction, respectively, before they turn to a temporal direction. It fits with the notion of a BM shift into the nasal direction in these eyes, since BM and the attached RPE may indirectly shift the overlying retina. Also fitting with the notion of a BMO shift as a cause for the disc shape in these eyes with inversio situs papillae is the finding of a reduced disc–fovea distance. The cause for the BMO and BM shift has remained unclear to date and will be discussed below.

In highly myopic eyes, the BMO enlarges, eventually leading to a circular gamma zone. During the BMO enlargement, the intrapapillarily overhanging part of BM will be retracted, leading to a circular gamma zone. The reason for the BMO enlargement may be an increase in the strain within BM perhaps caused by the axial elongation–associated enlargement of BM. A BMO enlargement has been noted mostly in eyes with an axial length >26.5 mm, which may be considered a cut-off value for differentiation between moderate and high myopia (Jonas, JB, 2005; Xu, L et al., 2010).

The gamma zone is dependent mostly on axial length, and it is not—or not profoundly—associated with glaucoma (Dai et al., 2013b; Jonas, JB et al., 2012). In contrast, the glaucomatous beta zone is associated with the prevalence and degree of glaucomatous optic nerve damage. A gamma zone leads to an enlargement of the parapapillary region without photoreceptors, and since it does not contain BM or RPE, it represents an absolute scotoma (i.e., an enlargement of the blind spot in the visual field). Since gamma zones do not include choriocapillaris (except for a choroidal crescent at the temporal border of the gamma zone in some eyes) or medium-sized choroidal vessels, the superficial peripapillary retinal capillary system is the only vascular system present in the gamma zone (besides few large choroidal vessels in some eyes). These anatomical characteristics may be taken into account when OCT-angiography findings in myopic eyes with a gamma zone are interpreted (Lee, K et al., 2020a; Park, HY et al., 2019; Suwan et al., 2018).

8.6.4. Delta zone

The delta zone has been defined as the region that is located, in some eyes, within the gamma zone at the optic disc border, and it is characterized by an elongated and thinned peripapillary scleral flange (Dai et al., 2013b; Jonas, JB et al., 2012) (Figs. 6, 7, 9, 16 and 17). Since the peripapillary scleral flange ends where the optic nerve dura mater merges with the posterior scleral, and since the peripapillary arterial circle Zinn–Haller is usually located at the dura mater–sclera junction, the peripapillary arterial circle can ophthalmoscopically delineate the delta zone from the remaining peripheral gamma zone (Jonas, JB et al., 2013b). The delta zone includes the ILM, the retinal nerve fiber layer, and the peripapillary scleral flange. All other retinal layers, the RPE, BM, and all choroidal layers (except for few large choroidal vessels stemming from the posterior short ciliary arteries) are absent in the delta zone. It remains unclear whether the retinal nerve fiver layer is fully covered by a normal ILM, since the Müller cells, forming the ILM as their basal membrane, are missing in gamma and delta zones. However, since the ILM may not contain a physiological opening in the region of the optic nerve canal (in contrast to the retina, RPE, BM, choroid, and peripapillary scleral flange), the development of delta and gamma zones may lead to a stretching of the ILM. Since the Müller cells may be firmly connected to their basal membrane (i.e., inner limiting membrane), the Müller cells themselves may become stretched and elongated. The effect of a potential gamma zone– and delta zone–associated stretching of Müller cells has not yet been explored. The potential effect of a stretching of the ILM with respect to the pathogenesis of a myopic macular retinoschisis is discussed below.

The peripapillary scleral flange forms the anterior border of the orbital CSF space, and it is the biomechanical anchor of the lamina cribrosa. The development of a delta zone in highly myopic eyes may, therefore, have consequences for the biomechanics of the lamina cribrosa and may be of importance for the pathogenesis of an increased prevalence of optic nerve damage in highly myopic eyes, as discussed in detail below (Jonas, JB et al., 2017a; Xu, L et al., 2007b).

9. Suprachoroidal parapapillary cavitation

Originally described as a peripapillary detachment, a suprachoroidal parapapillary cavitation (also called intrachoroidal parapapillary cavitation) is characterized by a cleavage between the choroid, which is connected to the BM, and the sclera in the parapapillary region (Freund et al., 2003; Spaide et al., 2012; Toranzo et al., 2005; You et al., 2013). It is typically found in highly myopic eyes in the inferior to temporal inferior parapapillary region, and it shows an orange-like color upon ophthalmoscopy and is positioned at the optic disc border. The

mechanism leading to the development of a suprachoroidal parapapillary cavitation may be associated with an optic nerve becoming too short to allow a complete adduction of markedly elongated eyes (Chang et al., 2017; Demer, 2016; Wang, X et al., 2016). As also discussed above, the optic nerve—presumably its dura mater—may exert a backward pull on the posterior sclera at the merging line of the dura mater with the sclera in markedly elongated adducted eyes. It could lead to a backward pull of the peripapillary sclera and to a secondary cleavage between the sclera and the choroid, which is adherent to BM. Taking into account the orbital origin of the optic nerve in the superior nasal region of the orbit, the backward traction at the end of the peripapillary sclera flange will be highest in the inferior temporal part of the parapapillary region, where the suprachoroidal parapapillary cavitations are most commonly located.

10. Peripapillary arterial circle of Zinn–Haller

The peripapillary arterial circle of Zinn–Haller is the origin for the arterial blood supply of the lamina cribrosa. It is located at the line where the posterior sclera splits off into the optic nerve dura mater (outer part) and into the peripapillary scleral flange (inner part) (Jonas, JB and Jonas, SB, 2010; Ohno-Matsui et al., 2013). The peripapillary arterial circle is, thus, positioned at the peripheral end of the peripapillary scleral flange and marks the border between the delta zone and the remaining gamma zone. The circle can be visualized by indocyanine green angiography (Ohno-Matsui et al., 2013). If visible upon ophthalmoscopy, the peripapillary arterial circle is helpful for the delineation of the delta zone. The axial elongation–related lengthening of the peripapillary scleral flange (i.e., delta zone) increases the distance between the arterial circle and the lamina cribrosa. The development and enlargement of the delta zone may be a reason for the increased prevalence of optic nerve damage found in highly myopic eyes.

11. Eye shape

Axial ocular elongation leads to increased ocular circumference; this increase is, to a minor degree, a result of increased length of the ciliary body (pars plicata and pars plana combined), and to a major degree a result of elongation of the retina (i.e., increased distance between the ora serrata and the optic disc and macula) (Panda-Jonas et al., 2022). The retinal length, measured from the ora serrata to the optic disc border, increases by approximately 0.73 mm, and the ciliary body length, measured from the scleral spur to the ora serrata, elongates by about 0.16 mm, for each mm increase in axial length. Both retinal length and ciliary body length are correlated with each other, with an increase of ciliary body length by 0.12 mm for each mm in increase in retinal length. Correspondingly, the myopic globe enlargement mainly affects the sagittal eye diameter, while the horizontal and vertical eye diameter increase, by a significantly lower amount (Atchison et al., 2004), in axial length was associated with an increase in the horizontal and vertical globe diameters by 0.44 mm and 0.51 mm, respectively, in eyes with an axial length $\leq$24 mm. However, in eyes with an axial length $>$24 mm, the horizontal and vertical globe diameters increased by a smaller amount (0.19 mm and 0.21 mm, respectively) for each millimeter increase in axial diameter (Jonas, JB et al., 2017d). The less pronounced enlargement of the coronal globe diameters relative to the anterior–posterior diameter falls in line with the change seen in the eye shape from a sphere in emmetropia to a prolate ellipsoid in myopia.

The change in the eye shape from a sphere to a prolate ellipsoid, as already described in many studies (Atchison et al., 2004; Cheng, HM et al., 1992; Guo, X et al., 2017; Heine, 1899; Jonas et al., 2017d; Lee et al., 2021; Logan et al., 2004; Matsumura et al., 2019; Meyer-Schwickerath et al., 1984), suggests that, for geometrical reasons, the eye wall enlargement takes place predominantly in the equatorial region and/or its vicinity. A primary wall enlargement at the anterior or posterior eye poles (i.e., cornea or macula) would not lead to a sagittal elongation of a sphere.

12. Definition of high myopia

To date, high axial myopia has not been generally defined by a cut-off value of myopic refractive error or of axial length. In many studies, a myopic refractive error of −6 diopters or more was used to differentiate moderate myopia from high myopia (Flitcroft et al., 2019). A myopic refractive error of −5 diopters, if uncorrected, leads to an uncorrected visual acuity of approximately 6/172, a level fulfilling the requirement of the definition of blindness (<3/60 in the better eye). An evidence-based consensus suggested a threshold of −6.00 diopters to define high myopia (Flitcroft et al., 2019; Morgan et al., 2012).

Morphologically, high myopia can be defined by an enlargement of the BMO, independently of additional pathological changes in the macular region or the optic nerve head (Jonas, JB, 2005; Zhang, Q et al., 2019). BMO enlargement may be an incipient sign of an axial elongation–related stretching of ocular tissues in the posterior ocular segment, prior to the development of secondary macular BM defects. BMO enlargement typically occurs beyond an axial length of about 26.0–26.5 mm or a myopic refractive error of approximately more than −6 to −8 diopters (Jonas, JB, 2005; Zhang, Q et al., 2019). Similarly, the prevalence of a glaucomatous or glaucoma-like optic neuropathy increased with axial length beyond a myopic refractive error of −6 to −8 diopters (Xu, L et al., 2007b).

Since the globe elongates in childhood and adolescence, the cut-off value for high myopia in children and adolescents may be defined in dependence of age, and it may be based on normograms, according to which a final axial length of more than 26.0–26.5 mm or a myopic refractive error of more than −6 to −8 diopters may eventually be reached in adulthood (Pärssinen et al., 2014; Pärssinen and Kauppinen, 2019; Tideman et al., 2018).

13. Secondary high axial myopia due to congenital glaucoma

Secondary high axial myopia due to congenital glaucoma is a special form of axial myopia caused by abnormally high intraocular pressure within the first 2 years of life. Assessment of similarities and differences between primary high myopia (with a yet unknown cause for axial elongation) and secondary high myopia may be helpful to elucidate the etiology of axial elongation in eyes with primary myopia.

A major morphological difference between eyes with secondary high myopia and eyes with primary high myopia is that in the former, the whole eye wall becomes elongated and thinned, including the cornea and BM (Bai et al., 2017; Jonas, JB et al., 2016c, 2020b; Shen et al., 2016b). The cornea is increased in its diameter and decreased in its thickness, and Descemet's membrane can show ruptures (Haab's striae) and secondary corneal edema. In contrast, the globe wall enlargement in primary high myopia occurs predominantly in the posterior segment. Subsequently, the corneal diameter is mostly independent of axial length in eyes with primary myopia, and the axial elongation–associated lengthening of the ciliary body is markedly smaller than the axial elongation–associated lengthening of the retina.

Other differences between eyes with primary vs. secondary high myopia are that in eyes with secondary high myopia, RPE cell density at the posterior pole decreases with longer axial length, while eyes with primary high myopia show no such relationship. Furthermore, in eyes with secondary high myopia, BM thickness at the posterior pole, midpoint posterior pole/equator, and equator decreases with longer axial length; whereas, in eyes with primary high myopia, BM thickness at any ocular region is not statistically significantly correlated with axial length. In secondary high myopia, but not in primary high myopia, lower BM thickness is associated with lower RPE cell density, and BM thickness and RPE cell density decrease in a parallel manner with longer axial length.

14. Myopic maculopathy

Myopic maculopathy is characterized by an increased degree of fundus tessellation (category or stage 1 of myopic maculopathy according to the Pathologic Myopia Study Group), "diffuse chorioretinal atrophy" (stage 2), extrafoveal patchy atrophies (stage 3), and foveally located patchy atrophies (stage 4) (Fang et al., 2018; Haarman et al., 2022a; Hashimoto et al., 2019; Ohno-Matsui et al., 2015; Ruiz-Medrano et al., 2019; Yokoi and Ohno-Matsui, 2018). "Plus" signs include lacquer cracks and macular neovascularization.

In the population-based Beijing Eye Study, a higher degree of fundus tessellation was related mainly to a thinner subfoveal choroidal thickness and to older age, while adjusting for parameters such as longer axial length, male sex, lower body mass index, worse best-corrected visual acuity, larger parapapillary beta zone, and lower prevalence of intermediate and late age-related macular degeneration (Wei et al., 2013). If semi-quantified into four grades (0–4), an increasing grade of fundus tessellation was associated with decreasing subfoveal choroidal thickness (grade 0: 322 ± 90 μm; grade 1: 229 ± 80 μm; grade 2: 122 ± 52 μm; grade 3: 81 ± 37 μm). Therefore, marked fundus tessellation is an ophthalmoscopical surrogate for a leptochoroidea. As also discussed above, the ratio of small-vessel choroidal layer thickness to total choroidal thickness increases with longer axial length, while the ratios of Sattler's layer (medium-sized choroidal vessel layer) and Haller's layer thickness (large-sized choroidal vessel layer) to total choroidal thickness decreases (Zhao et al., 2018). Axial elongation–associated (and ageing-associated) choroidal thinning thus affected Haller's and Sattler's layers more markedly than the small-vessel layer. Correspondingly, a histomorphometric study and a recent clinical study did not find a significant relationship between thickness of the choriocapillaris and axial length in enucleated human eyes (Cheng, W et al., 2022; Panda-Jonas et al., 2021).

Stage 2 of myopic maculopathy (i.e., diffuse chorioretinal atrophy) is characterized mainly by a pronounced thinning of the choroid, in the absence of any specific defects such as lesions in the RPE layer or BM defects. It remains unclear whether "diffuse chorioretinal atrophy" is indeed an atrophy of tissue, such as a loss of RPE cells or photoreceptors, or whether it is simply a further axial elongation–associated thinning of the choroid. Interestingly, studies have not shown an association between the foveal retinal thickness and axial length (Deng et al., 2019; Jonas, JB et al., 2016a).

Stage 3 of myopic maculopathy is characterized by extrafoveally located, so-called "patchy atrophies", formerly also called "chorioretinal atrophies" (Ohno-Matsui et al., 2016a). Upon OCT-based imaging and light microscopy, the patchy atrophies were found to represent a round defect in the layer of the RPE, often but not always, surrounding an additional defect in the BM (Jonas, JB et al., 2013a; Ohno-Matsui et al., 2016a). In a recent histomorphometric study, a higher prevalence and a larger diameter of patchy atrophies with central BM defects was associated with longer axial length and a higher prevalence of posterior staphylomas. The mean size of the largest BM defect per eye was 1.93 ± 1.62 mm (own unpublished data). The patchy atrophies with central BM defects are predominantly located in the macular region. The BM defects are smaller than the width of the defect in the overlying RPE layer, and they are marginally smaller than the defect in the overlying outer nuclear layer. The BM defects are larger than the defects in the overlying inner nuclear layer and inner limiting membrane bridges. The choriocapillaris thickness, BM thickness, and RPE cell density were not found to differ significantly between the region at the BM defect margin and neighboring regions.

In the region of the BM defect, the choriocapillaris and the RPE layer are absent. The sclera is thinner in the region of the BM defects than in neighboring regions. To date, the reason underlying the spatial association between the BM defects and a localized thinning of the sclera—found in addition to the axial elongation–associated general scleral thinning—has remained elusive. It can be discussed that, first, there is a scleral thinning, leading to a local overextension of BM and secondary BM defects, or that the BM defects are the primary changes, secondarily leading to a local extension of the sclera. Corresponding to the association between BM defects and localized scleral thinning, a higher prevalence of BM defects is associated with a higher prevalence of posterior staphylomas. In a recent histological study on enucleated highly myopic human eyes, all globes with posterior staphylomas showed BM defects in spatial association with the staphylomas (Jonas et al., 2020a). The ophthalmoscopically visible patchy atrophies mainly represent defects in the RPE, while the centrally located, smaller BM defects are better visible upon OCT-based imaging than by ophthalmoscopy. Due to the absence of RPE (and photoreceptors), the patchy atrophies represent an absolute scotoma in the visual field.

In stage 4 of myopic maculopathy, a patchy atrophy is located in the foveal center, in association with a marked reduction in central visual acuity and a scotoma in the central and paracentral visual field. In most eyes in the fourth stage of myopic maculopathy, the atrophy develops around a scarred macular neovascularization (Cheung et al., 2017; Ohno-Matsui et al., 2016c).

A lacquer crack is one of the plus lesions in the definition of myopic maculopathy (Figs. 6, 8 and 17). It represents most likely a linear defect in the RPE, while BM in the region of a lacquer crack is usually intact. The orientation of lacquer cracks is often perpendicular to the largest width of the parapapillary gamma zone. Lacquer cracks have been considered to be the precursor—or the first stage—of a patchy atrophy. In the longitudinal population-based Beijing Eye Study, with a follow-up of 10 years, newly developed or enlarged lacquer cracks/patchy atrophies were detected in 17 (19.1%) out of 89 highly myopic eyes (Yan, YN et al., 2018). Incident lacquer cracks, enlargement of a pre-existing lacquer crack, and enlargement of a lacquer crack to a patchy atrophy were observed in 3, 3, and 5 eyes, respectively. In 14 (82.4%) of 17 eyes with incident or enlarging lacquer cracks/patchy atrophies, the change occurred perpendicularly to, and widened in, the direction of the parapapillary gamma zone enlargement.

Overall, the frequency of a lacquer crack/patchy atrophy enlargement was lower than the frequency of changes in other myopic maculopathy features, such as an elongation of the optic disc–fovea distance, a choroidal vessel shift, and a change in the ophthalmoscopical optic disc size (Jonas, JB et al., 2022a). A recent observational report described the decrease in the width of lacquer cracks in eyes with an expanding parapapillary myopic beta/gamma zone (Jonas, RA et al., 2021a) (Fig. 18). A possible explanation is that an enlargement of the RPE opening (i.e., myopic beta zone) of the optic nerve head canal led to a relative relaxation of the axial elongation–related increased strain within the RPE layer, so that the linear defect in the RPE in the parafoveal region (lacquer crack) decreased in width.

Myopic macular retinoschisis is part of myopic traction maculopathy, as another feature of myopic maculopathy (Cheong et al., 2022; Matsumura et al., 2021; Parolini et al., 2021; Shinohara et al., 2018; Uramoto et al., 2022; You et al., 2014). It is characterized by a spreading of the retinal layers in the macular region, with the photoreceptors firmly connected to the RPE; the latter is fully adherent to BM. The inner retinal layers in association with the ILM appear to be drawn away, with schisis-like tissue dehiscences running parallel to the retinal surface between various retinal layers. Besides maculoschisis, the myopic traction maculopathy includes lamellar or full-thickness macular holes and foveal retinal detachment. A higher prevalence of myopic traction maculopathy is associated with pre-retinal tractional structures, with higher myopic refractive error and longer axial length, and with a higher prevalence of posterior staphylomas, dome-shaped macula, chorioretinal atrophy, and myopic maculopathy (Cheong et al., 2022).

The pathogenesis of myopic macular retinoschisis remains poorly understood. One explanation is that the ILM connected to the optic disc and, with the basal membrane being non-elastic, may become too short to completely follow the inner retinal surface in myopic eyes with an elongated retina; this may particularly be the case in regions with a

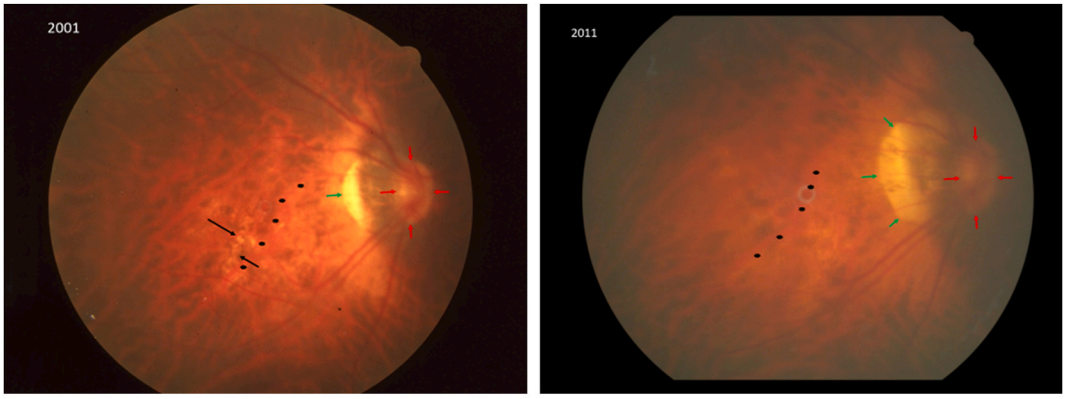

Fig. 18. Fundus photograph taken in 2001 (Figs. 18a) and 2011 (Fig. 18b) of a highly myopic eye with a refractive error of −20.0 diopters and an axial length of 30.69 mm. The image taken in 2001 shows a lacquer crack (black arrows) which is no longer detectable in the image obtained in 2011. Note: marked enlargement of parapapillary myopic beta/gamma zone (green arrows); black asterisks: markings of a large choroidal vessel as fundus landmark.

posterior staphyloma. While due to the lengthening of the peripapillary choroidal border tissue, BM can slip away from the optic disc border, and the ILM may get strained and partially elevated in such axially elongated eyes. This may resemble a washing-line phenomenon. Such an intraretinal detachment of the ILM could cause a secondary splitting of the retina, into an inner part clinging to the ILM, and an outer part with the retinal photoreceptors firmly connected to the RPE and BM.

Macular neovascularization is another plus lesion in the definition of myopic maculopathy and can eventually lead to a subretinal proliferation of RPE cells, forming a pseudo-fibrous metaplasia that is histologically similar to the fibrous pseudo-metaplasia of the lens epithelium in the case of secondary cataract (Jonas, SB et al., 2021d). It has remained unclear, why macular BM defects usually do not develop macular neovascularization despite a full access of the choroidal tissue to the retinal space.

Longitudinal studies revealed the sequence of the stages of myopic maculopathy, which we described earlier (Fang et al., 2018; Guo et al., 2021; Lin, C et al., 2018; Liu et al., 2010a; Ueda et al., 2020; Wong, YL et al., 2020; Yan, YN et al., 2018). In general, it has remained unclear whether the axial elongation–associated changes form a continuum, starting from mild abnormalities in moderate myopia to profound changes in high myopia and to pathological changes found in eyes with pathological myopia. It refers to the question of whether the marked increase in the prevalence of mild, moderate, and high myopia found in children and adolescents during the past three decades poses a risk for a substantial increase in the prevalence of pathological myopia when these children and adolescents reach the age of 40–60 years. Alternatively, pathological myopia may represent an entity different from the so-called “schoolchildren myopia”.

Interestingly, the prevalence of pathological myopia in a rural population of Central India was not associated with educational attainment level, in contrast to the prevalence of schoolchildren myopia, which strongly increased with higher educational level (Jonas, JB et al., 2017g). It also appears that the genetic backgrounds may partially differ between schoolchildren myopia and pathological myopia. To date, less than 20% of all myopias, including schoolchildren myopia, have been linked to a genetic pattern, while pathological myopia, in association with known syndromes such as Stickler’s syndrome, has a strong genetic basis (Haarman et al., 2022b; Ghorbani Mojarrad et al., 2020; Tideman et al., 2021).

14.1. Dome-shaped macula

A dome-shaped macula (DSM) is another characteristic feature occurring in some highly myopic eyes with myopic maculopathy. First reported by Gaudric and colleagues (Caillaux et al., 2013), a DSM is described as an inward protrusion of the macula, as visualized by optical coherence tomography (Ellabban et al., 2013; Errera et al., 2014; Gaucher et al., 2008; Ohno-Matsui et al., 2017; Saito et al., 2021; Soudier et al., 2016; Viola et al., 2015, 2021). Another study reported that a DSM was associated with a local thickening of the subfoveal sclera (Imamura et al., 2011). In a clinical study conducted by Fang and colleagues, a higher DSM prevalence correlated with a higher prevalence of macular BM defects (Fang et al., 2017; Meng et al., 2022b). The authors discussed that the BM defects may be pathogenetically associated with the DSM formation. Assuming a biomechanical role played by BM, the ruptures in BM may lead to a relaxation of the posterior sclera, allowing a relative thickening and relative inward protrusion of the central sclera (Fang et al., 2017). In a recent histomorphometric study, a dome-shaped configuration of the macula was associated with a relative thickening of the sclera and of the choroid in the foveal region, a central defect in BM and a subretinal RPE proliferation (own unpublished data). The latter was similar to a neovascular proliferative myopic maculopathy with a subretinal proliferation of RPE cells connected to a PAS (periodic acid–Schiff reaction)-positive membrane (Jonas, SB et al., 2021). It resembled the pseudo-fibrous metaplasia of the lens epithelium in the case of a secondary cataract, and corresponded to the embryological origin of both the RPE and the lens epithelium from the ectoderm.

The etiology of a DSM has remained elusive thus far. The assumed axial elongation–associated BM enlargement may lead to an increased strain within BM, primarily leading to an enlargement of the BM opening of the optic nerve head, and secondarily, to macular BM defects. In eyes that are not highly myopic, BM defects are associated with localized posterior staphylomas, such as in the case of macular toxoplasmotic scars and in congenital colobomas (Jonas, JB and Panda-Jonas, 2016). In a similar manner, congenital defects in BM in eyes with colobomas are associated with localized posterior staphylomas. It has remained unclear why, in some highly myopic eyes, BM defects located outside of the foveal region are associated with an outpouching of the sclera (i.e., staphylomas), while in other highly myopic eyes, BM defects located in the foveal region are related with a relative inward bowing of the sclera, forming a DSM. One possibility is that in highly myopic eyes, an increased orbital tissue pressure due to a compression of retrobulbar orbital fat (caused by the enlarging globe) may push the sclera inward, no longer meeting a strong biomechanical resistance by a now weakened BM.

14.2. Macular ridges

Macular elevations can occur in three patterns: DSMs with the

macular elevation detectable in both the (1) vertical and (2) horizontal OCT sections; and (3) ridge-shaped maculas (RSMs), in which case the macular elevation is observable only in the vertical or horizontal section (Coco et al., 2012; García-Zamora et al., 2021; Maruko et al., 2011). In a recent hospital-based study, 17 (9.2%) out of 185 highly myopic eyes (100 consecutive patients younger than 20 years) eyes showed macular elevations, all of which ran exclusively in the horizontal direction across the vertical optical coherence tomographic section (Xu, X et al., 2020). They fulfilled the definition of a macular ridge and showed no staphylomas or macular BM defects. Conversely, the macular elevations in patients with DSMs were significantly higher and had a narrower base than the macular ridges in younger patients and showed macular BM defects in their vicinity. The macular ridges usually have a wider basis and smoother elevation slope relative to DSMs.

The etiologies of RSMs and DSMs have remained unclear so far. In contrast to DSMs, macular ridges show no BM defects in their vicinity. One possibility is that a BM enlargement in the equatorial and retroequatorial fundus regions in axially elongating eyes may not occur in a completely symmetrical manner; rather, in some eyes the BM enlargement is larger in one meridian relative to the perpendicular meridian, which would result in a linear abundance of BM at the posterior pole, leading to an inward folding of BM, with a BM fold (macular ridge) running in the direction perpendicular to the meridian in which the surplus of BM was produced. With macular ridges running predominantly in the horizontal direction (and being detectable in vertical OCT scans), the relative overproduction of BM may have occurred in these eyes in the vertical meridian. Such an etiology of a macular elevation would be independent of the presence and location of macular BM defects. It has remained unclear whether a macular ridge in younger age is a risk factor for developing a dome-shaped macula in older age (Fang et al., 2020).

15. Myopia-associated optic neuropathy

15.1. Glaucomatous or glaucoma-like optic neuropathy

Although population-based studies have shown that pathologic myopia is one of the most common causes for irreversible blindness worldwide, they typically did not differentiate between the macular changes (caused by myopic maculopathy) and optic nerve damage as the main causes for the vision loss (Bikbov et al., 2020; Flaxman et al., 2017; Xu, L et al., 2006). The classification of myopic maculopathy by the Pathologic Myopia Study Group (fundus tessellation, diffuse chorioretinal atrophy, extrafoveal patchy atrophies, foveal patchy atrophy) did not include any optic nerve head alterations, although such alterations are frequently found in highly myopic eyes (Ohno-Matsui et al., 2015; Jonas, JB et al., 2017a; Xu et al., 2007a). However, epidemiological investigations and hospital-based studies have revealed an abnormally high prevalence of glaucomatous or glaucoma-like optic nerve damage in myopic and highly myopic eyes and have found myopia to be a risk factor for progression of glaucomatous optic neuropathy (Chihara et al., 1997; Ha et al., 2022; Jonas, JB et al., 2017a,e, 2020d; Kuzin et al., 2010; Lee, K et al., 2020b; Marcus et al., 2011; Mitchell et al., 1999; Pan, C et al., 2013; Suzuki et al., 2006; Tham et al., 2016; Xu et al., 2007a, Wang et al., 2022). It remains unclear whether the association between glaucoma and myopia is valid for high myopia exclusively, or for myopia of any degree (Jonas, JB et al., 2002; Xu, L et al., 2007a).

The association between glaucoma and (high) myopia suggests that a considerable subgroup of highly myopic patients lose vision due to an optic neuropathy (Bikbov et al., 2020; Jonas, JB et al., 2017a; Xu, L et al., 2007a). Vision loss induced by optic nerve damage in highly myopic patients can go unnoticed. In a clinical study of 519 highly myopic eyes (axial length: 29.5 ± 2.2 mm), the prevalence of glaucomatous or glaucoma-like optic neuropathy was 27.2%, and increased from 12.2% in the subgroup of eyes with an axial length <26.5 mm to 32.6% in the subgroup with an axial length ≥28 mm, and to 42.1% in the subgroup of eyes with an axial length ≥30 mm (Jonas, JB et al., 2017a).

The clinical diagnosis of glaucomatous or glaucoma-like optic neuropathy depends on the ophthalmoscopical examination of the optic nerve head, especially of the shape of the neuroretinal rim (Jonas, JB et al., 1999, 2020c; Wang, YX et al., 2021). As also discussed above, the neuroretinal rim shape follows the ISNT rule in myopic and highly myopic eyes, with the smallest rim part located in the temporal horizontal disc sector (Jonas, JB et al., 1988a). To delineate the neuroretinal rim from the optic cup in highly myopic eyes, it is important to detect an intrapapillary vessel kinking relatively near the optic disc border. Such kinking suggests a loss of neuroretinal rim in that disc sector, corresponding to a glaucomatous damage of the optic nerve.

Morphometric techniques for the detection of an optic nerve damage—mainly OCT-based measurements of the peripapillary retinal nerve fiber layer thickness and determination of the thickness and width of the neuroretina rim—usually fail in highly myopic eyes due to marked myopia-associated alterations in the morphology of the optic nerve head (Tan et al., 2019). These changes include a reduction in the spatial contrast between the height of the neuroretinal rim and the depth of the optic cup due to the stretching of the optic disc, including the BMO and the lamina cribrosa, with a subsequent flattening of the optic cup; a decrease in the color contrast between the pinkish color of the neuroretinal rim and the pale color of the bottom of the optic cup; a reduced visibility of the peripapillary retinal nerve fiber layer due to the bright underground in the parapapillary region in the gamma and delta zones; and unspecific causes of visual field defects, which may be due to myopic macular changes, non-glaucomatous reasons for an optic nerve damage in highly myopic eyes, refractive reasons, and irregularities of the posterior eye wall (e.g., staphylomas) (Chang and Singh, 2013; Jonas, JB and Dichtl, 1997; Lin, F et al., 2022; Rezapour et al., 2021a,b; Tan et al., 2019; Xu, L et al., 2007b). Furthermore, the intraocular pressure is not elevated in many highly myopic eyes with optic nerve damage (Jonas, JB et al., 2017h; Lin, FB et al., 2020).

Some of these problems may be addressed if the retinal ganglion cell–inner plexiform layer thickness in the macular region outside of areas with macular patchy atrophies are measured by OCT (Bowd et al., 2022; Rezapour et al., 2022b). In that context, it must be taken into account that within the patchy atrophic regions (stages 3 and 4 of myopic maculopathy), the retinal surface area is focally enlarged. This enlargement may lead to a geometrically explained thinning of the retinal ganglion cell layer and inner plexiform layer (Jonas, JB et al., 2013a). Another possibility may be the assessment of the radial peripapillary capillary network by OCT-angiography and the assessment of the retinal nerve fiber layer texture (Ang et al., 2018; Sung et al., 2018; Tan et al., 2019).

The difficulties in assessing an optic nerve damage in highly myopic eyes are compounded by even more severe difficulties in detecting progression of optic neuropathy in high myopia. Future studies may address whether the determination of the outer perimetric isopters and thickness measurements of the macular retinal ganglion cell–inner plexiform layer outside of patchy atrophic areas are helpful for examining progression of optic nerve damage in highly myopic eyes.

It should be noted that an association between intraocular pressure and the occurrence of a glaucomatous or glaucoma-like optic neuropathy, as defined by an abnormal shape of the neuroretinal rim, has not yet been conclusively demonstrated (Jonas, JB et al., 2017h; Lin, FB et al., 2020). Furthermore, the markedly thinned sclera in highly myopic eyes may lead to an inaccuracy in tonometry (Whitacre and Stein, 1993). However, an association of the optic nerve damage with intraocular pressure and with the protective effect of a lowering of intraocular pressure has been considered central for the definition of glaucoma (Garway-Heath et al., 2015). Until future studies address such a relationship, the occurrence of an optic nerve damage with an abnormal neuroretinal rim shape in highly myopic eyes may also be called “glaucoma-like” or “glaucomatoid” (Song et al., 2020).

15.2. Causes of increased prevalence of glaucomatous or glaucomatoid optic neuropathy in high myopia

Histological risk factors for the axial length–associated increase in the prevalence of a glaucomatous or glaucoma-like optic neuropathy in highly myopic eyes may be the enlargement and thinning of the lamina cribrosa, lengthening and thinning of the peripapillary choroidal border tissue—with potential consequences on the biomechanics of the connection between BM and the lamina cribrosa—the elongation and thinning of the peripapillary scleral flange as the biomechanical anchor of the lamina cribrosa, and the increased distance between the peripapillary arterial circle of Zinn–Haller and the lamina cribrosa. It remains unclear whether other axial elongation–associated changes in the region of the optic nerve head, such as the development of the parapapillary gamma zone in association with a temporal shifting of the BM opening, and the enlargement of gamma zone in association with an enlargement of the BM opening, may indirectly be associated with the prevalence of glaucoma (Jonas, JB et al., 2020c; Wang, YX et al., 2021).

As a corollary to the histological findings, clinical observations have suggested that the presence and size of parapapillary delta zone and an axial elongation-associated enlargement of the optic disc were the two main morphological risk factors for an increase in the glaucoma prevalence in axially elongated, highly myopic, eyes (Jonas, JB et al., 2017a; Nagaoka et al., 2015). Interestingly, presence and size of gamma zone (after subtraction of delta zone) after adjusting for axial length was not markedly associated with glaucoma in high myopia in that study, fitting with the notion, that it is the peripapillary scleral flange which is primarily connected with the lamina cribrosa.

15.3. Non-glaucomatous optic neuropathy

Clinical findings suggest that high axial myopia can be associated with a non-glaucomatous optic nerve damage. In the population-based Ufa Eye and Medical Study, a higher prevalence of myopic maculopathy was correlated with a thinner peripapillary retinal nerve fiber layer, after adjusting for the presence or degree of glaucomatous optic neuropathy or after excluding eyes with glaucomatous optic nerve damage (Bikbov et al., 2020). The thinner retinal nerve fiber layer in non-glaucomatous eyes with myopic maculopathy points at a non-glaucomatous type of optic nerve damage in highly myopic eyes with maculopathy.

Reasons for an increased prevalence of a non-glaucomatous optic neuropathy in highly myopic eyes may be the increase in the distance between the retinal ganglion cell bodies and the optic disc. Upon histomorphometry and as discussed above, the retina—over its whole region from the ora serrata to the optic disc—elongates by 4.3 mm if axial length increases from 24 mm in an emmetropic eye to 30 mm in a highly myopic eye (own unpublished data). This retinal lengthening primarily affects the retinal structures connecting the deeper retinal layers with the optic disc; these structures are the ILM and the retinal nerve fibers. Assuming that the axons of the retinal ganglion cells are not elastic or extendable, any lengthening of the retinal nerve fibers will lead to their stretching. Such mechanical strain may lead to damage to and loss of the retinal nerve fibers, ultimately resulting in a non-glaucomatous optic neuropathy.

In addition to the axial elongation–associated changes in the midperiphery of the fundus, an increase in the distance between the retinal ganglion cells and the optic disc occurs in the papillo-macular region via the development of a temporal parapapillary gamma and delta zone (Jonas, RA et al., 2021b). The gamma and delta zones, if located in the temporal parapapillary region, lead directly to an increase in the disc–fovea distance at a ratio of approximately 1:1 (Jonas, RA et al., 2015a). This increase is associated with a lengthening of the retinal nerve fibers in the papillomacular region, since these fibers already run in a straight course to the optic disc, prior to the commencement of axial elongation. The lengthening of the fibers may lead to their stretching with secondary damage.

In contrast, axons in the curved arcuate regions may compensate for an increase in the disc–fovea distance by becoming more straight-lined, without secondary fiber stretching. An elongation and stretching of the papillo-macular fibers may be associated with the development of central scotomas in highly myopic eyes; myopic macular changes could not otherwise explain these scotomas. The notion of a straightening of retinal nerve fibers with elongating distance to the optic disc is supported by a population-based 10-year follow-up study, in which a higher prevalence of a disc–fovea distance elongation was found in 71% of highly myopic eyes and was related to a straightening of the papillomacular retinal vessels; additionally, a widening of the gamma zone and a decrease in angle kappa were found (Jonas, RA et al., 2021b). Using the easily ophthalmoscopically detectable retinal vessels as landmarks, one may infer that the retinal nerve fibers become stretched throughout the course of a widening parapapillary gamma zone.

16. Axial elongation/emmetropization/myopization

Axial myopia can be regarded as the result of an overshooting of the physiological process of emmetropization. The process of emmetropization describes the physiological axial elongation of the eye by which the marked axial hyperopia present at birth is transformed into emmetropia in adulthood. For each millimeter of the ocular axial length that extends beyond the accepted threshold in relation to the combined refractive power of cornea and lens, a myopic refractive error of approximately −2 to −3 diopters results. Studies report that axial elongation usually ceases in the third decade of life in about two-thirds of moderately myopic individuals, while one-third of such individuals can show myopia progression during that period, albeit at lower rates than during childhood (Lee, SS et al., 2022b). In contrast, highly myopic patients, especially those with pathological changes in the macula (i.e., myopic maculopathy) or the optic nerve (high myopia–associated optic neuropathy), can experience further axial elongation in adulthood such that sagittal eye diameters exceeding 35 mm can eventually result (Du et al., 2021; Fang et al., 2018; Larsen, 1971; Lee, MW et al., 2020; Saka et al., 2010, 2013).

Continuous axial elongation is a main risk factor for the progression of myopic maculopathy (Fang et al., 2018; Lee MW et al., 2020; Saka et al., 2010, 2013). To cite an example, in the study by Du and colleagues, the mean axial length among 1877 patients increased from 29.66 ± 2.20 mm annually at baseline by 0.05 ± 0.24 mm (Du et al., 2021). Among the risk factors for marked axial elongation were female sex (OR: 1.46, 95%CI: 1.38–1.55), baseline axial length of 28.15 mm or greater (OR: 1.67, 95%CI: 1.54–1.81 to OR: 2.67, 95%CI: 2.46–2.88), presence of maculopathy (OR: 1.06, 95%CI: 0.96–1.17 to OR: 1.39, 95% CI: 1.24–1.55), and previous macular neovascularization (OR: 1.37, 95%CI: 1.29–1.47) (Du et al., 2021). These risk factors for elongation are not modifiable; therefore, Du and colleagues concluded that prevention of myopia may be the best approach to reduce the incidence of pathological myopia. Alternatively, procedures are warranted to decrease or completely stop further axial elongation and myopization in highly myopic eyes, in an attempt to prevent the development and progression of myopic maculopathy and high myopia–associated optic neuropathy. Blocking or neutralizing a hypothetical “myopia growth factor” has been suggested as a possible method to prevent or reduce further axial elongation, particularly in adult highly myopic patients with ongoing axial elongation.

Experimental and clinical studies reported that various molecules are potentially involved in the process of axial elongation. These molecules include dopamine, atropine, TGF-β, fibroblast growth factor, hepatocyte growth factor, insulin-like growth factor, and amphiregulin and other epidermal growth factor (EGF) family members, to name a few (Barathi et al., 2009; Cheng, T et al., 2020; Chua, WH et al., 2006; Chia et al., 2016; Dong et al., 2019b, 2020, 2022; Gao et al., 2006; Jiang, L et al., 2014; Jiang, WJ et al., 2017; Jobling et al., 2009, 2014; Li et al., 2014;

Mao et al., 2016; Seko et al., 1995). Recent studies conducted in young guinea pigs with or without lens-induced myopization showed that the repeated intravitreal application of antibodies against EGF family members, such as amphiregulin, neuregulin-1, and EGF itself, yielded a decrease in axial elongation, while repeated intravitreal injections of EGF family members themselves—namely, amphiregulin, neuregulin-1, and EGF—were associated with an increase in axial elongation (Dong et al., 2019b, 2020, 2022; Jiang, WJ et al., 2017). As a corollary, the intravitreal application of EGF receptor antibodies was associated with a reduction in the axial elongation in young guinea pigs (Dong et al., 2020). Based on the observations made in the experimental studies and in the histomorphometric investigations, the hypothesis was formulated that EGF and its family members, potentially produced by cells in the retina, may stimulate the RPE in the mid-periphery of the fundus to locally enlarge BM as its basal membrane. The RPE contains receptors for EGF (Anchan et al., 1991; Cheng, LB et al., 2014; Defoe and Grindstaff, 2004; Khaliq et al., 1996; Kociok et al., 1998; Liang et al., 2010; Liu, NP et al., 1992; Vatsyayan et al., 2011; Xu and Fu, 2007; Yan, F et al., 2007; Zhang, L et al., 2013). These findings place BM at the center of the efferent limb of the postulated feedback mechanism governing axial elongation in the process of emmetropization/myopization (Jonas, JB et al., 2017b).

The following findings were the basis for the formulation of the hypothesis (Table 1) (Fig. 19). The process of emmetropization can be regarded as a fitting of the optical axis length to the refractive power of the cornea and lens, starting approximately in the third year of life. In the first 2 years of life, the enlargement of the globe occurs by growth in all directions (i.e., the spherical shape of the eye remains preserved). In that period, the globe enlarges its anterior–posterior sagittal diameter from about 17 mm at full-term birth to about 21–22 mm at the end of the second year of life. This globe enlargement is related to an increase in the scleral volume, as also found histomorphometrically (Jonas, JB et al., 2014a). After that period, the eye further enlarges, mainly by an increase in its sagittal diameter up to an axial length of about 24 mm, with 1-mm increase in the anterior–posterior size corresponding to an increase of 0.5 mm in the equatorial plane in the horizontal and vertical direction (Jonas, JB et al., 2017d). Above an axial length of 24 mm, the equatorial diameters (horizontal and vertical) increase by approximately 0.20 mm or less for each millimeter elongation in the sagittal direction (Jonas, JB et al., 2017d). These measurements corroborate the observed change in the eye shape from a sphere in hyperopia and emmetropia to a prolate ellipsoid in axial myopia. The axial elongation–associated change in the globe's shape suggests an eye wall enlargement occurring predominantly in the equatorial region.

Axial elongation leads to a choroidal thinning and, to a relatively lower degree, to a scleral thinning (Hoseini-Yazdi et al., 2019; Flores-Moreno et al., 2013; Fujiwara et al., 2009; Jonas, JB et al., 2019; Moriyama et al., 2007; Spaide et al., 2008; Wei et al., 2013). The choroidal thinning is most pronounced at the posterior pole. Additionally, axial elongation is related to a retinal thinning and a reduction in the RPE cell density in the retro-equatorial region (Jonas, JB et al., 2016d, 2017c, 2020b). This contrasts with the retinal thickness and RPE cell density in the macular region; here, both parameters are independent of axial length. BM's thickness in any region was found to be independent of axial length in all ocular regions, except for eyes with secondary high myopia due to congenital glaucoma (Bai et al., 2017; Dong et al., 2019a; Jonas, JB et al., 2014b, 2020b). The axial elongation–associated increase in the fovea–optic disc distance is mainly due to the development and enlargement of a parapapillary gamma zone, which usually enlarges in the temporal to inferior temporal direction, towards the fovea (Jonas JB et al., 2012, 2016b, 2018c, 2022b,d; Jonas RA et al., 2015a). Since the distance between the temporal superior vascular arcade and the temporal inferior vascular arcade is independent of axial length, BM length in the macular region is not enlarged during axial elongation (Jonas JB et al., 2015, 2018a; Jonas RA et al., 2015b). The elongation of the optic disc–fovea distance leads to a

Table 1
Axial elongation–associated morphological changes.

Minor, moderate, and high myopia:	Thinning of the sclera, most marked at the posterior pole and least marked at the ora serrata or anterior to it. Scleral volume not correlated with axial length (and age) beyond an age of 3 years. Thinning of the choroid, most marked at the posterior pole and least marked at the ora serrata. Choroidal volume not correlated with axial length (and age) beyond an age of 3 years. Bruch's membrane not related to axial length. Bruch's membrane volume increase with longer axial length. Photoreceptor density decrease with longer axial length, most marked at the posterior pole/equator midpoint and in the equatorial region, and less marked close to the ora serrata. Retinal thickness decreases with longer axial length, most marked at the posterior pole/equator midpoint and in the equatorial region, and least—or not—marked at the posterior pole. Retinal pigment epithelium cell density decreases with longer axial length, most marked at the posterior pole/equator midpoint and in the equatorial region, and least—or not—marked at the posterior pole. Bruch's membrane opening shift in moderately myopic eyes, usually in the temporal/inferior direction; leading to an overhanging of Bruch's membrane into the nasal intrapapillary compartment and Bruch's membrane absence in the temporal region (i.e., parapapillary gamma zone), optic disc ovalization due to shortening of the ophthalmoscopically visible horizontal disc diameter, fovea–optic disc distance elongation, reduction in angle kappa, and straightening/stretching of the papillomacular retinal blood vessels and retinal nerve fibers
Minor and moderate myopia:	Bruch's membrane opening (BMO) shift, usually in the temporal (inferior) direction, with longer axial length in moderately myopic eyes, leading to an overhanging of Bruch's membrane (BM) into the intrapapillary compartment nasally, and an absence of BM in the temporal parapapillary region (parapapillary gamma zone).
Moderate and high myopia:	Enlargement of the retinal pigment epithelium layer opening of the optic nerve canal, leading to a parapapillary myopic beta zone; Elongation and thinning of the peripapillary choroidal border tissue (the volume of which is not related to axial length), due to the development of a gamma zone with an increased distance between the end of Bruch's membrane and the end of lamina cribrosa. High myopia: Enlargement of all layers of the optic nerve canal, including Enlargement of the retinal pigment epithelium layer opening of the optic nerve canal, leading to a parapapillary myopic beta zone. Enlargement of Bruch's membrane opening, leading to a retraction of a BM formerly overhanging into the intrapapillary compartment and eventually to a circular gamma zone. Enlargement of the lamina cribrosa, leading an elongation and thinning of the lamina cribrosa, with the consequence of the development of a secondary macrodiscs and a steepening of the trans-lamina cribrosa pressure gradient between the intraocular compartment (intraocular pressure) and the retro-laminar compartment (orbital cerebrospinal fluid pressure). Elongation and thinning of the peripapillary scleral flange (i.e., parapapillary delta zone). - Elongation and thinning of the peripapillary choroidal border tissue due to the circular enlargement of gamma zone, sometimes leading to a rupture of the elongated and thinned peripapillary choroidal border tissue, with the consequence of a loosening of the peripapillary BM end and a corrugation of BM.

(*continued on next page*)

Table 1 (*continued*)

	Development of linear defects of the RPE in the macular (extrafoveal) region, widening to round defects (patchy atrophies) with further axial elongation.
	Development of macular BM defects with a corresponding equally sized defect in the choriocapillaris, surrounded by a larger RPE layer defect; with a smaller defect in the retinal outer nuclear layer and an even smaller defect in the retinal inner nuclear layer, sometimes leading to inner limiting membrane (ILM) bridges.
	Macular neovascularization, often in association with a foveal patchy atrophy.
	Myopic macular retinoschisis, potentially in association with a washing line effect of the inner limiting membrane.
	Glaucomatous/glaucoma-like optic neuropathy.
	Non-glaucomatous optic neuropathy.

With Bruch's membrane unrelated to axial length, and considering the change in eye shape from a sphere in emmetropia to a prolate (rotational) ellipsoid in myopia, the features may be explained by a primary Bruch's membrane enlargement in the retro-equatorial/equatorial region, leading to axial elongation and secondary choroidal thinning at the posterior pole.

decrease in angle kappa between the temporal superior and the temporal inferior vascular arcade (Jonas RA et al., 2015b). The observation that the macular BM does not markedly change during axial elongation in eyes without myopic maculopathy (stage 3 or higher) aligns with the findings that the RPE cell density, retinal thickness and density of the choriocapillaris, and the best-corrected visual acuity were independent of axial length in axially elongated eyes without myopic maculopathy (Panda-Jonas, JB et al., 2021) (Fig. 19).

These morphological findings formed the basis for the hypothesis that axial elongation occurs through an enlargement of BM in the equatorial to retroequatorial region. An ocular wall enlargement taking place predominantly in the equatorial to retro-equatorial region would geometrically explain the change from a spherical eye shape in emmetropia to a prolate ellipsoid form in axial myopia. A BM enlargement in the equatorial to retro-equatorial region pushes the posterior part of BM backward, leading to a compression and secondary thinning of the choroid that is most pronounced at the posterior pole. The thinning of the sclera, less marked than the choroidal thinning when expressed in relative terms, might secondarily be induced by the backward push of the posterior BM. A BM enlargement in the equatorial to retro-equatorial region fits with the observed decrease in the RPE cell count and retinal layer thickness in these regions of axially elongated eyes. With BM in the macular region primarily not involved in the process of BM enlargement, the density of the retinal photoreceptors remains unaffected by axial elongation. This aligns with the observation that best-corrected visual acuity is independent of axial length in myopic eyes without myopic maculopathy.

With the macular BM primarily unaffected by axial elongation, the hypothesis also fits with the findings, that the thickness of the retina, the RPE cell density and the choriocapillaris density in the macular region were not related to axial length (Cheng, W et al., 2021, 2022; Panda-Jonas et al., 2021). By the same token, the distance between the

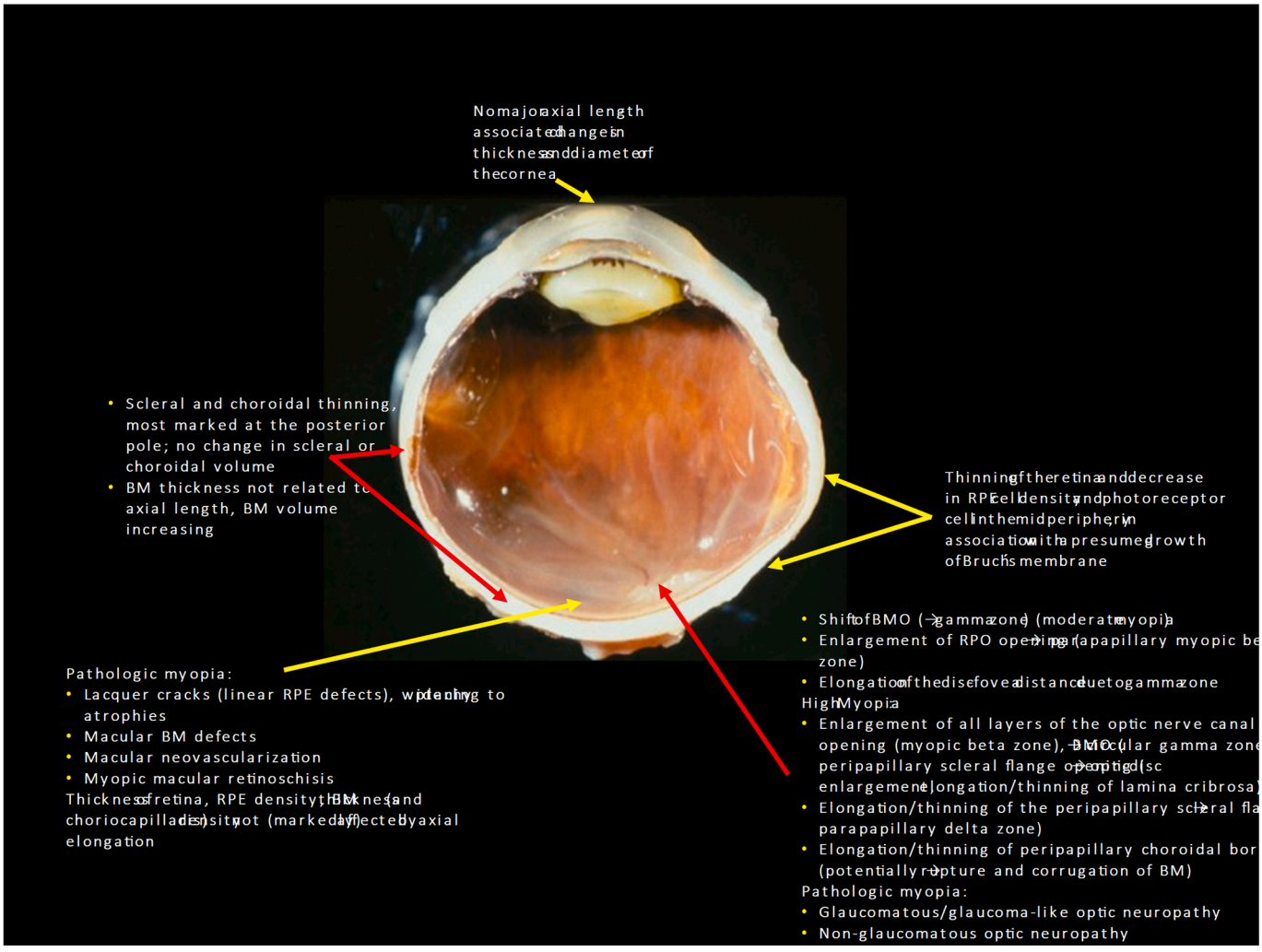

Fig. 19. Eye globe with general myopic changes topographically listed.

temporal superior vascular arcade and the temporal inferior vascular arcade was not related to axial length in eyes without stage 3 or higher of myopic maculopathy, supporting the notion that macular BM does not enlarge in axially elongated eyes. BM enlargement taking place predominantly in the equatorial to retro-equatorial region would also explain the shift of BM into the temporal direction towards the fovea, parallel to the development and enlargement of the gamma zone in the temporal parapapillary region in moderately myopic eyes.

Finally, an active BM production and enlargement would fit with the observation that the thickness of BM, in contrast to the thickness of the choroid and sclera, was independent of axial length. It remains unclear how an enlargement of BMO with longer axial length, and eventually the development and enlargement of lacquer cracks and BM defects in the macular region, could be explained by the hypothesis. One may discuss that the BM enlargement in the equatorial to retro-equatorial region, also slightly increasing the coronal diameters of the myopic eye, may increase the strain within BM, leading initially to a BMO enlargement. Should that be insufficient to release the strain, secondary new BM defects may develop in the macular region. The enlargement of the RPE opening of the optic nerve canal (i.e., the development of a myopic parapapillary beta zone) may result from enlargement of the inner surface of BM (due to the enlargement of BM), so that the RPE layer becomes stretched, leading initially to an increase in the RPE opening of the optic nerve canal, and in a second step, to secondary RPE layer defects in the macular region, beginning with linear lacquer cracks that then widened to round defect and then so-called "patchy atrophies". Fitting with this notion is that the orientation of the lacquer cracks (or linear RPE defects) is usually perpendicular to the direction of the widest section of the gamma zone.

The notion of defects in the RPE layer developing before or in association with the development of macular BM defects is supported by histological findings of macular BM defects. In all eyes with BM defects, as examined in a recent histomorphometric study, the overlying RPE defect was larger than the BM defect. This finding corroborates clinical OCT findings indicating that within a patchy atrophy, the RPE defect is larger than the BM defect in its center. Further support is lent by the finding that highly myopic eyes can show RPE defects in the macular region (patchy atrophies) without a concurrent BM defect, while all BM defects are associated with a (larger) surrounding RPE defect. Supporting the hypothesis of BM as a biomechanically important structure for the shape and size of the eye and for the process of axial elongation is the finding that the biomechanical strength of BM in relationship to the structure thickness was about 100 times higher than the strength of the sclera.

Experimental studies and clinical observations have suggested that the afferent, sensory part of the feedback mechanism governing the process of axial elongation is located in the mid-periphery of the fundus in the retro-equatorial region of the eye (Berntsen et al., 2013; Mutti et al., 2007, 2011; Sankaridurg et al., 2011; Smith et al., 2005, 2007, 2009). This suggestion is based on experimental results that a peripheral defocus leads to axial elongation of the eyes in animals, and on clinical observations that human eyes with a congenital macular scar (e.g., due to a toxoplasmotic retinochoroiditis) do not typically develop axial elongation, while eyes with a destruction of the retina in the mid-periphery, such as after peripheral and mid-peripheral laser coagulation therapy for retinopathy of prematurity, can develop marked axial myopia. In contrast, eyes with retinopathy of prematurity treated by intravitreal application of anti–vascular endothelial growth factor (VEGF) drugs develop axial myopia less often (Harder et al., 2013; Marlow et al., 2021).

The notion of the fundus mid-periphery as the location of the sensory arm of the process of emmetropization is also supported by clinical trials on myopic children, in which a peripheral myopization by circular progressive addition contact lenses or by orthokeratology (with a steepening of the corneal periphery) or other optical measures was associated with a reduction in the rate of myopia progression (Wildsoet et al., 2019). The presumed location of the sensory part of the feedback mechanism in the fundus mid-periphery is in line with the location of the presumed BM growth in the fundus mid-periphery, with the RPE cells–producing BM being located in close proximity to the retinal cells, which are part of the sensory arm of the feedback mechanism. It would also explain why BM in the macular region is not primarily affected during the process.

In summary, the hypothesis suggests that BM enlargement in the retro-equatorial/equatorial region actively leads to myopic axial elongation. This hypothesis is supported by histological, clinical, and experimental findings, such as that the elastic modulus of BM is comparable or higher than that of the sclera for an intraocular pressure of approximately 15 mm Hg (Table 1). The hypothesis conflicts with the usual assumption that the sclera is the primary structure involved in achieving the elongation of the eye (Liu, HH et al., 2010b; McBrien, 2013; McBrien et al., 2000, 2003, 2006, 2009; Morgan et al., 2012).

Previous studies have examined the axial elongation–associated changes in the sclera and have convincingly shown alterations at the microscopical, biochemical, and genetical levels (Liu, HH et al., 2010b; McBrien, 2013; McBrien et al., 2000, 2003, 2006, 2009; Morgan et al., 2012). It has remained unclear, however, whether these changes are primary changes leading to the elongation of the globe, or whether they occur in a secondary manner as a consequence of eye elongation. A major argument may be that if the sclera was the tissue elongating the eye, the distance between the sclera and BM would increase (i.e., the choroidal thickness would increase). All studies concur, however, that axial elongation is associated with a choroidal thinning. The posterior choroidal thinning implies that the posterior pole of BM is moving backward to a greater degree than the degree to which the posterior sclera moves backward.

An indirect argument in favor of BM and against the sclera as the structure primarily elongating the eye is that the process of emmetropization uses axial elongation to elongate the optical axis and not the sagittal diameter of the globe. The optical axis ends at the photoreceptor outer segments in close proximity to the RPE and BM. Since the choroid separates the sclera from the photoreceptor outer segments, and since the subfoveal choroidal thickness fluctuates between morning and evening—and may be dependent on additional parameters (such as cerebrospinal fluid pressure—the sclera is unlikely to govern the optical axis length with a sufficient precision of approximately 50–100 μm.

Another point for discussion is that the messenger molecule that may be produced in the retina would have to cross the RPE barrier, the rapid blood stream of the choriocapillaris, and the interstitial tissue of the choroid before it could arrive at the scleral inner surface. It may be unlikely that such as mechanism would lead to a predictable dose of the messenger molecule reaching the sclera. In addition, the density of fibrocytes in the sclera is relatively low, so that a fine-tuning of the length of the optic axis may be difficult. A fine-tuning is, however, necessary, since an axial length of merely 300 μm too long—resulting in a myopic refractive error of −1 diopter—would have been a major survival disadvantage in our ancestral environments. Future studies may address in greater detail which structure—the sclera, BM, or other morphological element—may be the primary catalysts of eye elongation.

17. Biomechanical aspects

Some potential biomechanical aspects of the myopic changes are as follows.

- During myopization in adolescence, the BMO shift described above leads to an anatomical stretching of the peripapillary choroidal border tissue on the nasal optic disc side (centripetally, in direction of the intrapapillary compartment) and at the temporal optic disc side in the gamma zone (centrifugally in a direction away from the optic disc). Any stretching of the peripapillary border tissue of the

choroid may be transferred onto the lamina cribrosa, since the choroidal border tissue is connected with the peripheral end of the lamina cribrosa.

- Anatomically, the eye can be considered to be composed of an inner ball and an outer coat. The inner ball, comprising the uvea, BM, RPE, retina, lens, and vitreous body, is connected to its outer coat (i.e., the sclera) at only two locations: anteriorly at the scleral spur, and posteriorly at the peripapillary border tissue of the choroid. The biomechanical importance of the peripapillary choroidal border tissue as the only posterior connection between the inner ball and the outer coat of the eye has not yet been explored, either with respect to the state of emmetropia or axial elongation.
- The eye performs movements with marked acceleration and deceleration, which may lead to a hurling of the inner ball against the outer shell (i.e., the sclera), buffered by the choroid. In that model, the choroid may play a similar role as the outer cerebrospinal fluid space plays for buffering body movement–induced shifting of the brain against the skull. The hurling of the inner ocular shell leads to stress and strain on the peripapillary choroidal border tissue, which is the only connection between the inner shell and the outer shell in the posterior hemisphere of the globe. The axial elongation–associated changes in the peripapillary choroidal border tissue (elongation and thinning, in some eyes perhaps rupture) with respect to the potential role of the choroid as mechanical buffer has not yet been explored.
- The potential enlargement of BM in the equatorial regions, also leading to an increase in the coronal diameters of the globe, may lead to a strain in BM at the posterior pole, leading to an enlargement of the BMO in highly myopic eyes (usually beyond an axial length of approximately 26.0–26.5 mm). This BMO enlargement leads to a centrifugal stretch on the peripapillary choroidal border tissue, and to the development of a circular gamma zone. The biomechanical importance of a circularly centrifugal stretch on the peripapillary choroidal border tissue has not been examined yet.
- The collagenous fibers of the peripapillary border tissue of the peripapillary scleral flange criss-cross with the collagenous fibers of the scleral flange, which continue into those of the lamina cribrosa. The biomechanics of this anchoring of the scleral flange/lamina cribrosa, running in the coronal plane, with the sagittally orientated peripapillary border tissues has remained unexplored. It is likely that this criss-crossing leads to a stabilization of the lamina cribrosa in the anterior–posterior direction.
- If in highly myopic eyes with a large gamma zone, the peripapillary choroidal border tissue (connecting the end of BM with the end of the lamina cribrosa) ruptures, the strain within BM may be released, leading to an undulation of BM in its vicinity (Jonas, JB et al., 2018a). A similar morphology can be detected close to macular BM defects in eyes with myopic maculopathy. The biomechanical importance of a ruptured peripapillary choroidal border tissue for the stability and morphology of the lamina cribrosa remains to be explored. Likewise, the biomechanical consequence of the end of BM loosened (due to the ruptured peripapillary choroidal border tissue) for the stability and function of the BM in the macular region has not yet been assessed.
- The development of BM defects in the macular region may lead to a release in the strain of BM around the BMO of the optic nerve, with a secondary reduction in the strain in the peripapillary choroidal border tissue.
- The potential enlargement of BM in the equatorial regions in axial myopization may lead to an increase in the strain within the sclera, potentially most pronounced at the posterior pole. It may cause not only to a reduction in the posterior sclera thickness, but also an enlargement of the peripapillary scleral flange opening (i.e., the optic disc), with a secondary stretching, elongation, and thinning of the lamina cribrosa. It may hold significant importance for the biomechanics of the lamina cribrosa, especially with respect to the increased prevalence of glaucomatous or glaucoma-like optic neuropathy in high myopia.
- The potential enlargement of BM in the equatorial regions in axial myopization may lead to a backward movement of the BM at posterior pole, leading to a compression and thinning of the choroid at the posterior pole.
- A large gamma zone in the temporal parapapillary region, increasing the distance between the retinal ganglion cell nuclei and the optic disc border, may lead to a stretching of the retinal ganglion cell axons in the papillo-macular region, and eventually to their loss, thereby potentially explaining the development of central scotoma in highly myopic eyes without maculopathy.
- Especially in highly myopic eyes, additional forces may be involved, such as an increased tissue pressure due to a compression of retrobulbar orbital fat, caused by the enlarging globe; an increased backward pull by the four rectus muscles the insertion position, which has moved forward due to the forward displacement of the anterior segment of the highly axially elongated globe; and a backward pull by the optic nerve (dura mater) becoming relatively too short to allow a full adduction of a markedly axially elongated eye.

18. Limitations

The limitations of this review must be considered. First, the scope of the topic at hand did not allow for a complete description of all morphological changes occurring in axially elongating, myopic eyes. Similarly, given that the principles of the process of axial elongation remain unknown, we focused on only one possible explanatory mechanism underlying axial elongation, without describing in detail other potential explanations of how axial elongation is associated with certain biomarkers and messenger molecules. That this study neglected other hypotheses, such as those on the role of the choroid and sclera in myopization, does not indicate that these hypotheses are not valid (Barathi and Beuerman, 2011; Guggenheim and McBrien, 1996; Guo, L et al., 2014; Gwiazda et al., 1993; Hung et al., 2018; Jiang, L et al., 2018; Markov et al., 2018; Mutti et al., 2006, 2007, 2011; Nickla and Wallman, 2010; Pan, M et al., 2021; Rymer and Wildsoet, 2005; Siegwart and Norton, 2002; Troilo and Wallman, 1991; Troilo et al., 2019; Wang, KK et al., 2017; Wallman et al., 1978, 1995; Wang, M et al., 2018; Wildsoet and Wallman, 1995; Wong, CW et al., 2017; Wu et al., 2018; Ye et al., 2020; Zhang and Wildsoet, 2015; Zhou, F et al., 2021; Zhou, X et al., 2021).

Second, it has remained elusive whether anatomical features of myopic eyes are effect of or are caused by the process of axial elongation. Third, there may be many counter-arguments against the hypothesis of BM as a driving structure in the process of axial elongation. It has been discussed that the choroid may have a tendency to mold itself to the supporting sclera such that there would be no reason for the development of a suprachoroidal cleavage or choroidal widening in the case the sclera were the structure primarily moving the back of the eye backward. It could hold true even more if BM would follow the choroid and sclera, if the sclera was the structure primarily elongating the globe. It also has to be considered that an enlargement of BM or increased production of basal membrane material by the RPE in the retro-equatorial region has not been directly demonstrated yet. Fourth, it has not generally been accepted yet that the mid-peripheral retina has a regulatory function in the process of emmetropization.

19. Future developments/questions addressable in the future

Some of the topics future studies may address are (1) the biomechanical properties of BM in axially elongated eyes; (2) the effect of measures, such as macula buckling, scleral banding, and scleral stiffening by cross-linking of scleral collagen, on further axial elongation and choroidal thinning (compression); (3) whether peripapillary suprachoroidal cavitations may prevent further optic disc rotation in highly

myopic eyes; (4) whether the BM defects in eyes with angioid streaks differ in some aspects from BM defects in highly myopic eyes; (5) the potential role of the choroid as a buffer for the inner ocular sphere against acceleration- and deceleration-induced whiplash injuries, including the role of the peripapillary choroidal border tissue and the effect of its axial elongation–related thinning and stretching; (6) the biomechanical consequences of a potential rupture of the peripapillary choroidal border tissue, potentially leading to a corrugation of BM; (7) the biomechanical consequence of a globe enlargement in the coronal diameters for the strain within BM, in particular at the posterior pole;

(8) the biomechanical importance of the criss-crossing of the collagenous fibers of the peripapillary border tissue of the peripapillary scleral flange with the collagenous fibers of the scleral flange at the border of the lamina cribrosa; (9) the consequence of an increased strain in BM on the biomechanics of the lamina cribrosa; and (10) the effects and associations of BM defects occurring in non–highly myopic eyes, such as in patients with Stargardt's disease or in eyes with pseudoxanthoma elasticum and peripapillary atrophy (Park, SP et al., 2012; Spaide and Jonas, 2015).

20. Conclusions

In primary myopia, axial elongation–associated non-pathological changes occur predominantly in the posterior half of the eye. Corresponding to a change in the eye shape from a sphere to a prolate ellipsoid, an axial length–related reduction in photoreceptor and RPE cell density and decrease in retinal nuclear layer thickness is most marked at the equator/posterior pole midpoint, followed by the equator region, and least—or not at all—marked at the posterior pole (Table 1). An axial length–associated thinning of the choroid and sclera is most pronounced at the posterior pole and least marked at the ora serrata. These changes in choroidal and scleral thickness occur without a change in choroidal and scleral volume. In contrast, the thickness of BM is not correlated with, and BM volume increases with, longer axial length. In moderate myopia, the BMO may shift, usually in direction to the fovea, leading to an overhanging of BM into the nasal intrapapillary compartment, an absence of BM in the temporal region (i.e., parapapillary gamma zone), an ovalization of the disc shape due to a shortening of the ophthalmoscopically visible horizontal optic disc diameter with a subsequent reduction in the ophthalmoscopical disc size, an elongation of the fovea–optic disc distance (due to the development of gamma zone and without an elongation of the macular BM), a reduction in angle kappa, and a straightening and stretching of the papillomacular retinal blood vessels and retinal nerve fibers. Anatomical characteristics in highly myopic eyes are an enlargement of the BMO with an optic disc enlargement, elongation and thinning of the lamina cribrosa, peripapillary scleral flange (i.e., parapapillary delta zone) and peripapillary choroidal border tissue, and development of circular gamma and delta zones. These features are anatomical characteristics of moderately myopic and highly myopic eyes and may be of interest to describe and better understand the psychophysical effects of myopia on visual acuity and visual field, and may help to further elucidate the mechanism of myopic axial elongation. Future studies may examine whether these anatomical findings can be explained by an enlargement of BM in the equatorial and retro-equatorial region, the location that has been considered the site of the afferent part of the feedback mechanism controlling the processes of emmetropization/myopization and axial elongation.

Funding

None.

Financial interest

Rahul A. Jonas, Jost B. Jonas, Songhomitra Panda-Jonas: European patent EP 3,271,392, JP 2021–119187, and US 2021 0340237 A1: Agents for use in the therapeutic or prophylactic treatment of myopia or hyperopia.

Author statement

Jost B. Jonas: Conceptualization; Data curation; Formal analysis; Investigation; Methodology; Project administration; Resources; Supervision; Validation; Visualization; Writing - original draft; Writing - review & editing.

Rahul A. Jonas: Conceptualization; Data curation; Formal analysis; Investigation; Methodology; Project administration; Resources; Supervision; Validation; Visualization; Writing - original draft; Writing - review & editing.

Mukharram M. Bukbov: Conceptualization; Data curation; Formal analysis; Investigation; Methodology; Project administration; Resources; Supervision; Validation; Visualization; Writing - original draft; Writing - review & editing.

Songhomitra Panda-Jonas: Conceptualization; Data curation; Formal analysis; Investigation; Methodology; Project administration; Resources; Supervision; Validation; Visualization; Writing - original draft; Writing - review & editing.

Data availability

Data will be made available on request.

References

Akagi, T., Hangai, M., Kimura, Y., Ikeda, H.O., Nonaka, A., Matsumoto, A., Akiba, M., Yoshimura, N., 2013. Peripapillary scleral deformation and retinal nerve fiber damage in high myopia assessed with swept-source optical coherence tomography. Am. J. Ophthalmol. 155, 927–936.

Anchan, R.M., Reh, T.A., Angello, J., Balliet, A., Walker, M., 1991. EGF and TGF-alpha stimulate retinal neuroepithelial cell proliferation in vitro. Neuron 6, 923–936.

Anderson, D.R., 1969. Ultrastructure of the human and monkey lamina cribrosa and optic nerve head. Arch. Ophthalmol. 82, 800–814.

Anderson, D.R., 1970. Ultrastructure of the optic nerve head. Arch. Ophthalmol. 83, 63–73.

Anderson, D.R., 1983. Correlation of the peripapillary damage with the disc anatomy and field abnormalities in glaucoma. Doc. Ophthalmol. Proc. Sers. 35, 1–10.

Ang, M., Tan, A.C.S., Cheung, C.M.G., Keane, P.A., Dolz-Marco, R., Sng, C.C.A., Schmetterer, L., 2018. Optical coherence tomography angiography: a review of current and future clinical applications. Graefes Arch. Clin. Exp. Ophthalmol. 256, 237–245.

Araie, M., Sekine, M., Suzuki, Y., Koseki, N., 1994. Factors contributing to the progression of visual field damage in eyes with normal-tension glaucoma. Ophthalmology 101, 1440–1444.

Araie, M., Iwase, A., Sugiyama, K., Nakazawa, T., Tomita, G., Hangai, M., Yanagi, Y., Murata, H., Tanihara, H., Burgoyne, C.F., Chauhan, B.C., 2017. Determinants and characteristics of Bruch's membrane opening and Bruch's membrane opening-minimum rim width in a normal Japanese population. Invest. Ophthalmol. Vis. Sci. 58, 4106–4113.

Asai, T., Ikuno, Y., Akiba, M., Kikawa, T., Usui, S., Nishida, K., 2016. Analysis of peripapillary geometric characters in high myopia using swept-source optical coherence tomography. Invest. Ophthalmol. Vis. Sci. 57, 137–144.

Atchison, D.A., Jones, C.E., Schmid, K.L., Pritchard, N., Pope, J.M., Strugnell, W.E., Riley, R.A., 2004. Eye shape in emmetropia and myopia. Invest. Ophthalmol. Vis. Sci. 45, 3380–3386.

Avetisov, E.S., Savitskaya, N.F., Vinetskaya, M.I., Iomdina, E.N., 1983. A study of biochemical and biomechanical qualities of normal and myopic eye sclera in humans of different age groups. Metab. Pediatr. Syst. Ophthalmol. 7, 183–188.

Al-Sheikh, M., Phasukkijwatana, N., Dolz-Marco, R., Rahimi, M., Iafe, N.A., Freund, K.B., Sadda, S.R., Sarraf, D., 2017. Quantitative OCT angiography of the retinal microvasculature and the choriocapillaris in myopic eyes. Invest. Ophthalmol. Vis. Sci. 58, 2063–2069.

Bak, E., Ha, A., Kim, Y.W., Lee, J., Han, Y.S., Kim, Y.K., Jeoung, J.W., Park, K.H., 2020. Ten years and beyond longitudinal change of ß-zone parapapillary atrophy: comparison of primary open-angle glaucoma with normal eyes. Ophthalmology 127 (8), 1054–1063, 2020 Aug.

Banc, A., Bianchi Marzoli, S., 2022. Parapapillary atrophy in optic neuropathies: histology and clinical relevance. Eur. J. Ophthalmol. 32, 95–101.

Bai, H.X., Mao, Y., Shen, L., Xu, X.L., Gao, F., Zhang, Z.B., Li, B., Jonas, J.B., 2017. Bruch's membrane thickness in relationship to axial length. PLoS One 12, e0182080.

Barathi, V.A., Weon, S.R., Beuerman, R.W., 2009. Expression of muscarinic receptors in human and mouse sclera and their role in the regulation of scleral fibroblasts proliferation. Mol. Vis. 15, 1277–1293.

Barathi, V.A., Beuerman, R.W., 2011. Molecular mechanisms of muscarinic receptors in mouse scleral fibroblasts: prior to and after induction of experimental myopia with atropine treatment. Mol. Vis. 17, 680–692.

Berntsen, D.A., Barr, C.D., Mutti, D.O., Zadnik, K., 2013. Peripheral defocus and myopia progression in myopic children randomly assigned to wear single vision and progressive addition lenses. Invest. Ophthalmol. Vis. Sci. 54, 5761–5770.

Bikbov, M.M., Gilmanshin, T.R., Kazakbaeva, G.M., Zainullin, R.M., Rakhimova, E.M., Rusakova, I.A., Bolshakova, N.I., Safiullina, K.R., Zaynetdinov, A.F., Zinatullin, A.A., Nuriev, I.F., Khalimov, T.A., Panda-Jonas, S., Arslangareeva, I.I., Bikbova, G.M., Yakupova, D.F., Uzianbaeva, Y.V., Jonas, J.B., 2020. Prevalence of myopic maculopathy among adults in a Russian population. JAMA Netw. Open 3, e200567.

Bowd, C., Belghith, A., Rezapour, J., Christopher, M., Hyman, L., Jonas, J.B., Weinreb, R. N., Zangwill, L.M., 2022. Diagnostic accuracy of macular thickness map and texture en-face images for detecting glaucoma in eyes with axial high myopia, 2022 May 2: S0002-9394(22)00168-4 Am. J. Ophthalmol.. https://doi.org/10.1016/j.ajo.2022.04.019 (Online ahead of print).

Bryant, M.R., McDonnell, P.J., 1998. Optical feedback controlled scleral remodeling as a mechanism for myopic eye growth. J. Theor. Biol. 193, 613–622.

Budde, W.M., Velten, I., Jonas, J.B., 1998. Optic disc size and iris color. Arch. Ophthalmol. 116, 545.

Bücklers, M., 1929. Anatomische Untersuchung über die Beziehung zwischen der senilen und myopischen circumpapillären Aderhautatrophie. Unter Beifügen eines Falles von hochgradiger Anisometropie. Arch. Ophthalmol. 121, 243–283.

Burgoyne, C.F., Downs, J.C., Bellezza, A.J., Francis Suh, J.K., Hart, R.T., 2005. The optic nerve head as a biomechanical structure: a new paradigm for understanding the role of IOP-related stress and strain in the pathophysiology of glaucomatous optic nerve head damage. Prog. Retin. Eye Res. 24, 39–73.

Caillaux, V., Gaucher, D., Gualino, V., Massin, P., Tadayoni, R., Gaudric, A., 2013. Morphologic characterization of dome-shaped macula in myopic eyes with serous macular detachment. Am. J. Ophthalmol. 156, 958–967.

Chang, M.Y., Shin, A., Park, J., Nagiel, A., Lalane, R.A., Schwartz, S.D., Demer, J.L., 2017. Deformation of optic nerve head and peripapillary tissues by horizontal duction. Am. J. Ophthalmol. 174, 85–94.

Chang, R.T., Singh, K., 2013. Myopia and glaucoma: diagnostic and therapeutic challenges. Curr. Opin. Ophthalmol. 24, 96–101.

Cheng, D., Ruan, K., Wu, M., Qiao, Y., Gao, W., Lian, H., Shen, M., Bao, F., Yang, Y., Zhu, J., Huang, H., Meng, X., Shen, L., Ye, Y., 2022. Characteristics of the optic nerve head in myopic eyes using swept-source optical coherence tomography. Invest. Ophthalmol. Vis. Sci. 63, 20.

Cheng, H.M., Singh, O.S., Kwong, K.K., Xiong, J., Woods, B.T., Brady, T.J., 1992. Shape of the myopic eye as seen with high resolution magnetic resonance imaging. Optom. Vis. Sci. 69, 698–701.

Cheng, L.B., Chen, C.M., Zhong, H., Zhu, L.J., 2014. Squamosamide derivative FLZ protects retinal pigment epithelium cells from oxidative stress through activation of epidermal growth factor receptor (EGFR)-AKT signaling. Int. J. Mol. Sci. 15, 18762–18775.

Cheng, T., Wang, J., Xiong, S., Zhang, B., Li, Q., Xu, X., He, X., 2020. Association of IGF1 single-nucleotide polymorphisms with myopia in Chinese children. PeerJ 8, e8436.

Cheng, W., Song, Y., Lin, F., Jin, L., Wang, Z., Jonas, J.B., Wang, W., Zhang, X., 2021. Choriocapillaris flow deficits in normal Chinese imaged by swept-source Optical coherence tomographic angiography. Am. J. Ophthalmol. 235, 143–153.

Cheng, W., Wang, W., Song, Y., Gao, X., Lin, F., Li, F., Wang, P., Hu, K., Li, H., Li, Y., Chen, L., Jonas, J.B., Zhang, X., GSHM study group, 2022. Axial length and choriocapillaris flow deficits in non-pathological high myopia, 2022 Aug 12:S0002-9394(22)00309-9 Am. J. Ophthalmol.. https://doi.org/10.1016/j.ajo.2022.08.005 (Online ahead of print).

Cheong, K.X., Xu, L., Ohno-Matsui, K., Sabanayagam, C., Saw, S.M., Hoang, Q.V., 2022. An evidence-based review of the epidemiology of myopic traction maculopathy. Surv. Ophthalmol. 67, 1603–1630.

Cheung, C.M.G., Arnold, J.J., Holz, F.G., Park, K.H., Lai, T.Y.Y., Larsen, M., Mitchell, P., Ohno-Matsui, K., Chen, S.J., Wolf, S., Wong, T.Y., 2017. Myopic choroidal neovascularization: review, guidance, and consensus statement on management. Ophthalmology 124, 1690–1711.

Chi, T., Ritch, R., Stickler, D., Pitman, B., Tsai, C., Hsieh, F.Y., 1989. Racial differences in optic nerve head parameters. Arch. Ophthalmol. 107, 836–839.

Chia, A., Lu, Q.S., Tan, D., 2016. Five-year clinical trial on atropine for the treatment of myopia 2: myopia control with atropine 0.01% eye drops. Ophthalmology 123, 391–399.

Chihara, E., Liu, X., Dong, J., Takashima, Y., Akimoto, M., Hangai, M., Kuriyama, S., Tanihara, H., Hosoda, M., Tsukahara, S., 1997. Severe myopia as a risk factor for progressive visual field loss in primary open-angle glaucoma. Ophthalmologica 211, 66–71.

Chua, S.Y.L., Dhillon, B., Aslam, T., Balaskas, K., Yang, Q., Keane, P.A., Tufail, A., Reisman, C., Foster, P.J., Patel, P.J., , UK Biobank Eye, Consortium, Vision, 2019. Associations with photoreceptor thickness measures in the UK Biobank. Sci. Rep. 9, 19440.

Chua, W.H., Balakrishnan, V., Chan, Y.H., Tong, L., Ling, Y., Quah, B.L., Tan, D., 2006. Atropine for the treatment of childhood myopia. Ophthalmology 113, 2285–2291.

Chui, T.Y., Yap, M.K., Chan, H.H., Thibos, L.N., 2005. Retinal stretching limits peripheral visual acuity in myopia. Vision Res 45, 593–605.

Coco, R.M., Sanabria, M.R., Alegria, J., 2012. Pathology associated with optical coherence tomography macular bending due to either dome-shaped macula or inferior staphyloma in myopic patients. Ophthalmologica 228, 7–12.

Cohen, S.Y., Vignal-Clermont, C., Trinh, L., Ohno-Matsui, K., 2022. Tilted disc syndrome (TDS): new hypotheses for posterior segment complications and their implications in other retinal diseases. Prog. Retin. Eye Res. 88, 101020.

Coudrillier, B., Tian, J., Alexander, S., Myers, K.M., Quigley, H.A., Nguyen, T.D., 2012. Biomechanics of the human posterior sclera: age- and glaucoma-related changes measured using inflation testing. Invest. Ophthalmol. Vis. Sci. 53, 1714–1728.

Curcio, C.A., Johnson, M., 2012. In: Ryan, S.J., Schachat, A.P., Wilkinson, C.P., Hinton, D.R., Sadda, S.R., Wiedemann, P. (Eds.), Structure, Function and Pathology of Bruch's Membrane, Retina fifth ed. Saunders Co. (Chapter 20).

Curtin, B.J., 1977. The posterior staphyloma of pathologic myopia. Trans. Am. Ophthalmol. Soc. 75 (1977), 67–86.

Dabir, S., Mangalesh, S., Schouten, J.S., Berendschot, T.T., Kurian, M.K., Kumar, A.K., Yadav, N.K., Shetty, R., 2015. Axial length and cone density as assessed with adaptive optics in myopia. Indian J. Ophthalmol. 63, 423–426.

Dai, Y., Jonas, J.B., Ling, Z., Sun, X., 2013a. Parapapillary gamma zone hole. J. Glaucoma 22, e33–e35.

Dai, Y., Jonas, J.B., Huang, H., Wang, M., Sun, X., 2013b. Microstructure of parapapillary atrophy: beta zone and gamma zone. Invest. Ophthalmol. Vis. Sci. 54, 2013–2018.

Dai, Y., Jonas, J.B., Ling, Z., Wang, X., Sun, X., 2015a. Unilateral peripapillary intrachoroidal cavitation and optic disc rotation. Retina 35, 655–659.

Dai, Y., Jonas, J.B., Ling, Z., Sun, X., 2015b. Ophthalmoscopic-perspectively distorted optic disc diameters and real disc diameters. Invest. Ophthalmol. Vis. Sci. 56, 7076–7083.

Defoe, D.M., Grindstaff, R.D., 2004. Epidermal growth factor stimulation of RPE cell survival: contribution of phosphatidylinositol 3-kinase and mitogen-activated protein kinase pathways. Exp. Eye Res. 79, 51–59.

Deng, J., Jin, J., Lv, M., Jiang, W., Sun, S., Yao, C., Zhu, J., Zou, H., Wang, L., He, X., Xu, X., 2019. Distribution of scleral thickness and associated factors in 810 Chinese children and adolescents: a swept-source optical coherence tomography study. Acta Ophthalmol. 97, e410–e418.

Demer, J.L., 2016. Optic nerve sheath as a novel mechanical load on the globe in ocular duction. Invest. Ophthalmol. Vis. Sci. 57, 1826–1838.

De Moraes, C.G., Murphy, J.T., Kaplan, C.M., Reimann, J.J., Skaat, A., Blumberg, D.M., Al-Aswad, L., Cioffi, G.A., Girkin, C.A., Medeiros, F.A., Weinreb, R.N., Zangwill, L., Liebmann, J.M., 2017. β-Zone parapapillary atrophy and rates of glaucomatous visual field progression: African Descent and Glaucoma Evaluation Study. JAMA Ophthalmol 135, 617–623.

Dhakal, R., Vupparaboina, K.K., Verkicharla, P.K., 2020. Anterior sclera undergoes thinning with increasing degree of myopia. Invest. Ophthalmol. Vis. Sci. 61, 6.

Dichtl, A., Jonas, J.B., Naumann, G.O.H., 1998. Histomorphometry of the optic disc in highly myopic eyes with glaucoma. Br. J. Ophthalmol. 82, 286–289.

Dong, L., Shi, X.H., Kang, Y.K., Wei, W.B., Wang, Y.X., Xu, X.L., Gao, F., Jonas, J.B., 2019a. Bruch's membrane thickness and retinal pigment epithelium cell density in experimental axial elongation. Sci. Rep. 9, 6621.

Dong, L., Shi, X.H., Kang, Y.K., Wei, W.B., Wang, Y.X., Xu, X.L., Gao, F., Yuan, L.H., Zhen, J., Jiang, W.J., Jonas, J.B., 2019b. Amphiregulin and ocular axial length. Acta Ophthalmol. 97, e460–e470.

Dong, L., Shi, X.H., Li, Y.F., Jiang, X., Wang, Y.X., Li, Y., Lan, Y.J., Wu, H.T., Gao, F., Xu, X.L., Jonas, J.B., Wei, W.B., 2020. Blockade of epidermal growth factor and its receptor and axial elongation in experimental myopia. Faseb. J. 34, 13654–13670.

Dong, L., Zhang, R.H., Zhou, W.D., Li, Y.F., Li, H.Y., Wu, H.T., Shi, X.H., Jonas, J.B., Wei, W.B., 2022. Epiregulin, epigen and betacellulin antibodies and axial elongation in young Guinea pigs with lens-induced myopization. BMC Ophthalmol. 22, 193.

Du, R., Fang, Y., Jonas, J.B., Yokoi, T., Takahashi, H., Uramoto, K., Kamoi, K., Yoshida, T., Ohno-Matsui, K., 2020. Clinical features of patchy chorioretinal atrophy in pathological myopia. Retina 40, 951–959.

Du, R., Xie, S., Igarashi-Yokoi, T., Watanabe, T., Uramoto, K., Takahashi, H., Nakao, N., Yoshida, T., Fang, Y., Ohno-Matsui, K., 2021. Continued increase of axial length and its risk factors in adults with high myopia. JAMA Ophthalmol 139, 1096–1103.

Ellabban, A.A., Tsujikawa, A., Matsumoto, A., Yamashiro, K., Oishi, A., Ooto, S., Nakata, I., Akagi-Kurashige, Y., Miyake, M., Elnahas, H.S., Radwan, T.M., Zaky, K.A., Yoshimura, N., 2013. Three-dimensional tomographic features of dome-shaped macula by swept-source optical coherence tomography. Am. J. Ophthalmol. 155, 320–328.

Eckmann-Hansen, C., Hansen, M.H., Laigaard, P.P., Sander, B.A., Munch, I.C., Olsen, E. M., Skovgaard, A.M., Larsen, M., 2021. Cone photoreceptor density in the Copenhagen Child Cohort at age 16-17 years. Ophthalmic Physiol. Opt. 41, 1292–1299.

Elschnig, A., 1900. Das Colobom am Sehnerveneintritte und der Conus nach unten. Arch. Ophthalmol. 51, 391–430.

Elschnig, A., 1901. Der normale Sehnerveneintritt des menschlichen Auges. Denkschrift der kais Akad der Wiss. Wien, Math.-Naturw. Kl. 70, 219–310.

Elsheikh, A., Alhasso, D., Rama, P., 2008. Biomechanical properties of human and porcine corneas. Exp. Eye Res. 86, 783–790.

Errera, M.H., Michaelides, M., Keane, P.A., Restori, M., Paques, M., Moore, A.T., Yeoh, J., Chan, D., Egan, C.A., Patel, P.J., Tufail, A., 2014. The extended clinical phenotype of dome-shaped macula. Graefes Arch. Clin. Exp. Ophthalmol. 252, 499–508.

Fantes, F.E., Anderson, D.R., 1989. Clinical histologic correlation of human peripapillary anatomy. Ophthalmology 96, 20–25.

Fang, Y., Jonas, J.B., Yokoi, T., Cao, K., Shinohara, K., Ohno-Matsui, K., 2017. Macular Bruch's membrane defect and dome-shaped macula in high myopia. PLoS One 12, e0178998.

Fang, Y., Yokoi, T., Nagaoka, N., Shinohara, K., Onishi, Y., Ishida, T., Yoshida, T., Xu, X., Jonas, J.B., Ohno-Matsui, K., 2018. Progression of myopic maculopathy during 18-year follow-up. Ophthalmology 125, 863–877.

Fang, Y., Du, R., Jonas, J.B., Watanabe, T., Uramoto, K., Yokoi, T., Onishi, Y., Yoshida, T., Kamoi, K., Ohno-Matsui, K., 2020. Ridge-shaped macula progressing to Bruch membrane defects and macular suprachoroidal cavitation. Retina 40, 456–460.

Faridi, O.S., Park, S.C., Kabadi, R., Su, D., De Moraes, C.G., Liebmann, J.M., Ritch, R., 2014. Effect of focal lamina cribrosa defect on glaucomatous visual field progression. Ophthalmology 121, 1524–1530.

Flaxman, S.R., Bourne, R.R.A., Resnikoff, S., Ackland, P., Braithwaite, T., Cicinelli, M.V., Das, A., Jonas, J.B., Keeffe, J., Kempen, J.H., Leasher, J., Limburg, H., Naidoo, K., Pesudovs, K., Silvester, A., Stevens, G.A., Tahhan, N., Wong, T.Y., Taylor, H.R., Vision Loss Expert Group of the Global Burden of Disease Study, 2017. Global causes of blindness and distance vision impairment 1990-2020: a systematic review and meta-analysis. Lancet Global Health 5, e1221–e1234.

Fledelius, H.C., Jacobsen, N., Li, X.Q., Goldschmidt, E., 2019. The Longitudinal Danish High Myopia Study, Cohort 1948: at age 66 years visual ability is only occasionally affected by visual field defects. Acta Ophthalmol. 97, 36–43.

Flitcroft, D.I., He, M., Jonas, J.B., Jong, M., Naidoo, K., Ohno-Matsui, K., Rahi, J., Resnikoff, S., Vitale, S., Yannuzzi, L., 2019. MI - defining and classifying myopia: a proposed set of standards for clinical and epidemiologic studies. Invest. Ophthalmol. Vis. Sci. 60, M20–M30.

Flores-Moreno, I., Lugo, F., Duker, J.S., Ruiz-Moreno, J.M., 2013. The relationship between axial length and choroidal thickness in eyes with high myopia. Am. J. Ophthalmol. 155, 314–319 e1.

Freund, K.B., Ciardella, A.P., Yannuzzi, L.A., Pece, A., Goldbaum, M., Kokame, G.T., Orlock, D., 2003. Peripapillary detachment in pathologic myopia. Arch. Ophthalmol. 121, 197–204.

Friberg, T.R., Lace, J.W., 1988. A comparison of the elastic properties of human choroid and sclera. Exp. Eye Res. 47, 429–436.

Fujiwara, T., Imamura, Y., Margolis, R., Slakter, J.S., Spaide, R.F., 2009. Enhanced depth imaging optical coherence tomography of the choroid in highly myopic eyes. Am. J. Ophthalmol. 148, 445–450.

Gao, Q., Liu, Q., Ma, P., Zhong, X., Wu, J., Ge, J., 2006. Effects of direct intravitreal dopamine injections on the development of lid-suture induced myopia in rabbits. Graefes Arch. Clin. Exp. Ophthalmol. 244, 1329–1335.

García-Zamora, M., Flores-Moreno, I., Ruiz-Medrano, J., Vega-González, R., Puertas, M., Almazán-Alonso, E., González-Buendía, L., Ruiz-Moreno, J.M., 2021. Dome-shaped macula versus ridge-shaped macula eyes in high myopia based on the 12-line radial optical coherence tomography scan pattern. Differences in clinical features. Diagnostics 11, 1864.

Garway-Heath, D.F., Crabb, D.P., Bunce, C., Lascaratos, G., Amalfitano, F., Anand, N., et al., 2015. Latanoprost for open-angle glaucoma (UKGTS): a randomised, multicentre, placebo-controlled trial. Lancet 385, 1295–1304.

Gaucher, D., Erginay, A., Lecleire-Collet, A., Haouchine, B., Puech, M., Cohen, S.Y., Massin, P., Gaudric, A., 2008. Dome-shaped macula in eyes with myopic posterior staphyloma. Am. J. Ophthalmol. 145, 909–914.

Ghazi, N.G., Dibernardo, C., Ying, H., Mori, K., Gehlbach, P.L., 2006. Optical coherence tomography of peripheral retinal lesions in enucleated human eye specimens with histologic correlation. Am. J. Ophthalmol. 141, 740–742.

Ghorbani Mojarrad, N., Plotnikov, D., Williams, C., Guggenheim, J.A., , UK Biobank Eye, Consortium, Vision, 2020. Association between polygenic risk score and risk of myopia. JAMA Ophthalmol 138, 7–13.

Girard, M.J.A., Downs, J.C., Bottlang, M., Burgoyne, C.F., Suh, J.K., 2009. Peripapillary and posterior scleral mechanics—part ii: experimental and inverse finite element characterization. J. Biomech. Eng. 131, 051012.

Girkin, C.A., Fazio, M.A., Yang, H., Reynaud, J., Burgoyne, C.F., Smith, B., Wang, L., Downs, J.C., 2017. Variation in the three-dimensional histomorphometry of the normal human optic nerve head with age and race: lamina cribrosa and peripapillary scleral thickness and position. Invest. Ophthalmol. Vis. Sci. 58, 3759–3769.

Grossniklaus, H.E., Green, W.R., 1992. Pathologic findings in pathologic myopia. Retina 12, 127–133.

Guggenheim, J.A., McBrien, N.A., 1996. Form-deprivation myopia induces activation of scleral matrix metalloproteinase-2 in tree shrew. Invest. Ophthalmol. Vis. Sci. 37, 1380–1395.

Guo, X., Xiao, O., Chen, Y., Wu, H., Chen, L., Morgan, I.G., He, M., 2017. Three-dimensional eye shape, myopic maculopathy, and visual acuity: the Zhongshan ophthalmic center-brien holden vision institute high myopia cohort study. Ophthalmology 124, 679–687.

Guo, L., Frost, M.R., Siegwart Jr., J.T., Norton, T.T., 2014. Scleral gene expression during recovery from myopia compared with expression during myopia development in tree shrew. Mol. Vis. 20, 1643–1659.

Guo, Y., Liu, L.J., Xu, L., Lv, Y.Y., Tang, P., Feng, Y., Zhou, J.Q., Meng, M., Jonas, J.B., 2015. Optic disc ovality in primary school children in Beijing. Invest. Ophthalmol. Vis. Sci. 56, 4547–4553.

Guo, Y., Liu, L.J., Tang, P., Feng, Y., Lv, Y.Y., Wu, M., Xu, L., Jonas, J.B., 2018a. Parapapillary gamma zone and progression of myopia in school children: the Beijing Children Eye Study. Invest. Ophthalmol. Vis. Sci. 59, 1609–1616.

Guo, Y., Liu, L.J., Tang, P., Feng, Y., Wu, M., Lv, Y.Y., Xu, L., Jonas, J.B., 2018b. Optic disc-fovea distance and myopia progression in school children: the Beijing Children Eye Study. Acta Ophthalmol. 96, e606–e613.

Guo, Y., Liu, L., Tang, P., Lv, Y., Wu, M., Liang, X., Zhang, L., Jonas, J.B., Wang, Y., 2021. Progression of myopic maculopathy in Chinese children with high myopia: a long-term follow-up study. Retina 41, 1502–1511.

Guymer, R., Luthert, P., Bird, A., 1999. Changes in Bruch's membrane and related structures with age. Prog. Retin. Eye Res. 18, 59–90.

Guymer, R., Bird, A., 2006. Age changes in Bruch's membrane and related structures. In: Ryan, S.J. (Ed.), Retina. Mosby, St Louis, pp. 1030–1039.

Gwiazda, J., Thorn, F., Bauer, J., Held, R., 1993. Myopic children show insufficient accommodative response to blur. Invest. Ophthalmol. Vis. Sci. 34, 690–694.

Ha, A., Kim, C.Y., Shim, S.R., Chang, I.B., Kim, Y.K., 2022. Degree of myopia and glaucoma risk: a dose-response meta-analysis. Am. J. Ophthalmol. 236, 107–119.

Haarman, A.E.G., Enthoven, C.A., Tideman, J.W.L., Tedja, M.S., Verhoeven, V.J.M., Klaver, C.C.W., 2020. The complications of myopia: a review and meta-analysis. Invest. Ophthalmol. Vis. Sci. 61, 49.

Haarman, A.E.G., Tedja, M.S., Brussee, C., Enthoven, C.A., van Rijn, G.A., Vingerling, J. R., Keunen, J.E.E., Boon, C.J.F., Geerards, A.J.M., Luyten, G.P.M., Verhoeven, V.J. M., Klaver, C.C.W., 2022a. Prevalence of myopic macular features in Dutch individuals of European ancestry with high myopia. JAMA Ophthalmol 140, 115–123.

Haarman, A.E.G., Thiadens, A.A.H.J., van Tienhoven, M., Loudon, S.E., de Klein, J.E.M. M.A., Brosens, E., Polling, J.R., van der Schoot, V., Bouman, A., Kievit, A.J.A., Hoefsloot, L.H., Klaver, C.C.W., Verhoeven, V.J.M., 2022b. Whole exome sequencing of known eye genes reveals genetic causes for high myopia. Hum. Mol. Genet. 31, 3290–3298.

Harder, B.C., von Baltz, S., Schlichtenbrede, F.C., Jendritza, W., Jendritza, B., Jonas, J.B., 2013. Intravitreal bevacizumab for retinopathy of prematurity: refractive error results. Am. J. Ophthalmol. 155, 1119–1124.

Harper, A.R., Summers, J.A., 2015. The dynamic sclera: extracellular matrix remodeling in normal ocular growth and myopia development. Exp. Eye Res. 133, 100–111.

Hashimoto, S., Yasuda, M., Fujiwara, K., Ueda, E., Hata, J., Hirakawa, Y., Ninomiya, T., Sonoda, K.H., 2019. Association between axial length and myopic maculopathy: the Hisayama Study. Ophthalmol. Retina 3, 867–873.

Hayashi, K., Tomidokoro, A., Lee, K.Y.C., Konno, S., Saito, H., Mayama, C., Aihara, M., Iwase, A., Araie, M., 2012. Spectral-domain optical coherence tomography of β-zone peripapillary atrophy: influence of myopia and glaucoma. Invest. Ophthalmol. Vis. Sci. 53, 1499–1505.

Hayashi, M., Ito, Y., Takahashi, A., Kawano, K., Terasaki, H., 2013. Scleral thickness in highly myopic eyes measured by enhanced depth imaging optical coherence tomography. Eye 27, 410–417.

Hayreh, S.S., 1974. Anatomy and physiology of the optic nerve head. Trans. Am. Acad. Ophthalmol. Otolaryngol. 78, OP240–254.

Hayreh, S.S., Vrabec, F., 1966. The structure of the head of the optic nerve in rhesus monkey. Am. J. Ophthalmol. 61, 136–150.

Heine, L., 1899. Beiträge zur Anatomie des myopischen Auges. Arch. Augenheilkd. 38, 277–290.

Hogan, M.J., Alvarado, J.A., Weddell, J.E., 1971. Histology of the Human Eye. An Atlas and Textbook. Saunders, Philadelphia, p. 606 (Chapter 10) Optic nerve, 523.537,544,561.

Hong, S., Yang, H., Gardiner, S.K., Luo, H., Hardin, C., Sharpe, G.P., Caprioli, J., Demirel, S., Girkin, C.A., Liebmann, J.M., Mardin, C.Y., Quigley, H.A., Scheuerle, A. F., Fortune, B., Chauhan, B.C., Burgoyne, C.F., 2019. OCT-detected optic nerve head neural canal direction, obliqueness, and minimum cross-sectional area in healthy eyes. Am. J. Ophthalmol. 208, 185–205.

Horn, F., Jonas, J.B., Jünemann, A., Korth, M., Gründler, A.E., 1997. The full-field flicker test in early diagnosis of chronic open-angle glaucoma. Am. J. Ophthalmol. 123, 313–319.

Hoseini-Yazdi, H., Vincent, S.J., Collins, M.J., Read, S.A., Alonso-Caneiro, D., 2019. Wide-field choroidal thickness in myopes and emmetropes. Sci. Rep. 9, 3474.

How, A.C., Tan, G.S., Chan, Y.H., Wong, T.T.L., Seah, S.K., Foster, P.J., Aung, T., 2009. Population prevalence of tilted and torted optic discs among an adult Chinese population in Singapore: the Tanjong Pagar Study. Arch. Ophthalmol. 127, 894–899.

Hu, X., Dai, Y., Jonas, J., Sun, X., 2016. Peripapillary gamma zone pit as dehiscence between Elschnig's border tissue and Bruch's membrane with herniation and defect of the retinal nerve fiber layer. BMC Ophthalmol. 16, 143.

Hu, X., Shang, K., Chen, X., Sun, X., Dai, Y., 2021. Clinical features of microvasculature in subzones of parapapillary atrophy in myopic eyes: an OCT-angiography study. Eye 35, 455–463.

Hung, L.F., Arumugam, B., She, Z., Ostrin, L., Smith 3rd, E.L., 2018. Narrow-band, long-wavelength lighting promotes hyperopia and retards vision-induced myopia in infant rhesus monkeys. Exp. Eye Res. 176, 147–160.

Hwang, Y.H., Yoo, C., Kim, Y.Y., 2012. Myopic optic disc tilt and the characteristics of peripapillary retinal nerve fiber layer thickness measured by spectral-domain optical coherence tomography. J. Glaucoma 21, 260–265.

Ikuno, Y., Tano, Y., 2009. Retinal and choroidal biometry in highly myopic eyes with spectral-domain optical coherence tomography. Invest. Ophthalmol. Vis. Sci. 50, 3876–3880.

Imamura, Y., Iida, T., Maruko, I., Zweifel, S.A., Spaide, R.F., 2011. Enhanced depth imaging optical coherence tomography of the sclera in dome-shaped macula. Am. J. Ophthalmol. 151, 297–302.

Jacoby, E., 1905. Über die Neuroglia des Sehnerven. Klein. Mbl. Augenheilk. 43, 129–137.

Javitt, J.C., Spaeth, G.L., Katz, L.J., Poryzees, E., Addiego, R., 1990. Acquired pits of the optic nerve. Increased prevalence in patients with low-tension glaucoma. Ophthalmology 97, 1038–1044.

Jiang, L., Long, K., Schaeffel, F., Zhou, X., Zheng, Y., Ying, H., Lu, F., Stell, W.K., Qu, J., 2014. Effects of dopaminergic agents on progression of naturally occurring myopia in albino Guinea pigs (Cavia porcellus). Invest. Ophthalmol. Vis. Sci. 55, 7508–7519.

Jiang, L., Zhang, S., Chen, R., Ma, L., Wang, X., Wen, Y., Qu, J., Zhou, X., 2018. Effects of the tyrosinase-dependent dopaminergic system on refractive error development in Guinea pigs. Invest. Ophthalmol. Vis. Sci. 59, 4631–4638.

Jiang, W.J., Song, H.X., Li, S.Y., Guo, B., Wu, J.F., Li, G.P., Guo, D.D., Shi, L., Bi, H.S., Jonas, J.B., 2017. Amphiregulin antibody and reduction of axial elongation in experimental myopia. EBioMedicine 17, 134–144.

Jiang, Y., Lou, S., Li, Y., Chen, Y., Lu, T.C., 2021. High myopia and macular vascular density: an optical coherence tomography angiography study. BMC Ophthalmol. 21, 407.

Jobling, A.I., Wan, R., Gentle, A., Bui, B.V., McBrien, N.A., 2009. Retinal and choroidal TGF-beta in the tree shrew model of myopia: isoform expression, activation and effects on function. Exp. Eye Res. 88, 458–466.
Jonas, J.B., 2005. Optic disk size correlated with refractive error. Am. J. Ophthalmol. 139, 346–348.
Jonas, J.B., Dichtl, A., 1997. Optic disc morphology in myopic primary open-angle glaucoma. Graefes Arch. Clin. Exp. Ophthalmol. 235, 627–633.
Jonas, J.B., Jonas, S.B., 2010. Histomorphometry of the circular arterial ring of Zinn-Haller in normal and glaucomatous eyes. Acta Ophthalmol. 88, e317–e322.
Jonas, J.B., Naumann, G.O.H., 1987. Papillengruben in großen papillae nervi optici. Papillometrische charakteristika in 15 Augen. Klin. Monatsbl. Augenheilkd. 191, 287–291.
Jonas, J.B., Königsreuther, K.A., 1994. Macrodiscs in eyes with flat and large corneas. Ger. J. Ophthalmol. 3, 179–181.
Jonas, J.B., Panda-Jonas, S., 2016. Secondary Bruch's membrane defects and scleral staphyloma in toxoplasmosis. Acta Ophthalmol. 94, e664–e666.
Jonas, J.B., Gusek, G.C., Naumann, G.O.H., 1988a. Optic disc, cup and neuroretinal rim size, configuration, and correlations in normal eyes. Invest. Ophthalmol. Vis. Sci. 29, 1151–1158.
Jonas, J.B., Gusek, G.C., Naumann, G.O.H., 1988b. Optic disk morphometry in high myopia. Graefes Arch. Clin. Exp. Ophthalmol. 226, 587–590.
Jonas, J.B., Gusek, G.C., Guggenmoos-Holzmann, I., Naumann, G.O.H., 1988c. Size of the optic nerve scleral canal and comparison with intravital determination of optic disk dimensions. Graefes Arch. Clin. Exp. Ophthalmol. 226, 213–215.
Jonas, J.B., Koniszewski, G., Naumann, G.O.H., 1989a. Morning-Glory-Syn¬drom" bzw. "Handmannsche Anomalie" in kongenitalen Makropapil¬len. Extremvariante "konfluierender Papillengruben. Klin. Monatsbl. Augenheilkd. 195, 371–374.
Jonas, J.B., Nguyen, X.N., Gusek, G.C., Naumann, G.O.H., 1989b. Parapapillary chorioretinal atrophy in normal and glaucoma eyes. I. Morphometric data. Invest. Ophthalmol. Vis. Sci. 30, 908–918.
Jonas, J.B., Gusek, G.C., Fernández, M.C., 1991. Correlation of the blind spot size to the area of the optic disc and parapapillary atrophy. Am. J. Ophthalmol. 111, 559–565.
Jonas, J.B., Königsreuther, K.A., Naumann, G.O.H., 1992a. Optic disc histomorphometry in normal eyes and eyes with secondary angle-closure glaucoma. I. Intrapapillary region. Graefes Arch. Clin. Exp. Ophthalmol. 230, 129–133.
Jonas, J.B., Fernández, M.C., Naumann, G.O.H., 1992b. Glaucomatous parapapillary atrophy. Occurrence and correlations. Arch. Ophthalmol. 110, 214–222.
Jonas, J.B., Budde, W.M., Panda-Jonas, S., 1999. Ophthalmoscopic evaluation of the optic nerve head. Surv. Ophthalmol. 43, 293–320.
Jonas, J.B., Budde, W.M., 2000. Diagnosis and pathogenesis of glaucomatous optic neuropathy: morphological aspects. Prog. Retin. Eye Res. 19, 1–40.
Jonas, J.B., Budde, W.M., Németh, J., Gründler, A.E., Mistlberger, A., Hayler, J.K., 2001. Central retinal vessel trunk exit and location of glaucomatous parapapillary atrophy in glaucoma. Ophthalmology 108, 1059–1064.
Jonas, J.B., Martus, P., Budde, W.M., 2002. Anisometropia and degree of optic nerve damage in chronic open-angle glaucoma. Am. J. Ophthalmol. 134, 547–551.
Jonas, J.B., Berenshtein, E., Holbach, L., 2003. Anatomic relationship between lamina cribrosa, intraocular space, and cerebrospinal fluid space. Invest. Ophthalmol. Vis. Sci. 44, 5189–5195.
Jonas, J.B., Berenshtein, E., Holbach, L., 2004. Lamina cribrosa thickness and spatial relationships between intraocular space and cerebrospinal fluid space in highly myopic eyes. Invest. Ophthalmol. Vis. Sci. 45, 2660–2665.
Jonas, J.B., Jonas, S.B., Jonas, R.A., Holbach, L., Panda-Jonas, S., 2011. Histology of the parapapillary region in high myopia. Am. J. Ophthalmol. 152, 1021–1029.
Jonas, J.B., Jonas, S.B., Jonas, R.A., Holbach, L., Dai, Y., Sun, X., Panda-Jonas, S., 2012. Parapapillary atrophy: histological gamma zone and delta zone. PLoS One 7, e47237.
Jonas, J.B., Ohno-Matsui, K., Spaide, R.F., Holbach, L., Panda-Jonas, S., 2013a. Macular Bruch's membrane defects and axial length: association with gamma zone and delta zone in peripapillary region. Invest. Ophthalmol. Vis. Sci. 54, 1295–1302.
Jonas, J.B., Holbach, L., Panda-Jonas, S., 2013b. Peripapillary arterial circle of Zinn-Haller: location and spatial relationships. PLoS One 8, e78867.
Jonas, J.B., Holbach, L., Panda-Jonas, S., 2014a. Scleral cross section area and volume and axial length. PLoS One 9, e93551.
Jonas, J.B., Holbach, L., Panda-Jonas, S., 2014b. Bruch's membrane thickness in high myopia. Acta Ophthalmol. 92, e470–e474.
Jonas, J.B., Holbach, L., Panda-Jonas, S., 2014c. Peripapillary ring: histology and correlations. Acta Ophthalmol. 92, e273–e279.
Jonas, J.B., Wang, Y.X., Zhang, Q., Liu, Y., Xu, L., Wei, W.B., 2015. Macular Bruch's membrane length and axial length. The Beijing Eye Study. PLoS One 10, e0136833.
Jonas, J.B., Dai, Y., Panda-Jonas, S., 2016a. Peripapillary suprachoroidal cavitation, parapapillary gamma zone and optic disc rotation due to the biomechanics of the optic nerve dura mater. Invest. Ophthalmol. Vis. Sci. 57, 4373.
Jonas, J.B., Wang, Y.X., Zhang, Q., Fan, Y.Y., Xu, L., Wei, W.B., Jonas, R.A., 2016b. Parapapillary gamma zone and axial elongation-associated optic disc rotation: the Beijing Eye Study. Invest. Ophthalmol. Vis. Sci. 57, 396–402.
Jonas, J.B., Holbach, L., Panda-Jonas, S., 2016c. Histologic differences between primary high myopia and secondary high myopia due to congenital glaucoma. Acta Ophthalmol. 94, 147–153.
Jonas, J.B., Xu, L., Wei, W.B., Pan, Z., Yang, H., Holbach, L., Panda-Jonas, S., Wang, Y.X., 2016d. Retinal thickness and axial length. Invest. Ophthalmol. Vis. Sci. 57, 1791–1797.
Jonas, J.B., Weber, P., Nagaoka, N., Ohno-Matsui, K., 2017a. Glaucoma in high myopia and parapapillary delta zone. PLoS One 12, e0175120.
Jonas, J.B., Ohno-Matsui, K., Jiang, W.J., Panda-Jonas, S., 2017b. Bruch membrane and the mechanism of myopization: a new theory. Retina 37, 1428–1440.
Jonas, J.B., Ohno-Matsui, K., Holbach, L., Panda-Jonas, S., 2017c. Retinal pigment epithelium cell density in relationship to axial length in human eyes. Acta Ophthalmol. 95, e22–e28.
Jonas, J.B., Ohno-Matsui, K., Holbach, L., Panda-Jonas, S., 2017d. Association between axial length and horizontal and vertical globe diameters. Graefes Arch. Clin. Exp. Ophthalmol. 255, 237–242.
Jonas, J.B., Aung, T., Bourne, R.R., Bron, A.M., Ritch, R., Panda-Jonas, S., 2017e. Glaucoma. Lancet 390, 2183–2193.
Jonas, J.B., Ohno-Matsui, K., Panda-Jonas, S., 2017f. Optic nerve head histopathology in high axial myopia. J. Glaucoma 26, 187–193.
Jonas, J.B., Nangia, V., Gupta, R., Bhojwani, K., Nangia, P., Panda-Jonas, S., 2017g. Prevalence of myopic retinopathy in rural Central India. Acta Ophthalmol. 95, e399–e404.
Jonas, J.B., Nagaoka, N., Fang, Y.X., Weber, P., Ohno-Matsui, K., 2017h. Intraocular pressure and glaucomatous optic neuropathy in high myopia. Invest. Ophthalmol. Vis. Sci. 58, 5897–5906.
Jonas, J.B., Weber, P., Nagaoka, N., Ohno-Matsui, K., 2018a. Temporal vascular arcade width and angle in high myopia. Retina 38, 1839–1847.
Jonas, J.B., Jonas, R.A., Ohno-Matsui, K., Holbach, L., Panda-Jonas, S., 2018b. Corrugated Bruch's membrane in high myopia. Acta Ophthalmol. 96, e147–e151.
Jonas, J.B., Fang, Y., Weber, P., Ohno-Matsui, K., 2018c. Parapapillary gamma and delta zones in high myopia. Retina 38, 931–938.
Jonas, J.B., Ohno-Matsui, K., Panda-Jonas, S., 2019. Myopia: anatomic changes and consequences for its etiology. Asia Pac. J. Ophthalmol. (Phila). 8, 355–359.
Jonas, J.B., Ohno-Matsui, K., Holbach, L., Panda-Jonas, S., 2020a. Histology of myopic posterior scleral staphylomas. Acta Ophthalmol. 98, e856–e863.
Jonas, J.B., Li, D., Holbach, L., Panda-Jonas, S., 2020b. Retinal pigment epithelium cell density and Bruch's membrane thickness in secondary versus primary high myopia and emmetropia. Sci. Rep. 10 (2020), 5159.
Jonas, J.B., Wang, Y.X., Dong, L., Panda-Jonas, S., 2020c. High myopia and glaucoma-like optic neuropathy. Asia Pac J Ophthalmol (Phila). 9, 234–238.
Jonas, J.B., Panda-Jonas, S., Wang, Y.X., 2020d. Glaucoma neurodegeneration and myopia. Prog. Brain Res. 257, 1–17.
Jonas, J.B., Yan, Y.N., Zhang, Q., Jonas, R.A., Wang, Y.X., 2021. Choroidal shift in myopic eyes in the 10-year follow-up Beijing eye study. Sci. Rep. 11, 14658.
Jonas, J.B., Xu, L., Wei, W.B., Jonas, R.A., Wang, Y.X., 2022a. Progression and associated factors of lacquer cracks/patchy atrophies in high myopia: the Beijing Eye Study 2001-2011, 2022 May 24 Graefes Arch. Clin. Exp. Ophthalmol.. https://doi.org/10.1007/s00417-022-05705-7 (Online ahead of print).
Jonas, J.B., Yan, Y.N., Zhang, Q., Zhang, Q., Wei, W.B., Jonas, R.A., Wang, Y.X., 2022b. Retinal nerve fibre layer thickness in association with gamma zone width and disc-fovea distance, 2022 Jan 25 Acta Ophthalmol.. https://doi.org/10.1111/aos.15088 (Online ahead of print).
Jonas, J.B., Zhang, Q., Xu, L., Wei, W.B., Jonas, R.A., Wang, Y.X., 2022c. Change in the ophthalmoscopical optic disc size and shape in a 10-year follow-up: the Beijing Eye Study 2001-2011, 2021 Sep 2:bjophthalmol-2021-319632 Br. J. Ophthalmol.. https://doi.org/10.1136/bjophthalmol-2021-319632 (Online ahead of print).
Jonas, J.B., Zhang, Q., Xu, L., Wei, W.B., Jonas, R.A., Wang, Y.X., 2022d. Parapapillary gamma zone enlargement in a 10-year follow-up: the Beijing Eye Study 2001-2011, 2022 Feb 23 Eye. https://doi.org/10.1038/s41433-022-01978-8 (Online ahead of print).
Jonas, R.A., Holbach, L., 2020. Peripapillary border tissue of the choroid and peripapillary scleral flange in human eyes. Acta Ophthalmol. 98, e43–e49.
Jonas, R.A., Wang, Y.X., Yang, H., Li, J.J., Xu, L., Panda-Jonas, S., Jonas, J.B., 2015a. Optic disc - fovea distance, axial length and parapapillary zones. The Beijing Eye Study 2011. PLoS One 10, e0138701.
Jonas, R.A., Wang, Y.X., Yang, H., Li, J.J., Xu, L., Panda-Jonas, S., Jonas, J.B., 2015b. Optic disc-fovea angle: the beijing eye study. PLoS One 10 (11), e0141771, 2015.
Jonas, R.A., Wie, C.C., Jonas, J.B., Wang, Y.X., 2021a. Decreasing myopic lacquer crack and widening parapapillary gamma zone: case report. BMC Ophthalmol. 21, 443.
Jonas, R.A., Yan, Y.N., Zhang, Q., Wang, Y.X., Jonas, J.B., 2021b. Elongation of the disc-fovea distance and retinal vessel straightening in high myopia in a 10-year follow-up of the Beijing eye study. Sci. Rep. 11, 9006.
Jonas, R.A., Brandt, C.F., Zhang, Q., Wang, Y.X., Jonas, J.B., 2021c. Location of parapapillary gamma zone and vertical fovea location. The Beijing Eye Study 2011. Invest. Ophthalmol. Vis. Sci. 62 (1), 18.
Jonas, S.B., Panda-Jonas, S., Jonas, J.B., Jonas, R.A., 2021d. Histology of neovascular myopic macular degeneration. Sci. Rep. 11, 21908.
Jonas, S.B., Jonas, R.A., Panda-Jonas, S., Jonas, J.B., 2022. Histopathology of myopic cobble stones. Acta Ophthalmol. 100, 111–117.
Khaliq, A., Jarvis-Evans, J., McLeod, D., Boulton, M., 1996. Oxygen modulates the response of the retinal pigment epithelium to basic fibroblast growth factor and epidermal growth factor by receptor regulation. Invest. Ophthalmol. Vis. Sci. 37, 436–443.
Kiilgaard, J.F., Prause, J.U., Prause, M., Scherfig, E., Nissen, M.H., la Cour, M., 2007. Subretinal posterior pole injury induces selective proliferation of RPE cells in the periphery in in vivo studies in pigs. Invest. Ophthalmol. Vis. Sci. 48, 355–360.
Kim, H.R., Weinreb, R.N., Zangwill, L.M., Suh, M.H., 2020. Characteristics of focal gamma zone parapapillary atrophy. Invest. Ophthalmol. Vis. Sci. 61, 17.
Kim, M., Choung, H.K., Lee, K.M., Oh, S., Kim, S.H., 2018. Longitudinal changes of optic nerve head and peripapillary structure during childhood myopia progression on OCT: boramae Myopia Cohort Study Report 1. Ophthalmology 125, 1215–1223.
Kim, M.J., Kim, S.H., Hwang, Y.H., Park, K.H., Kim, T.W., Kim, D.M., 2014. Novel screening method for glaucomatous eyes with myopic tilted discs: the crescent moon sign. JAMA. Ophthalmol. 132, 1407–1413.

Kim, T.W., Kim, M., Weinreb, R.N., Woo, S.J., Park, K.H., Hwang, J.M., 2012. Optic disc change with incipient myopia of childhood. Ophthalmology 119 (2012), 21–26.
Kimura, Y., Akagi, T., Hangai, M., Takayama, K., Hasegawa, T., Suda, K., Yoshikawa, M., Yamada, H., Nakanishi, H., Unoki, N., Ikeda, H.O., Yoshimura, N., 2014. Lamina cribrosa defects and optic disc morphology in primary open angle glaucoma with high myopia. PLoS One 9, e115313.
Ko, M.W., Leung, L.K., Lam, D.C., Leung, C.K., 2013. Characterization of corneal tangent modulus in vivo. Acta Ophthalmol. 91, e263–e269.
Kociok, N., Heppekausen, H., Schraermeyer, U., Esser, P., Thumann, G., Grisanti, S., Heimann, K., 1998. The mRNA expression of cytokines and their receptors in cultured iris pigment epithelial cells: a comparison with retinal pigment epithelial cells. Exp. Eye Res. 67, 237–250.
Kubota, T., Jonas, J.B., Naumann, G.O.H., 1993. Direct clinico-histological correlation of parapapillary chorioretinal atrophy. Br. J. Ophthalmol. 77, 103–106.
Kuhnt, H., 1879. Zur Kenntniss des Sehnerven und der Netzhaut. Albrecht Von Graefes Arch. Ophthalmol. 25, 179–288.
Kuzin, A.A., Varma, R., Reddy, H.S., Torres, M., Azen, S.P., Los Angeles Latino Eye Study Group, 2010. Ocular biometry and open-angle glaucoma: the Los Angeles Latino eye study. Ophthalmology 117, 1713–1719.
Larsen, J.S., 1971. The sagittal growth of the eye. IV. ultrasonic measurement of the axial length of the eye from birth to puberty. Acta Ophthalmol. 49, 873–886.
Lee, E.J., Kim, T.W., Kim, J.A., Kim, J.A., 2017. Parapapillary deep-layer microvasculature dropout in primary open-angle glaucoma eyes with a parapapillary γ-zone. Invest. Ophthalmol. Vis. Sci. 58, 5673–5680.
Lee, K., Maeng, K.J., Kim, J.Y., Yang, H., Choi, W., Lee, S.Y., Seong, G.J., Kim, C.Y., Bae, H.W., 2020a. Diagnostic ability of vessel density measured by spectral-domain optical coherence tomography angiography for glaucoma in patients with high myopia. Sci. Rep. 10, 3027.
Lee, K., Yang, H., Kim, J.Y., Seong, G.J., Kim, C.Y., Bae, H.W., 2020b. Risk factors associated with structural progression in normal-tension glaucoma: intraocular pressure, systemic blood pressure, and myopia. Invest. Ophthalmol. Vis. Sci. 61, 35.
Lee, K.M., Choung, H.K., Kim, M., Oh, S., Kim, S.H., 2018a. Positional change of optic nerve head vasculature during axial elongation as evidence of lamina cribrosa shifting: boramae Myopia Cohort Study Report 2. Ophthalmology 125, 1224–1233.
Lee, K.M., Choung, H.K., Kim, M., Oh, S., Kim, S.H., 2018b. Change of β-zone parapapillary atrophy during axial elongation: boramae myopia cohort study report 3. Invest. Ophthalmol. Vis. Sci. 59, 4020–4030.
Lee, K.M., Park, S.W., Kim, M., Oh, S., Kim, S.H., 2021. Relationship between three-dimensional magnetic resonance imaging eyeball shape and optic nerve head morphology. Ophthalmology 128, 532–544.
Lee, M.W., Lee, S.E., Lim, H.B., Kim, J.Y., 2020. Longitudinal changes in axial length in high myopia: a 4-year prospective study. Br. J. Ophthalmol. 104, 600–603.
Lee, S., Han, S.X., Young, M., Beg, M.F., Sarunic, M.V., Mackenzie, P.J., 2014. Optic nerve head and peripapillary morphometrics in myopic glaucoma. Invest. Ophthalmol. Vis. Sci. 55, 4378–4393.
Lee, S., Schimmenti, L.A., King, R.A., Brilliant, M., Anderson, J.L., Schoonveld, C., Summers, C.G., 2015. Posterior staphyloma in oculocutaneous albinism: another possible cause of reduced visual acuity. J. AAPOS. 19, 562–564.
Lee, S.S., Alonso-Caneiro, D., Lingham, G., Chen, F.K., Sanfilippo, P.G., Yazar, S., Mackey, D.A., 2022a. Choroidal thickening during young adulthood and baseline choroidal thickness predicts refractive error change. Invest. Ophthalmol. Vis. Sci. 63, 34.
Lee, S.S., Lingham, G., Sanfilippo, P.G., Hammond, C.J., Saw, S.M., Guggenheim, J.A., Yazar, S., Mackey, D.A., 2022b. Incidence and progression of myopia in early adulthood. JAMA Ophthalmol 140, 162–169.
Lejoyeux, R., Benillouche, J., Ong, J., Errera, M.H., Rossi, E.A., Singh, S.R., Dansingani, K.K., da Silva, S., Sinha, D., Sahel, J.A., Freund, K.B., Sadda, S.R., Lutty, G.A., Chhablani, J., 2022. Choriocapillaris: fundamentals and advancements. Prog. Retin. Eye Res. 87, 100997.
Leung, L.K.K., Ko, M.W.L., Ye, C., Lam, D.C.C., Leung, C.K.S., 2014. Noninvasive measurement of scleral stiffness and tangent modulus in porcine eyes. Invest. Ophthalmol. Vis. Sci. 55, 3721–3726.
Li, X.J., Yang, X.P., Wan, G.M., Wang, Y.Y., Zhang, J.S., 2014. Effects of hepatocyte growth factor on MMP-2 expression in scleral fibroblasts from a Guinea pig myopia model. Int. J. Ophthalmol. 7, 239–244.
Liang, C.M., Tai, M.C., Chang, Y.H., Chen, Y.H., Chen, C.L., Chien, M.W., Chen, J.T., 2010. Glucosamine inhibits epidermal growth factor-induced proliferation and cell-cycle progression in retinal pigment epithelial cells. Mol. Vis. 16, 2559–2571.
Lin, C., Li, S.M., Ohno-Matsui, K., Wang, B.S., Fang, Y.X., Cao, K., Gao, L.Q., Hao, J., Zhang, Y., Wu, J., Wang, N.L., Handan Eye Study Group, 2018. Five-year incidence and progression of myopic maculopathy in a rural Chinese adult population: the Handan Eye Study. Ophthalmic Physiol. Opt. 38, 337–345.
Lin, F., Chen, S., Song, Y., Li, F., Wang, W., Zhao, Z., Gao, X., Wang, P., Jin, L., Liu, Y., Chen, M., Liang, X., Yang, B., Ning, G., Cheng, C.Y., Healey, P.R., Park, K.H., Zangwill, L.M., Aung, T., Ohno-Matsui, K., Jonas, J.B., Weinreb, R.N., Zhang, X., GSHM study group, 2022. Classification of visual field abnormalities in highly myopic eyes without pathological change, 2022 Mar 11:S0161-6420(22)00193-2 Ophthalmology. https://doi.org/10.1016/j.ophtha.2022.03.001 (Online ahead of print).
Lin, F.B., Da Chen, S., Song, Y.H., Wang, W., Jin, L., Liu, B.Q., Liu, Y.H., Chen, M.L., Gao, K., Friedman, D.S., Jonas, J.B., Aung, T., Lv, L., Liu, Y.Z., Zhang, X.L., GSHM study group, 2020. Effect of medically lowering intraocular pressure in glaucoma suspects with high myopia (GSHM study): study protocol for a randomized controlled trial. Trials 21, 813.
Liu, H.H., Xu, L., Wang, Y.X., Wang, S., You, Q.S., Jonas, J.B., 2010a. Prevalence and progression of myopic retinopathy in Chinese adults: the Beijing Eye Study. Ophthalmology 117, 1763–1768.
Liu, H.H., Gentle, A., Jobling, A.I., McBrien, N.A., 2010b. Inhibition of matrix metalloproteinase activity in the chick sclera and its effect on myopia development. Invest. Ophthalmol. Vis. Sci. 51, 2865–2871.
Liu, H.H., Kenning, M.S., Jobling, A.I., McBrien, N.A., Gentle, A., 2017. Reduced scleral TIMP-2 expression is associated with myopia development: TIMP-2 supplementation stabilizes scleral biomarkers of myopia and limits myopia development. Invest. Ophthalmol. Vis. Sci. 58, 1971–1981.
Liu, J., He, X., 2009. Corneal stiffness affects IOP elevation during rapid volume change in the eye. Invest. Ophthalmol. Vis. Sci. 50, 2224–2229.
Liu, L., Fang, Y., Igarashi-Yokoi, T., Takahashi, H., Ohno-Matsui, K., 2021. Clinical and morphologic features of posterior staphyloma edges by ultra-widefield imaging in pathologic myopia. Retina 41, 2278–2287.
Liu, N.P., Fitzgibbon, F., Nash, M., Osborne, N.N., 1992. Epidermal growth factor potentiates the transmitter-induced stimulation of C-AMP and inositol phosphates in human pigment epithelial cells in culture. Exp. Eye Res. 55, 489–497.
Liu, T.X., Wang, Z., 2013. Collagen crosslinking of porcine sclera using genipin. Acta Ophthalmol. 91, e253–e257.
Logan, N.S., Gilmartin, B., Wildsoet, C.F., Dunne, M.C., 2004. Posterior retinal contour in adult human anisomyopia. Invest. Ophthalmol. Vis. Sci. 45, 2152–2162.
Manjunath, V., Shah, H., Fujimoto, J.G., Duker, J.S., 2011. Analysis of peripapillary atrophy using spectral domain optical coherence tomography. Ophthalmology 118, 531–536.
Manalastas, P.I.C., Belghith, A., Weinreb, R.N., Jonas, J.B., Suh, M.H., Yarmohammadi, A., Medeiros, F.A., Girkin, C.A., Liebmann, J.M., Zangwill, L.M., 2018. Automated beta zone parapapillary area measurement to differentiate between healthy and glaucoma eyes. Am. J. Ophthalmol. 191, 140–148.
Mao, J., Liu, S., Fu, C., 2016. Citicoline retards myopia progression following form deprivation in Guinea pigs. Exp. Biol. Med. 241, 1258–1263.
Marcus, M.W., de Vries, M.M., Junoy, M.F., Jansonius, N.M., 2011. Myopia as a risk factor for open-angle glaucoma: a systematic review and meta-analysis. Ophthalmology 118, 1989–1994.
Margolis, R., Spaide, R.F., 2009. A pilot study of enhanced depth imaging optical coherence tomography of the choroid in normal eyes. Am. J. Ophthalmol. 147, 811–815.
Markov, P.P., Eliasy, A., Pijanka, J.K., Htoon, H.M., Paterson, N.G., Sorensen, T., Elsheikh, A., Girard, M.J.A., Boote, C., 2018. Bulk changes in posterior scleral collagen microstructure in human high myopia. Mol. Vis. 24, 818–833.
Marlow, N., Stahl, A., Lepore, D., Fielder, A., Reynolds, J.D., Zhu, Q., Weisberger, A., Stiehl, D.P., Fleck, B., RAINBOW investigators group, 2021. 2-year outcomes of ranibizumab versus laser therapy for the treatment of very low birthweight infants with retinopathy of prematurity (RAINBOW extension study): prospective follow-up of an open label, randomised controlled trial. Lancet Child Adolesc. Health 5, 698–707.
Maruko, I., Iida, T., Sugano, Y., Oyamada, H., Sekiryu, T., 2011. Morphologic choroidal and scleral changes at the macula in tilted disc syndrome with staphyloma using optical coherence tomography. Invest. Ophthalmol. Vis. Sci. 52, 8763–8768.
Maruko, I., Iida, T., Sugano, Y., Oyamada, H., Akiba, M., Sekiryu, T., 2012. Morphologic analysis in pathologic myopia using high-penetration optical coherence tomography. Invest. Ophthalmol. Vis. Sci. 53, 3834–3838.
Matsumura, S., Kuo, A.N., Saw, S.M., 2019. An update of eye shape and myopia. Eye Contact Lens 45, 279–285.
Matsumura, S., Sabanayagam, C., Wong, C.W., Tan, C.S., Kuo, A., Wong, Y.L., Ohno-Matsui, K., Wong, T.Y., Cheng, C.Y., Hoang, Q.V., Saw, S.M., 2021. Characteristics of myopic traction maculopathy in myopic Singaporean adults. Br. J. Ophthalmol. 105, 531–537.
McBrien, N.A., 2013. Regulation of scleral metabolism in myopia and the role of transforming growth factor-beta. Exp. Eye Res. 114, 128–140.
McBrien, N.A., Lawlor, P., Gentle, A., 2000. Scleral remodeling during the development of and recovery from axial myopia in the tree shrew. Invest. Ophthalmol. Vis. Sci. 41, 3713–3719.
McBrien, N.A., Cornell, L.M., Gentle, A., 2001. Structural and ultrastructural changes to the sclera in a mammalian model of high myopia. Invest. Ophthalmol. Vis. Sci. 42, 2179–2187.
McBrien, N.A., Gentle, A., 2003. Role of the sclera in the development and pathological complications of myopia. Prog. Retin. Eye Res. 22, 307–338.
McBrien, N.A., Metlapally, R., Jobling, A.I., Gentle, A., 2006. Expression of collagen-binding integrin receptors in the mammalian sclera and their regulation during the development of myopia. Invest. Ophthalmol. Vis. Sci. 47, 4674–4682.
McBrien, N.A., Jobling, A.I., Gentle, A., 2009. Biomechanics of the sclera in myopia: extracellular and cellular factors. Optom. Vis. Sci. 86, E23–E30.
Meng, L.H., Yuan, M.Z., Zhao, X.Y., Chen, Y.X., 2022a. Macular Bruch's membrane defects and other myopic lesions in high myopia. Int. J. Ophthalmol. 15, 466–473.
Meng, L.H., Yuan, M.Z., Zhao, X.Y., Chen, Y.X., 2022b. Macular Bruch's membrane defects and other myopic lesions in high myopia. Int. J. Ophthalmol. 15, 466–473.
Mehta, P., Dinakaran, S., Squirrell, D., Talbot, J., 2006. Retinal pigment epithelial changes and choroidal neovascularisation at the edge of posterior staphylomas; a case series and review of the literature. Eye 20 (2), 150–153, 2006 Feb.
Meyer, J.H., Guhlmann, M., Funk, J., 1997. Blind spot size depends on the optic disc topography a study using SLO controlled scotometry and the Heidelberg retina tomograph. Br. J. Ophthalmol. 81, 355–359.
Meyer-Schwickerath, G., Gerke, E., 1984. Biometric studies of the eyeball and retinal detachment. Br. J. Ophthalmol. 68, 29–31.

Miki, A., Ikuno, Y., Weinreb, R.N., Yokoyama, J., Asai, T., Usui, S., Nishida, K., 2017. Measurements of the parapapillary atrophy zones in en face optical coherence tomography images. PLoS One 12, e0175347.
Miki, A., Ikuno, Y., Weinreb, R.N., Asai, T., Usui, S., Nishida, K., 2019. En face optical coherence tomography imaging of beta and gamma parapapillary atrophy in high myopia. Ophthalmol. Glaucoma 2, 55–62.
Mirhajianmoghadam, H., Jnawali, A., Musial, G., Queener, H.M., Patel, N.B., Ostrin, L.A., Porter, J., 2020. In vivo assessment of foveal geometry and cone photoreceptor density and spacing in children. Sci. Rep. 10, 8942.
Mitchell, P., Hourihan, F., Sandbach, J., Wang, J.J., 1999. The relationship between glaucoma and myopia: the blue mountains eye study. Ophthalmology 106, 2010–2025.
Mo, J., Duan, A., Chan, S., Wang, X., Wie, W., 2017. Vascular flow density in pathological myopia: an optical coherence tomography angiography study. BMJ Open 7, e013571.
Morgan, I.G., Ohno-Matsui, K., Saw, S.M., 2012. Myopia. Lancet 379, 1739–1748.
Moriyama, M., Ohno-Matsui, K., Futagami, S., Yoshida, T., Hayashi, K., Shimada, N., Kojima, A., Tokoro, T., Mochizuki, M., 2007. Morphology and long-term changes of choroidal vascular structure in highly myopic eyes with and without posterior staphyloma. Ophthalmology 114, 1755–1762.
Moriyama, M., Ohno-Matsui, K., Hayashi, K., Shimada, N., Yoshida, T., Tokoro, T., Morita, I., 2011. Topographical analyses of shape of eyes with pathologic myopia by high-resolution three dimensional magnetic resonance imaging. Ophthalmology 118, 1626–1637.
Mutti, D.O., Mitchell, G.L., Hayes, J.R., Jones, L.A., Moeschberger, M.L., Cotter, S.A., Kleinstein, R.N., Manny, R.E., Twelker, J.D., Zadnik, K., CLEERE Study Group, 2006. Accommodative lag before and after the onset of myopia. Invest. Ophthalmol. Vis. Sci. 47, 837–846.
Mutti, D.O., Hayes, J.R., Mitchell, G.L., 2007. Refractive error, axial length, and relative peripheral refractive error before and after the onset of myopia. Invest. Ophthalmol. Vis. Sci. 48, 2510–2519.
Mutti, D.O., Sinnott, L.T., Mitchell, G.L., 2011. Relative peripheral refractive error and the risk of onset and progression of myopia in children. Invest. Ophthalmol. Vis. Sci. 52, 199–205.
Nagaoka, N., Jonas, J.B., Morohoshi, K., Moriyama, M., Shimada, N., Yoshida, T., Ohno-Matsui, K., 2015. Glaucomatous-type optic discs in high myopia. PLoS One 10, e0138825.
Nakao, N., Igarashi-Yokoi, T., Takahashi, H., Xie, S., Shinohara, K., Ohno-Matsui, K., 2022. Quantitative evaluations of posterior staphylomas in highly myopic eyes by ultra-widefield optical coherence tomography. Invest. Ophthalmol. Vis. Sci. 63, 20.
Nakazawa, M., Kurotaki, J., Ruike, H., 2008. Longterm findings in peripapillary crescent formation in eyes with mild or moderate myopia. Acta Ophthalmol. 86, 626–629.
Nangia, V., Jonas, J.B., Sinha, A., Matin, A., Kulkarni, M., 2010. Central corneal thickness and its association with ocular and general parameters in Indians: the Central India Eye and Medical Study. Ophthalmology 117, 705–710.
Nickla, D.L., Wallman, J., 2010. The multifunctional choroid. Prog. Retin. Eye Res. 29, 144–168.
Norman, R.E., Flanagan, J.G., Rausch, S.M., Sigal, I.A., Tertinegg, I., Eilaghi, A., Portnoy, S., Sled, J.G., Ethier, C.E., 2010. Dimensions of the human sclera: thickness measurement and regional changes with axial length. Exp. Eye Res. 90, 277–284.
O'Brart, D.P., de Souza Lima, M., Bartsch, D.U., Freeman, W., Weinreb, R.N., 1997. Indocyanine green angiography of the peripapillary region in glaucomatous eyes by confocal scanning laser ophthalmoscopy. Am. J. Ophthalmol. 123, 657–666.
Ohno-Matsui, K., Akiba, M., Moriyama, M., Shimada, N., Ishibashi, T., Tokoro, T., Spaide, R.F., 2012. Acquired optic nerve and peripapillary pits in pathologic myopia. Ophthalmology 119, 1685–1692.
Ohno-Matsui, K., Kasahara, K., Moriyama, M., 2013. Detection of Zinn-Haller arterial ring in highly myopic eyes by simultaneous indocyanine green angiography and optical coherence tomography. Am. J. Ophthalmol. 155, 920–926.
Ohno-Matsui, K., 2014. Proposed classification of posterior staphylomas based on analyses of eye shape by three-dimensional magnetic resonance imaging and wide-field fundus imaging. Ophthalmology 121, 1798–1809.
Ohno-Matsui, K., Kawasaki, R., Jonas, J.B., Cheung, C.M., Saw, S.M., Verhoeven, V.J., Klaver, C.C., Moriyama, M., Shinohara, K., Kawasaki, Y., Yamazaki, M., Meuer, S., Ishibashi, T., Yasuda, M., Yamashita, H., Sugano, A., Wang, J.J., Mitchell, P., Wong, T.Y., META-analysis for Pathologic Myopia (META-PM) Study Group, 2015. International photographic classification and grading system for myopic maculopathy. Am. J. Ophthalmol. 159, 877–883 e7.
Ohno-Matsui, K., Jonas, J.B., Spaide, R.F., 2016a. Macular Bruch membrane holes in highly myopic patchy chorioretinal atrophy. Am. J. Ophthalmol. 166, 22–28.
Ohno-Matsui, K., Jonas, J.B., Spaide, R.F., 2016b. Macular Bruch's membrane holes in highly myopic patchy chorioretinal atrophy. Am. J. Ophthalmol. 166, 22–28.
Ohno-Matsui, K., Lai, T.Y., Lai, C.C., Cheung, C.M., 2016c. Updates of pathologic myopia. Prog. Retin. Eye Res. 52, 156–187.
Ohno-Matsui, K., Fang, Y., Uramoto, K., Shinohara, K., Yokoi, T., Ishida, T., Jonas, J.B., 2017. Peri-dome choroidal deepening in highly myopic eyes with dome-shaped maculas. Am. J. Ophthalmol. 183, 134–140.
Ohno-Matsui, K., Jonas, J.B., 2019. Posterior staphyloma in pathologic myopia. Prog. Retin. Eye Res. 70, 99–109.
Ohno-Matsui, K., Wu, P.C., Yamashiro, K., Vutipongsatorn, K., Fang, Y., Cheung, C.M.G., Lai, T.Y.Y., Ikuno, Y., Cohen, S.Y., Gaudric, A., Jonas, J.B., 2021. IMI pathologic myopia. Invest. Ophthalmol. Vis. Sci. 62, 5.
Oliveira, C., Tello, C., Liebmann, J., Ritch, R., 2006. Central corneal thickness is not related to anterior scleral thickness or axial length. J. Glaucoma 15, 190–194.
Olsen, T.W., Aaberg, S.Y., Geroski, D.H., Edelhauser, H.F., 1998. Human sclera: thickness and surface area. Am. J. Ophthalmol. 125, 237–241.
Omari, A., Carniciu, A.L., Desai, M., Schimmel, O., Schlachter, D.M., Folberg, R., Kahana, A., 2022. Globe dislocation and optic nerve avulsion following all-terrain vehicle accidents. Am. J. Ophthalmol. Case Rep. 27, 101621.
Pan, C.W., Cheung, C.Y., Aung, T., Cheung, C.M., Zheng, Y.F., Wu, R.Y., Mitchell, P., Lavanya, R., Baskaran, M., Wang, J.J., Wong, T.Y., Saw, S.M., 2013. Differential associations of myopia with major age-related eye diseases: the Singapore Indian Eye Study. Ophthalmology 120, 284–291.
Pan, M., Guan, Z., Reinach, P.S., Kang, L., Cao, Y., Zhou, D., Srinivasalu, N., Zhao, F., Qu, J., Zhou, X., 2021. PPARγ modulates refractive development and form deprivation myopia in Guinea pigs. Exp. Eye Res. 202, 108332.
Panda-Jonas, S., Jonas, J.B., Jakobczyk, M., Schneider, U., 1994. Retinal photoreceptor count, retinal surface area, and optic disc size in normal human eyes. Ophthalmology 101, 519–523.
Panda-Jonas, S., Jonas, J.B., Jakobczyk-Zmija, M., 1996. Retinal pigment epithelial cell count, distribution, and correlations in normal human eyes. Am. J. Ophthalmol. 121, 181–189.
Panda-Jonas, S., Holbach, L., Jonas, J.B., 2021. Choriocapillaris thickness and density in axially elongated eyes. Acta Ophthalmol. 99, 104–110.
Panda-Jonas, S., Auffarth, G.U., Jonas, J.B., Jonas, R.A., 2022. Elongation of the retina and ciliary body in dependence of the sagittal eye diameter. Invest. Ophthalmol. Vis. Sci. 63, 18.
Papastathopoulos, K.I., Jonas, J.B., Panda-Jonas, S., 1995. Large optic discs in large eyes, small optic discs in small eyes. Exp. Eye Res. 60, 459–461.
Park, H.Y., Choi, S.I., Choi, J.A., Park, C.K., 2015. Disc torsion and vertical disc tilt are related to subfoveal scleral thickness in open-angle glaucoma patients with myopia. Invest. Ophthalmol. Vis. Sci. 56, 4927–4935.
Park, H.Y., Shin, D.Y., Jeon, S.J., Park, C.K., 2019. Association between parapapillary choroidal vessel density measured with optical coherence tomography angiography and future visual field progression in patients with glaucoma. JAMA Ophthalmol 137, 681–688.
Park, J.H., Choi, K.R., Kim, C.Y., Kim, S.S., 2016. The height of the posterior staphyloma and corneal hysteresis is associated with the scleral thickness at the staphyloma region in highly myopic normal-tension glaucoma eyes. Br. J. Ophthalmol. 100, 1251–1256.
Park, K.H., Tomita, G., Liou, S.Y., Kitazawa, Y., 1996. Correlation between peripapillary atrophy and optic nerve damage in normal-tension glaucoma. Ophthalmology 103, 1899–1906.
Park, U.C., Lee, E.K., Kim, B.H., Oh, B.L., 2021. Decreased choroidal and scleral thicknesses in highly myopic eyes with posterior staphyloma. Sci. Rep. 11, 7987.
Park, S.P., Chang, S., Allikmets, R., Smith, R.T., Burke, T.R., Gregory-Roberts, E., Tsang, S.H., 2012. Disruption in Bruch membrane in patients with Stargardt disease. Ophthalmic Genet. 33, 49–52.
Parolini, B., Palmieri, M., Finzi, A., Besozzi, G., Frisina, R., 2021. Myopic traction maculopathy: a new perspective on classification and management. Asia. Pac. J. Ophthalmol (Phila). 10 (1), 49–59.
Pärssinen, O., Kauppinen, M., 2019. Risk factors for high myopia: a 22-year follow-up study from childhood to adulthood. Acta Ophthalmol. 97, 510–518.
Pärssinen, O., Kauppinen, M., Viljanen, A., 2014. The progression of myopia from its onset at age 8-12 to adulthood and the influence of heredity and external factors on myopic progression. A 23-year follow-up study. Acta Ophthalmol. 92, 730–739.
Pauleikhoff, D., Harper, C.A., Marshall, J., Bird, A.C., 1990. Aging changes in Bruch's membrane: a histochemical and morphological study. Ophthalmology 97, 171–178.
Pierscionek, B.K., Asejczyk-Widlicka, M., Schachar, R.A., 2007. The effect of changing intraocular pressure on the corneal and scleral curvatures in the fresh porcine eye. Br. J. Ophthalmol. 91, 801–803.
Rada, J.A., Shelton, S., Norton, T.T., 2006. The sclera and myopia. Exp. Eye Res. 82, 185–200.
Ramrattan, R.S., van der Schaft, T.L., Mooy, C.M., de Bruijn, W.C., Mulder, P.G., de Jong, P.T., 1994. Morphometric analysis of Bruch's membrane,the choriocapillaris, and the choroid in aging. Invest. Ophthalmol. Vis. Sci. 35, 2857–2864.
Ramrattan, R.S., Wolfs, R.C., Jonas, J.B., Hofman, A., de Jong, P.T., 1999. Determinants of optic disc characteristics in a general population: the Rotterdam Study. Ophthalmology 106, 1588–1596.
Rebolleda, G., Casado, A., Oblanca, N., Muñoz-Negrete, F.J., 2016. The new Bruch's membrane opening–minimum rim width classification improves optical coherence tomography specificity in tilted discs. Clin. Ophthalmol. 10, 2417–2425.
Reis, A.S., O'Leary, N., Yang, H., Sharpe, G.P., Nicolela, M.T., Burgoyne, C.F., Chauhan, B.C., 2012. Influence of clinically invisible, but optical coherence tomography detected, optic disc margin anatomy on neuroretinal rim evaluation. Invest. Ophthalmol. Vis. Sci. 53, 1852–1860.
Ren, R., Wang, N., Li, B., Li, L., Gao, F., Xu, X., Jonas, J.B., 2009. Lamina cribrosa and peripapillary sclera histomorphometry in normal and advanced glaucomatous Chinese eyes with normal and elongated axial length. Invest. Ophthalmol. Vis. Sci. 50, 2175–2184.
Rensch, F., Jonas, J.B., 2008. Direct microperimetry of alpha zone and beta zone parapapillary atrophy. Br. J. Ophthalmol. 92, 1617–1619.
Rezapour, J., Proudfoot, J.A., Bowd, C., Dohleman, J., Christopher, M., Belghith, A., Vega, S.M., Dirkes, K., Hee, M.S., Jonas, J.B., Hyman, L., Fazio, M.A., Sella, R., Afshari, N.A., Weinreb, R.N., Zangwill, L.M., 2021. Bruch's membrane opening detection accuracy in healthy and glaucoma eyes with and without axial high myopia in an American and Korean cohort. Am. J. Ophthalmol. 237, 221–234.
Rezapour, J., Bowd, C., Dohleman, J., Belghith, A., Proudfoot, J.A., Christopher, M., Hyman, L., Jonas, J.B., Fazio, M.A., Weinreb, R.N., Zangwill, L.M., 2021b. The influence of axial myopia on optic disc characteristics of glaucoma eyes. Sci. Rep. 11 (1), 8854, 2021 Apr 23.

Rezapour, J., Tran, A.Q., Bowd, C., El-Nimri, N.W., Belghith, A., Christopher, M., Brye, N., Proudfoot, J.A., Dohleman, J., Fazio, M.A., Jonas, J.B., Weinreb, R.N., Zangwill, L.M., 2022a. Comparison of optic disc ovality index and rotation angle measurements in myopic eyes using photography and OCT based techniques. Front. Med. 9, 872658, 2022 Jun 24.

Rezapour, J., Bowd, C., Dohleman, J., Belghith, A., Proudfoot, J.A., Christopher, M., Hyman, L., Jonas, J.B., Penteado, R.C., Moghimi, S., Hou, H., El-Nimri, N.W., Micheletti, E., Fazio, M.A., Weinreb, R.N., Zangwill, L.M., 2022b. Macula structural and vascular differences in glaucoma eyes with and without high axial myopia, 2022 Jun 20:bjophthalmol-2021-320430 Br J Ophtalmol. https://doi.org/10.1136/bjophthalmol-2021-320430 (Online ahead of print).

Ruiz-Medrano, J., Montero, J.A., Flores-Moreno, I., Arias, L., García-Layana, A., Ruiz-Moreno, J.M., 2019. Myopic maculopathy: current status and proposal for a new classification and grading system (ATN). Prog. Retin. Eye Res. 69, 80–115.

Rymer, J., Wildsoet, C.F., 2005. The role of the retinal pigment epithelium in eye growth regulation and myopia: a review. Vis. Neurosci. 22, 251–261.

Saito, R., Shinohara, K., Tanaka, N., Takahashi, H., Yoshida, T., Ohno-Matsui, K., 2021. Association between dome-shaped macula and posterior staphyloma in highly myopic eyes investigated by ultra-widefield optical coherence tomography. Retina 41, 646–652.

Saka, N., Ohno-Matsui, K., Shimada, N., Sueyoshi, S., Nagaoka, N., Hayashi, W., Hayashi, K., Moriyama, M., Kojima, A., Yasuzumi, K., Yoshida, T., Tokoro, T., Mochizuki, M., 2010. Long-term changes in axial length in adult eyes with pathologic myopia. Am. J. Ophthalmol. 150, 562–568.

Saka, N., Moriyama, M., Shimada, N., Nagaoka, N., Fukuda, K., Hayashi, K., Yoshida, T., Tokoro, T., Ohno-Matsui, K., 2013. Changes of axial length measured by IOL master during 2 years in eyes of adults with pathologic myopia. Graefes Arch. Clin. Exp. Ophthalmol. 251, 495–499.

Sakaguchi, K., Higashide, T., Udagawa, S., Ohkubo, S., Sugiyama, K., 2017. Comparison of sectoral structure-function relationships in glaucoma: vessel density versus thickness in the peripapillary retinal nerve fiber layer. Invest. Ophthalmol. Vis. Sci. 58, 5251–5262.

Salzmann, M., 1912. The Anatomy and Histology of the Human Eyeball in the Normal State; its Development and Senescence. University of Chicago Press, Chicago, p. 94.

Samarawickrama, C., Mitchell, P., Tong, L., Gazzard, G., Lim, L., Wong, T.-Y., Saw, S.-M., 2011. Myopia-related optic disc and retinal changes in adolescent children from Singapore. Ophthalmology 118, 2050–2057.

Sanfilippo, P.G., Cardini, A., Hewitt, A.W., Crowston, J.G., Mackey, D.A., 2009. Optic disc morphology–rethinking shape. Prog. Retin. Eye Res. 28, 227–248.

Sankaridurg, P., Holden, B., Smith III., E., 2011. Decrease in rate of myopia progression with a contact lens designed to reduce relative peripheral hyperopia: one-year results. Invest. Ophthalmol. Vis. Sci. 52, 9362–9367.

Sayanagi, K., Ikuno, Y., Uematsu, S., Nishida, K., 2017. Features of the choriocapillaris in myopic maculopathy identified by optical coherence tomography angiography. Br. J. Ophthalmol. 101, 1524–1529.

Sawada, Y., Araie, M., Shibata, H., Ishikawa, M., Iwata, T., Yoshitomi, T., 2018. Optic disc margin anatomic features in myopic eyes with glaucoma with spectral-domain OCT. Ophthalmology 125, 1886–1897.

Schachat, A.P., Wilkinson, C.P., Hinton, D.R., Sadda, S.R., Wiedemann, P., 2017. Ryan's Retina, 6 ed. Elsevier Health Sciences. 2017.

Scherm, P., Pettenkofer, M., Maier, M., Lohmann, C.P., Feucht, N., 2019. Choriocapillary blood flow in myopic subjects measured with OCT angiography. Ophthalmic Surg. Lasers Imaging Retina 50, e133–e139.

Scott, A., Kashani, S., Towler, H.M., 2005. Progressive myopia due to posterior staphyloma in Type I Osteogenesis Imperfecta. Int. Ophthalmol. 26, 167–169.

Seko, Y., Shimokawa, H., Tokoro, T., 1995. Expression of bFGF and TGF-beta 2 in experimental myopia in chicks. Invest. Ophthalmol. Vis. Sci. 36, 1183–1187.

Shao, L., Xu, L., Wei, W.B., Chen, C.X., Du, K.F., Li, X.P., Yang, M., Wang, Y.X., You, Q.S., Jonas, J.B., 2014. Visual acuity and subfoveal choroidal thickness. The Beijing Eye Study. Am. J. Ophthalmol. 158, 702–709 e1.

Shang, K., Dai, Y., Liu, H., Qu, X., Wen, W., Jonas, J.B., 2019a. Optic disc shape in patients with long-lasting unilateral esotropia and exotropia. BMC Ophthalmol. 19, 185.

Shang, K., Hu, X., Dai, Y., 2019b. Morphological features of parapapillary beta zone and gamma zone in chronic primary angle-closure glaucoma. Eye 33, 1378–1386.

Shang, K., Zhuang, D., Dai, Y., 2022. Comparative analysis of OCT-defined parapapillary beta and gamma zones between primary open angle glaucoma and primary angle closure glaucoma. Sci. Rep. 12, 11070.

Shen, L., Xu, X., You, Q.S., Gao, F., Zhang, Z., Li, B., Jonas, J.B., 2015. Scleral thickness in Chinese eyes. Invest. Ophthalmol. Vis. Sci. 56, 2720–2727.

Shen, L., You, Q.S., Xu, X., Gao, F., Zhang, Z., Li, B., Jonas, J.B., 2016a. Scleral and choroidal volume in relation to axial length in infants with retinoblastoma versus adults with malignant melanomas or end-stage glaucoma. Graefes Arch. Clin. Exp. Ophthalmol. 254, 1779–1786.

Shen, L., You, Q.S., Xu, X., Gao, F., Zhang, Z., Li, B., Jonas, J.B., 2016b. Scleral and choroidal thickness in secondary high axial myopia. Retina 36, 1579–1585.

Shinohara, K., Moriyama, M., Shimada, N., Yoshida, T., Ohno-Matsui, K., 2016. Characteristics of peripapillary staphylomas associated with high myopia determined by swept-source optical coherence tomography. Am. J. Ophthalmol. 169, 138–144.

Shinohara, K., Shimada, N., Moriyama, M., Yoshida, T., Jonas, J.B., Yoshimura, N., Ohno-Matsui, K., 2017. Posterior staphylomas in pathologic myopia imaged by widefield optical coherence tomography. Invest. Ophthalmol. Vis. Sci. 58, 3750–3758.

Shinohara, K., Tanaka, N., Jonas, J.B., Shimada, N., Moriyama, M., Yoshida, T., Ohno-Matsui, K., 2018. Ultrawide-field OCT to investigate relationships between myopic macular retinoschisis and posterior staphyloma. Ophthalmology 125, 1575–1586.

Siegwart Jr., J.T., Norton, T.T., 2002. The time course of changes in mRNA levels in tree shrew sclera during induced myopia and recovery. Invest. Ophthalmol. Vis. Sci. 43, 2067–2075.

Skaat, A., De Moraes, C.G., Bowd, C., Sample, P.A., Girkin, C.A., Medeiros, F.A., Ritch, R., Weinreb, R.N., Zangwill, L.M., Liebmann, J.M., Diagnostic Innovations in Glaucoma Study and African Descent and Glaucoma Evaluation Study Groups, 2016. African Descent and Glaucoma Evaluation Study (ADAGES): racial differences in optic disc hemorrhage and beta-zone parapapillary atrophy. Ophthalmology 123, 1476–1483.

Smith 3rd, E.L., Kee, C.S., Ramamirtham, R., Qiao-Grider, Y., Hung, L.F., 2005. Peripheral vision can influence eye growth and refractive development in infant monkeys. Invest. Ophthalmol. Vis. Sci. 46, 3965–3972.

Smith 3rd, E.L., Ramamirtham, R., Qiao-Grider, Y., Hung, L.F., Huang, J., Kee, C.S., Coats, D., Paysse, E., 2007. Effects of foveal ablation on emmetropization and form-deprivation myopia. Invest. Ophthalmol. Vis. Sci. 48, 3914–3922.

Smith III, E.L., Hung, L.F., Huang, J., 2009. Relative peripheral hyperopic defocus alters central refractive development in infant monkeys. Vision Res 49, 2386–2392.

Song, Y., Wang, W., Lin, F., Chen, S., Jin, L., Li, F., Gao, K., Cheng, W., Xiong, J., Zhou, R., Chen, M., Liang, J., Zhang, J., Jonas, J.B., Zhang, X., 2020. Natural history of glaucomatous optic neuropathy in highly myopic Chinese: study protocol for a registry cohort study. BMJ Open 10, e039183.

Soudier, G., Gaudric, A., Gualino, V., Massin, P., Nardin, M., Tadayoni, R., Speeg-Schatz, C., Gaucher, D., 2016. Long-term evolution of dome-shaped macula: increased macular bulge is associated with extended macular atrophy. Retina 36, 944–952.

Spaide, R.F., Koizumi, H., Pozzoni, M.C., 2008. Enhanced depth imaging spectral-domain optical coherence tomography. Am. J. Ophthalmol. 146, 496–500.

Spaide, R.F., Akiba, M., Ohno-Matsui, K., 2012. Evaluation of peripapillary intrachoroidal cavitation with swept source and enhanced depth imaging optical coherence tomography. Retina 32, 1037–1044.

Spaide, R.F., 2013. Staphyloma: Part 1. Springer, New York, pp. 167–176.

Spaide, R.F., Jonas, J.B., 2015. Peripapillary Atrophy with Large Dehiscences in Bruch Membrane in Pseudoxanthoma Elasticum Retina, vol. 35, pp. 1507–1510.

Strouthidis, N.G., Yang, H., Fortune, B., Downs, J.C., Burgoyne, C.F., 2009. Detection of optic nerve head neural canal opening within histomorphometric and spectral domain optical coherence tomography data sets. Invest. Ophthalmol. Vis. Sci. 50, 214–223.

Strouthidis, N.G., Grimm, J., Williams, G.A., Cull, G.Al, Wilson, D.J., Burgoyne, C.F., 2010. A comparison of optic nerve head morphology viewed by spectral domain optical coherence tomography and by serial histology. Invest. Ophthalmol. Vis. Sci. 51, 1464–1474.

Sugiyama, K., Tomita, G., Kitazawa, Y., Onda, E., Shinohara, H., Park, K.H., 1997. The associations of optic disc hemorrhage with retinal nerve fiber layer defect and peripapillary atrophy in normal-tension glaucoma. Ophthalmology 104, 1926–1933.

Sung, M.S., Heo, H., Park, S.W., 2018. Microstructure of parapapillary atrophy Is associated with parapapillary microvasculature in myopic eyes. Am. J. Ophthalmol. 192, 157–168.

Sung, M.S., Heo, M.Y., Heo, H., Park, S.W., 2019. Bruch's membrane opening enlargement and its implication on the myopic optic nerve head. Sci. Rep. 9, 19564 (TBC).

Sung, M.S., Heo, H., Piao, H., Guo, Y., Park, S.W., 2020. Parapapillary atrophy and changes in the optic nerve head and posterior pole in high myopia. Sci. Rep. 10, 4607.

Sung, M.S., Ji, Y.S., Moon, H.S., Heo, H., Park, S.W., 2021. Anterior scleral thickness in myopic eyes and its association with ocular parameters. Ophthalmic Res. 64, 567–576.

Suwan, Y., Aghsaei Fard, M., Geyman, L.S., Tantraworasin, A., Chui, T.Y., Rosen, R.B., Ritch, R., 2018. Association of myopia with peripapillary perfused capillary density in patients with glaucoma an optical coherence tomography angiography study. JAMA. Ophthalmol. 136, 507–513.

Suzuki, Y., Iwase, A., Araie, M., Yamamoto, T., Abe, H., Shirato, S., Kuwayama, Y., Mishima, H.K., Shimizu, H., Tomita, G., Inoue, Y., Kitazawa, Y., Tajimi Study Group., 2006. Risk factors for open-angle glaucoma in a Japanese population: the Tajimi Study. Ophthalmology 113, 1613–1617.

Tan, N.Y.Q., Sng, C.C.A., Jonas, J.B., Wong, T.Y., Jansonius, N.M., Ang, M., 2019. Glaucoma in myopia: diagnostic dilemmas. Br. J. Ophthalmol. 103, 1347–1355.

Tanaka, N., Shinohara, K., Yokoi, T., Uramoto, K., Takahashi, H., Onishi, Y., Horie, S., Yoshida, T., Ohno-Matsui, K., 2019. Posterior staphylomas and scleral curvature in highly myopic children and adolescents investigated by ultra-widefield optical coherence tomography. PLoS One 14, e0218107.

Tay, E., Seah, S.K., Chan, S.P., Lim, A.T.H., Chew, S.-J., Foster, P.J., Aung, T., 2005. Optic disk ovality as an index of tilt and its relationship to myopia and perimetry. Am. J. Ophthalmol. 139, 247–252.

Tezel, G., Kolker, A.E., Wax, M.B., Kass, M.A., Gordon, M., Siegmund, K.D., 1997. Parapapillary chorioretinal atrophy in patients with ocular hypertension. II. An evaluation of progressive changes. Arch. Ophthalmol. 115, 1509–1514.

Tham, Y.C., Aung, T., Fan, Q., Saw, S.M., Siantar, R.G., Wong, T.Y., Cheng, C.Y., 2016. Joint effects of intraocular pressure and myopia on risk of primary open-angle glaucoma: the Singapore Epidemiology of Eye Diseases Study. Sci. Rep. 6, 19320.

Tideman, J.W.L., Polling, J.R., Vingerling, J.R., Jaddoe, V.W.V., Williams, C., Guggenheim, J.A., Klaver, C.C.W., 2018. Axial length growth and the risk of developing myopia in European children. Acta Ophthalmol. 96, 301–309.

Tideman, J.W.L., Pärssinen, O., Haarman, A.E.G., Khawaja, A.P., Wedenoja, J., Williams, K.M., Biino, G., Ding, X., Kähönen, M., Lehtimäki, T., Raitakari, O.T.,

Cheng, C.Y., Jonas, J.B., Young, T.L., Bailey-Wilson, J.E., Rahi, J., Williams, C., He, M., Mackey, D.A., Guggenheim, J.A., UK Biobank Eye and Vision Consortium and the Consortium for Refractive Error and Myopia (CREAM Consortium), 2021. Evaluation of shared genetic susceptibility to high and low myopia and hyperopia. JAMA Ophthalmol 139, 601–609.

Toranzo, J., Cohen, S.Y., Erginay, A., Gaudric, A., 2005. Peripapillary intrachoroidal cavitation in myopia. Am. J. Ophthalmol. 140, 731–732.

Trinh, M., Kalloniatis, M., Alonso-Caneiro, D., Nivison-Smith, L., 2022. High-density optical coherence tomography analysis provides insights into early/intermediate age-related macular degeneration retinal layer changes. Invest. Ophthalmol. Vis. Sci. 63, 36.

Troilo, D., Wallman, J., 1991. The regulation of eye growth and refractive state: an experimental study of emmetropization. Vision Res 31, 1237–1250.

Troilo, D., Smith III, E.L., Nickla, D.L., Ashby, R., Tkatchenko, A.V., Ostrin, L.A., Gawne, T.J., Pardue, M.T., Summers, J.A., Kee, C.S., Schroedl, F., Wahl, S., Jones, L., 2019. Imi – report on experimental models of emmetropization and myopia. Invest. Ophthalmol. Vis. Sci. 60, M31–M88.

Tsai, C.S., Zangwill, L., Gonzales, C., Irak, I., Garden, V., Hoffmann, R., Weinreb, R., 1995. Ethnic differences in optic nerve head topography. J. Glaucoma 4, 248–257.

Tuulonen, A., Jonas, J.B., Välimäki, S., Alanku, H.I., Airaksinen, P.J., 1996. Interobserver variation in the measurements of peripapillary atrophy in glaucoma. Ophthalmology 103, 535–541.

Uchida, H., Ugurlu, S., Caprioli, J., 1998. Increasing peripapillary atrophy is associated with progressive glaucoma. Ophthalmology 105, 1541–1545.

Ueda, E., Yasuda, M., Fujiwara, K., Hashimoto, S., Ohno-Matsui, K., Hata, J., Ishibashi, T., Ninomiya, T., Sonoda, K.H., 2020. Five-year incidence of myopic maculopathy in a general Japanese population: the Hisayama Study. JAMA Ophthalmol 138, 887–893.

Ugarte, M., Hussain, A.A., Marshall, J., 2006. An experimental study of the elastic properties of the human Bruch's membrane-choroid complex: relevance to ageing. Br. J. Ophthalmol. 90, 621–626.

Uramoto, K., Azuma, T., Watanabe, T., Takahashi, H., Igarashi-Yokoi, T., Noriaki, S., Ohno-Matsui, K., 2022. Extreme macular schisis simulating retinal detachment in eyes with pathologic myopia, 2022 Aug 17 Retina. https://doi.org/10.1097/IAE.0000000000003544 (Online ahead of print).

van Soest, S.S., de Wit, G.M., Essing, A.H., ten Brink, J.B., Kamphuis, W., de Jong, P.T., Bergen, A.A., 2007. Comparison of human retinal pigment epithelium gene expression in macula and periphery highlights potential topographic differences in Bruch's membrane. Mol. Vis. 13, 1608–1617.

Varma, R., Tielsch, J.M., Quigley, H.A., Hilton, S.C., Katz, L., Spaeth, G.L., Sommer, A., 1994. Race-, age-, gender-, and refractive error-related differences in the normal optic disc. Arch. Ophthalmol. 112, 1068–1076.

Vatsyayan, R., Chaudhary, P., Sharma, A., Sharma, R., Lelsani, P.C.R., Awasthi, S., Awasthi, Y.C., 2011. Role of 4-hydroxynonenal in epidermal growth factor receptor-mediated signaling in retinal pigment epithelial cells. Exp. Eye Res. 92, 147–154.

Vianna, J.R., Malik, R., Danthurebandara, V.M., Sharpe, G.P., Belliveau, A.C., Shuba, L. M., Chauhan, B.C., Nicolela, M.T., 2016. Beta and gamma peripapillary atrophy in myopic eyes with and without glaucoma. Invest. Ophthalmol. Vis. Sci. 57, 3103–3111.

Viola, F., Dell'Arti, L., Benatti, E., Invernizzi, A., Mapell, i C., Ferrari, F., Ratiglia, R., Staurenghi, G., Barteselli, G., 2015. Choroidal findings in dome-shaped macula in highly myopic eyes: a longitudinal study. Am. J. Ophthalmol. 159, 44–52.

Viola, F., Leone, G., Garoli, E., Mainetti, C., Galli, D., Invernizzi, A., 2021. Long-term natural history of highly myopic eyes with a dome-shaped macula with or without untreated serous retinal detachment: a 4-year follow-up study. Br. J. Ophthalmol. 105, 1405–1409.

Vurgese, S., Panda-Jonas, S., Jonas, J.B., 2012. Sclera thickness in human eyes. PLoS One 7, e29692.

Wallman, J., Turkel, J., Trachtman, J., 1978. Extreme myopia produced by modest change in early visual experience. Science 201, 1249–1251.

Wallman, J., Wildsoet, C., Xu, A., Gottlieb, M.D., Nickla, D.L., Marran, L., Krebs, W., Christensen, A.M., 1995. Moving the retina: choroidal modulation of refractive state. Vision Res 35, 37–50.

Wang, K.K., Metlapally, R., Wildsoet, C.F., 2017. Expression profile of the integrin receptor subunits in the Guinea pig sclera. Curr. Eye Res. 42, 857–863.

Wang, M., Schaeffel, F., Jiang, B., Feldkaemper, M., 2018. Effects of light of different spectral composition on refractive development and retinal dopamine in chicks. Invest. Ophthalmol. Vis. Sci. 59, 4413–4424.

Wang, N.K., Wu, Y.M., Wang, J.P., Liu, L., Yeung, L., Chen, Y.P., Chen, Y.H., Yeh, L.K., Wu, W.C., Chuang, L.H., Lai, C.C., 2016. Clinical characteristics of posterior staphylomas in myopic eyes with axial length shorter than 26.5 millimeters. Am. J. Ophthalmol. 162, 180–190 e1.

Wang, X., Rumpel, H., Lim, W.E., Baskaran, M., Perera, S.A., Nongpiur, M.E., Aung, T., Milea, D., Girard, M.J.A., 2016a. Finite element analysis predicts large optic nerve head strains during horizontal eye movements. Invest. Ophthalmol. Vis. Sci. 57, 2452–2462.

Wang, X., Beotra, M.R., Tun, T.A., Baskaran, M., Perera, S., Aung, T., Strouthidis, N.G., Milea, D., Girard, M.J.A., 2016b. In vivo 3-dimensional strain mapping confirms large optic nerve head deformations following horizontal eye movements. Invest. Ophthalmol. Vis. Sci. 57, 5825–5833.

Wang, X., Teoh, C.K.G., Chan, A.S.Y., Thangarajoo, S., Jonas, J.B., Girard, M.J.A., 2018. Biomechanical properties of Bruch's membrane-choroid complex and their influence on optic nerve head biomechanics. Invest. Ophthalmol. Vis. Sci. 59, 2808–2817.

Wang, X., Chang, S., Grinband, J., Yannuzzi, L.A., Freund, K.B., Hoang, Q.V., Girard, M. J., 2021. Optic nerve tortuosity and displacements during horizontal eye movements in healthy and highly myopic subjects, 2021 May 26:bjophthalmol-2021-318968 Br. J. Ophthalmol.. https://doi.org/10.1136/bjophthalmol-2021-318968 (Online ahead of print).

Wang, Y., Bensaid, N., Tiruveedhula, P., Ma, J., Ravikumar, S., Roorda, A., 2019. Human foveal cone photoreceptor topography and its dependence on eye length. Elife 8, e47148.

Wang, Y.X., Jiang, R., Wang, N.L., Xu, L., Jonas, J.B., 2015a. Acute peripapillary retinal pigment epithelium changes associated with acute intraocular pressure elevation. Ophthalmology 122, 2022–2028.

Wang, Y.X., Ran, J., Yang, L.H., Xu, L., Jonas, J.B., 2015b. Reversibility of retinal pigment epithelium detachment parallel to acute intraocular pressure rise. J. Glaucoma 24, e16–e18.

Wang, Y.X., Jiang, R., Wang, N.L., Xu, L., Jonas, J.B., 2015c. Acute peripapillary retinal pigment epithelium changes associated with acute intraocular pressure elevation. Ophthalmology 122, 2022–2028.

Wang, Y.X., Yang, H., Luo, H., Hong, S.W., Gardiner, S.K., Jeoung, J.W., Hardin, C., Sharpe, G.P., Nouri-Mahdavi, K., Caprioli, J., Demirel, S., Girkin, C.A., Liebmann, J. M., Mardin, C.Y., Quigley, H.A., Scheuerle, A.F., Fortune, B., Chauhan, B.C., Burgoyne, C.F., 2020. Peripapillary scleral bowing increases with age and is inversely associated with peripapillary choroidal thickness in healthy eyes. Am. J. Ophthalmol 127, 91–103.

Wang, Y.X., Yang, H., Wie, C.C., Xu, L., Wie, W.B., Jonas, J.B., 2022. High myopia as risk factor for the 10-year incidence of open-angle glaucoma in the Beijing Eye Study, 2022 Feb 22:bjophthalmol-2021-320644 Br. J. Ophthalmol.. https://doi.org/10.1136/bjophthalmol-2021-320644 (Online ahead of print).

Wei, W.B., Xu, L., Jonas, J.B., Shao, L., Du, K.F., Wang, S., Chen, C.X., Xu, J., Wang, Y.X., Zhou, J.Q., You, Q.S., 2013. Subfoveal choroidal thickness: the beijing eye study. Ophthalmology 120, 175–180.

Whitacre, M.M., Stein, R., 1993. Sources of error with use of Goldmann-type tonometers. Surv. Ophthalmol. 38, 1–30.

Whitcomb, J.E., Barnett, V.A., Olsen, T.W., Barocas, V.H., 2009. Ex vivo porcine iris stiffening due to drug stimulation. Exp. Eye Res. 89, 456–461.

1995 Wildsoet, C., Wallman, J., 1995. Choroidal and scleral mechanisms of compensation for spectacle lenses in chicks. Vision Res 35, 1175–1194.

Wildsoet, C.F., Chia, A., Cho, P., Guggenheim, J.A., Polling, J.R., Read, S., Sankaridurg, P., Saw, S.M., Trier, K., Walline, J.J., Wu, P.C., Wolffsohn, J.S., 2019. Imi - interventions Myopia Institute: interventions for controlling myopia onset and progression report. Invest. Ophthalmol. Vis. Sci. 60, M106–M131.

Wong, C.W., Phua, V., Lee, S.Y., Wong, T.Y., Cheung, C.M., 2017. Is choroidal or scleral thickness related to myopic macular degeneration? Invest. Ophthalmol. Vis. Sci. 58, 907–913.

Wong, C.W., Teo, Y.C.K., Tsai, S.T.A., Ting, S.W.D., Yeo, Y.S.I., Wong, W.K.D., Lee, S.Y., Wong, T.Y., Cheung, C.M.G., 2019. Characterization of the choroidal vasculature in myopic maculopathy with optical coherence tomographic angiography. Retina 39, 1742–1750.

Wong, Y.L., Zhu, X., Tham, Y.C., Yam, J.C., Zhang, K., Sabanayagam, C., Lanca, C., Zhang, X., Han, S.Y., Susvar, P., Trivedi, M., Yuan, N., Lambat, S., Raman, R., Song, S.J., Wang, Y.X., Bikbov, M.M., Nangia, V., Chen, L.J., Wong, T.Y., Lamoureux, E., Pang, C.P., Cheng, C.Y., Lu, Y., Jonas, J.B., Saw, S.M., 2020. Prevalence and Predictors of myopic macular degeneration among adults: pooled analysis from the Asian Eye Epidemiology Consortium: a pooled analysis, 2020 Sep 2;bjophthalmol-2020-316648 Br. J. Ophthalmol.. https://doi.org/10.1136/bjophthalmol-2020-316648 (Online ahead of print.f).

Woog, K., Legras, R., 2019. Distribution of mid-peripheral cones in emmetropic and myopic subjects using adaptive optics flood illumination camera. Ophthalmic Physiol. Opt. 39, 94–103.

Worthington, K.S., Wiley, L.A., Bartlett, A.M., Stone, E.M., Mullins, R.F., Salem, A.K., Guymon, C.A., Tucker, B.A., 2014. Mechanical properties of murine and porcine ocular tissues in compression. Exp. Eye Res. 121, 194–199.

Wu, H., Chen, W., Zhao, F., Zhou, Q., Reinach, P.S., Deng, L., Ma, L., Luo, S., Srinivasalu, N., Pan, M., Hu, Y., Pei, X., Sun, J., Ren, R., Xiong, Y., Zhou, Z., Zhang, S., Tian, G., Fang, J., Zhang, L., Lang, J., Wu, D., Zeng, C., Qu, J., Zhou, X., 2018. Scleral hypoxia is a target for myopia control. Proc. Natl. Acad. Sci. U.S.A. 115, E7091–E7100.

Wu, H., Zhang, G., Shen, M., Xu, R., Wang, P., Guan, Z., Xie, Z., Jin, Z., Chen, S., Mao, X., Qu, J., Zhou, X., 2021. Assessment of choroidal vascularity and choriocapillaris blood perfusion in anisomyopic adults by SS-OCT/OCTA. Invest. Ophthalmol. Vis. Sci. 62, 8.

Xie, J., Chen, Q., Hu, G., Yin, Y., Zou, H., He, J., Zhu, J., Fan, Y., Xu, X., 2021. Morphological differences between two types of Bruch's membrane defects in pathologic myopia. Graefes Arch. Clin. Exp. Ophthalmol. 259, 1411–1418.

Xu, J., Wang, Y.X., Jiang, R., Wie, W.B., Xu, L., Jonas, J.B., 2017. Peripapillary choroidal vascular layers: the beijing eye study. Acta Ophthalmol. 95, 619–628 (fvfv).

Xu, K.P., Yu, F.S., 2007. Cross talk between c-Met and epidermal growth factor receptor during retinal pigment epithelial wound healing. Invest. Ophthalmol. Vis. Sci. 48, 2242–2248.

Xu, L., Wang, Y., Li, Y., Li, J., Wang, Y., Cu, i .T., Li, J., Jonas, J.B., 2006. Causes of blindness and visual impairment in urban and rural areas in Beijing: the Beijing Eye Study. Ophthalmology 113, 1134–1141.

Xu, L., Wang, Y., Wang, S., Wang, Y., Jonas, J.B., 2007a. High myopia and glaucoma susceptibility. The beijing eye study. Ophthalmology 114, 216–220.

Xu, L., Li, Y., Wang, S., Wang, Y., Wang, Y., Jonas, J.B., 2007b. Characteristics of highly myopic eyes. The beijing eye study. Ophthalmology 114, 121–126.

Xu, L., Wang, Y.X., Wang, S., Jonas, J.B., 2010. Definition of high myopia by parapapillary atrophy. The Beijing Eye Study. Acta Ohthalmol 88, e350–e351.

Xu, X., Fang, Y., Yokoi, T., Shinohara, K., Hirakata, A., Iwata, T., Tsunoda, K., Jonas, J.B., Ohno-Matsui, K., 2019a. Posterior staphylomas in eyes with retinitis pigmentosa without high myopia. Retina 39, 1299–1304.

Xu, X., Fang, Y., Uramoto, K., Nagaoka, N., Shinohara, K., Yokoi, T., Tanaka, N., Ohno-Matsui, K., 2019b. Clinical features of lacquer cracks in eyes with pathological myopia. Retina 39, 1265–1277.

Xu, X., Fang, Y., Jonas, J.B., Du, R., Shinohara, K., Tanaka, N., Yokoi, T., Onishi, Y., Uramoto, K., Kamoi, K., Yoshida, T., Ohno-Matsui, K., 2020. Ridge-shaped macula in young myopic patients and its differentiation from typical dome-shaped macula in elderly myopic patients. Retina 40, 225–232.

Yan, F., Hui, Y.N., Li, Y.J., Guo, C.M., Meng, H., 2007. Epidermal growth factor receptor in cultured human retinal pigment epithelial cells. Ophthalmologica 221, 244–250.

Yan, Y.N., Wang, Y.X., Yang, Y., Xu, L., Xu, J., Wang, Q., Yang, J.Y., Yang, X., Zhou, W.J., Ohno-Matsui, K., Wei, W.B., Jonas, J.B., 2018. Ten-year progression of myopic maculopathy: the beijing eye study 2001-2011. Ophthalmology 125, 1253–1263.

Ye, J., Wang, M., Shen, M., Huang, S., Xue, A., Lin, J., Fan, Y., Wang, J., Lu, F., Shao, Y., 2020. Deep retinal capillary plexus decreasing correlated with the outer retinal layer alteration and visual acuity impairment in pathological myopia. Invest. Ophthalmol. Vis. Sci. 61, 45.

Yokoi, T., Ohno-Matsui, K., 2018. Diagnosis and treatment of myopic maculopathy. Asia Pac. J. Ophthalmol. 7, 415–421.

Yoo, Y.J., Lee, E.J., Kim, T.W., 2016. Intereye difference in the microstructure of parapapillary atrophy in unilateral primary open-angle glaucoma. Invest. Ophthalmol. Vis. Sci. 57, 4187–4193.

Yoon, J.Y., Sung, K.R., Yun, S.C., Shin, J.W., 2019. Progressive optic disc tilt in young myopic glaucomatous eyes. Kor. J. Ophthalmol. 33, 520–527.

You, Q.S., Xu, L., Jonas, J.B., 2008. Tilted optic discs: the beijing eye study. Eye 22, 728–729.

You, Q.S., Peng, X.Y., Chen, C.X., Xu, L., Jonas, J.B., 2013. Peripapillary intrachoroidal cavitations. The beijing eye study. PLoS One 8, e78743.

You, Q.S., Peng, X.Y., Xu, L., Chen, C.X., Wang, Y.X., Jonas, J.B., 2014. Myopic maculopathy imaged by optical coherence tomography: the beijing eye study. Ophthalmology 121, 220–224.

You, Q.S., Peng, X.Y., Xu, L., Chen, C.X., Wei, W.B., Wang, Y.X., Jonas, J.B., 2016. Macular Bruch's membrane defects in highly myopic eyes. The Beijing Eye Study. Retina 36, 517–523.

Zhang, L., Wang, F., Jiang, Y., Xu, S., Lu, F., Wang, W., Sun, X., Sun, X., 2013. Migration of retinal pigment epithelial cells is EGFR/PI3K/AKT dependent. Front. Biosci. 5, 661–671.

Zhang, Q., Wang, Y.X., Wei, W.B., Xu, L., Jonas, J.B., 2018. Parapapillary beta zone and gamma zone in a normal population: the Beijing Eye Study 2011. Invest. Ophthalmol. Vis. Sci. 59, 3320–3329.

Zhang, Q., Xu, L., Wei, W.B., Wang, Y.X., Jonas, J.B., 2019. Size and shape of Bruch's membrane opening in relationship to axial length, gamma zone and macular Bruch's membrane defects. Invest. Ophthalmol. Vis. Sci. 60, 2591–2598.

Zhang, Q., Xu, L., Zhao, L., Jonas, R.A., Wang, Y.X., Jonas, J.B., 2021. Peaks of circumpapillary retinal nerve fibre layer and associations in healthy eyes: the Beijing Eye Study 2011. Br. J. Ophthalmol. https://doi.org/10.1136/bjophthalmol-2021-318869, 2021 Apr 15:bjophthalmol-2021-318869, (Online ahead of print).

Zhang, Y., Wildsoet, C.F., 2015. RPE and choroid mechanisms underlying ocular growth and myopia. Prog. Mol. Biol. Transl. Sci. 134, 221–240.

Zhao, J., Wang, Y.X., Zhang, Q., Wie, W.B., Xu, L., Jonas, J.B., 2018. Macular choroidal small-vessel layer, Sattler's layer and Haller's layer thicknesses: the Beijing Eye Study. Sci. Rep. 8, 4411.

Zhou, X., Zhang, S., Yang, F., Yang, Y., Huang, Q., Huang, C., Qu, J., Zhou, X., 2021. Decreased choroidal blood perfusion induces myopia in Guinea pigs. Invest. Ophthalmol. Vis. Sci. 62, 30.

Zhu, X., McBrien, N.A., Smith 3rd, E.L., Troilo, D., Wallman, J., 2013. Eyes in various species can shorten to compensate for myopic defocus. Invest. Ophthalmol. Vis. Sci. 54, 2634–2644.